WRH

Exh. AES000051

Special Paper 353

Geology, Hydrogeology, and Environmental Remediation: Idaho National Engineering and Environmental Laboratory, Eastern Snake River Plain, Idaho

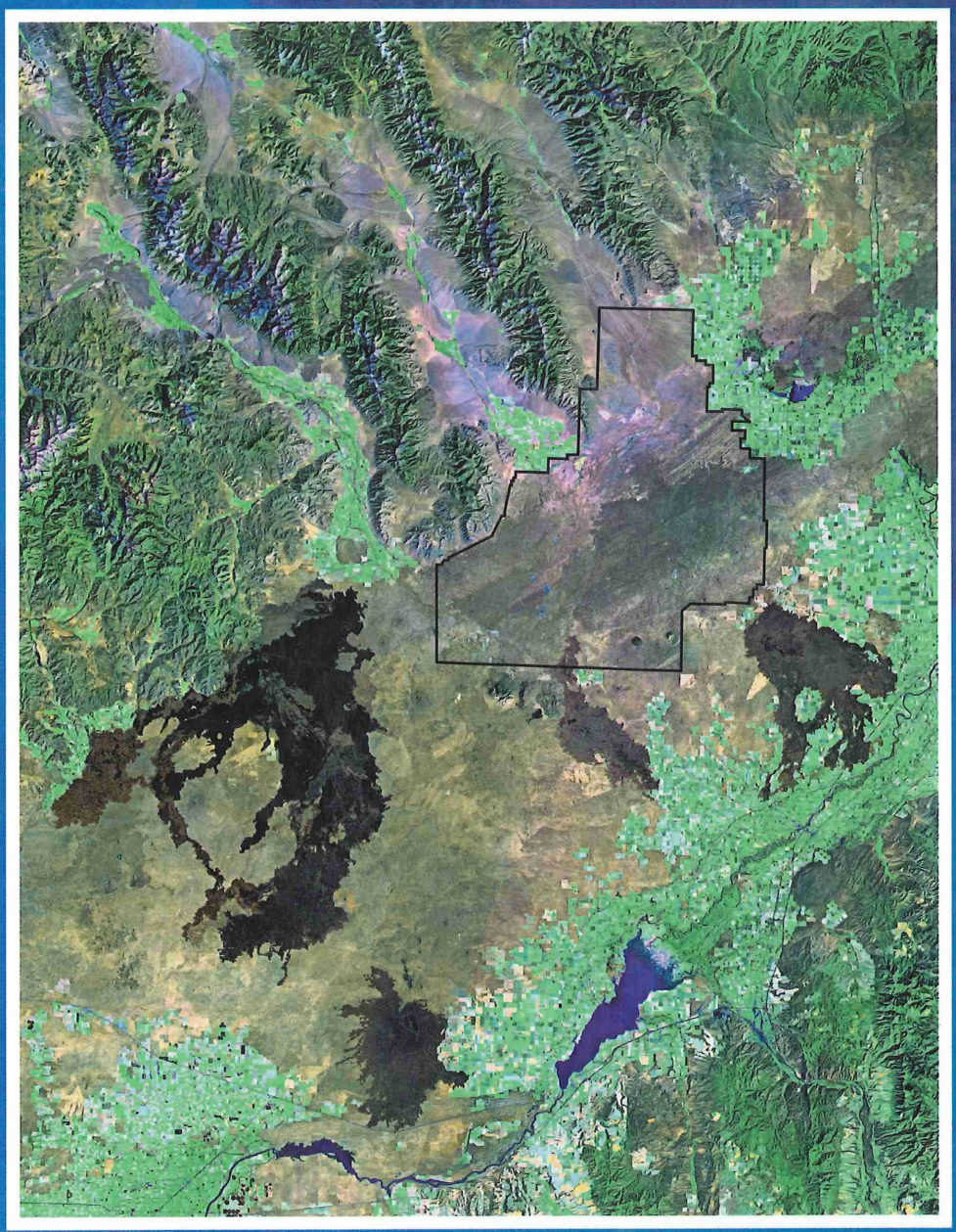

Paul Karl Link and L.L. Mink, Editors

Geology, Hydrogeology, and Environmental Remediation: Idaho National Engineering and Environmental Laboratory, Eastern Snake River Plain, Idaho

Edited by

Paul Karl Link
Department of Geosciences
Idaho State University
Pocatello, Idaho 83209
USA

and

L. L. Mink
Idaho Water Resources Research Institute
205 Morrill Hall
University of Idaho
Moscow, Idaho 83844-3011
USA

SPECIAL PAPER

353

Geological Society of America
3300 Penrose Place
P.O. Box 9140
Boulder, Colorado 80301-9140
2002

Published by The Geological Society of America, Inc.
3300 Penrose Place, P.O. Box 9140, Boulder, Colorado 80301
www.geosociety.org

Printed in U.S.A.

GSA Books Science Editor Abhijit Basu
GSA Books Editor Rebecca Herr
Cover design by Margo Good

Library of Congress Cataloging-in-Publication Data

Geology, hydrogeology, and environmental remediation: Idaho National Engineering and Environmental Laboratory, Eastern Snake River Plain, Idaho / edited by Paul Karl Link and Leland L. Mink.

p. cm. — (Special Paper ; 353)
Includes bibliographical references and index.
ISBN 0-8137-2353-1
1. Geology—Idaho. 2. Geology—Snake River Plain (Idaho and Or.) 3. Hydrogeology—Idaho. 4. Hydrogeology—Snake River Plain (Idaho and Or.) 5. Idaho Natinal Engineering an Environmental Laboratory—Environmental aspects. I. Link, P. K. II. Mink, Leland L. III. Special papers (Geological Society of America) ; 353.

QE104.S59 G46 2001
557.96—dc21 2001023206

Cover: Landsat Thematic Mapper false color composite image of the eastern Snake River Plain. Area of the Idaho National Engineering and Environmental Laboratory outlined in black. Image processing by John C. Dohrenwend, Southwest Satellite Imaging, 223 South State Street, Teasdale, Utah, 84773-0141; e-mail: dohrenwend@rkymtnhi.com.

10 9 8 7 6 5 4 3 2 1

Contents

Geological Society of America
Special Paper 353
2002

Foreword

Robert J. Creed
Trish St. Clair
U.S. Department of Energy, Idaho Operations Office, Idaho Falls, Idaho 83401, USA

The eastern Snake River Plain (ESRP) is a northeast-trending subsiding volcanic trough bounded by northerly trending Basin and Range structures to the north and south. The lithology, trend, and age of the ESRP are consistent with an origin related to the movement of the North American plate in a southwesterly direction over the Yellowstone hotspot. From a distance the ESRP seems to be a flat, featureless basaltic plain. At this perspective one could conclude that the subsurface features that control important geohydrologic properties would be similarly featureless and easily characterized. However, at the meter to tens of meters scales that are important for risk assessment at the Idaho National Engineering and Environmental Laboratory (INEEL) and geohydrological characterization for other water-resource issues, the forces and processes that have shaped the ESRP over the past 4 m.y. have produced a complex system of basalts, sedimentary interbeds, and structural features.

In this Geological Society of America Special Paper, the editors and authors have made significant contributions to our understanding of the composition, geometry, and evolution of the ESRP. Although the U.S. Department of Energy (DOE) and other risk assessment and remediation plans will always require thorough and site-specific investigations, these papers provide a robust and independent context within which various characterization and remediation models can be developed and assessed. This book is of special significance because it will be the first multidisciplinary peer-reviewed regional geoscience summary of any DOE site.

The editors and authors are to be commended in reaching a very productive middle ground between the scientific prerogatives of generating and testing hypotheses (wherever this process might lead) and the need for acceptable characterization data and methods to support risk assessment and resource management needs of the INEEL and the State of Idaho. We hope that the collaboration and multidisciplinary techniques reflected in these papers will serve as an example of how this integrated approach can be applied fruitfully to other sites and regions.

The independent and robust nature of these investigations should give stakeholders and regulators confidence that key characterization issues are or can be well defined. This volume will also give scientists and science and remediation research managers a better understanding of the nature and magnitude of uncertainties and knowledge gaps in important aspects of the ESRP. This knowledge will contribute to the systematic evolution of a productive consensus on how to focus resources and hypotheses to fill these gaps and reduce uncertainties in the assessment of risk associated with remediation strategies and water-resource characterization and development.

Confidence in this process will be essential as organizations with groundwater risk-assessment responsibilities across the country pursue the scientifically and politically defensible characterization of vadose-zone contaminant fate and transport. The INEEL in particular is organizing a systematic scientific effort to understand, coordinate, and integrate vadose-zone characterization efforts across the DOE complex. This book serves as an excellent example of how such issues can be addressed while scientists across the region benefit from pursuing the science needs of the Department of Energy.

A truly outstanding aspect of this volume is the depth, breadth, and coordination of the multidisciplinary techniques used to enhance our understanding of the ESRP and its aquifer. As one studies the systematics of fracture flow and flow in heterogeneous systems, it becomes clear that such a multidisciplinary approach is required. Thus, in this volume there are papers on the microbiology, geochemistry, sedimentology, and hydrology of the ESRP.

We hope that this book will encourage others to support and participate in the evolution of the field of earth sciences as a multidisciplinary problem-solving discipline. A necessary aspect of this evolution is the formulation and pursuit of scientific ideas. Some of these ideas will fail in the validation process and others will lead to concepts and technology that we cannot envision today. The generation and testing of these ideas is a source of endless fascination to earth scientists everywhere.

All involved are indebted to the DOE Environmental Management Office of Technology and Development (EM-50),

Creed, R.J., and St. Clair, T., 2002, Foreword, *in* Link, P.K., and Mink, L.L., eds., Geology, Hydrogeology, and Environmental Remediation: Idaho National Engineering and Environmental Laboratory, Eastern Snake River Plain, Idaho: Boulder, Colorado, Geological Society of America Special Paper 353, p. 1–2.

which provided the money; volume coeditor Roy Mink (Idaho Water Resources Research Institute [IWRRI], Idaho Universities Consortium), who led the research; Clay Nichols, U.S. Department of Energy Idaho Operations Office; Don Maiers (INEEL); and Sarah Bigger and Kathy Owens (IWRRI), who managed Idaho Universities Consortium grants and successfully encouraged collaboration among Idaho university, INEEL laboratory, and U.S. Geological Survey personnel.

MANUSCRIPT ACCEPTED BY THE SOCIETY NOVEMBER 2, 2000

Printed in the U.S.A.

Geological Society of America
Special Paper 353
2002

Introduction to the hydrogeology of the eastern Snake River Plain

Roy C. Bartholomay*
Linda C. Davis
U.S. Geological Survey, Pocatello, Idaho 83209, USA
Paul Karl Link
Department of Geosciences, Idaho State University, Pocatello, Idaho 83209, USA

ABSTRACT

This chapter gives a general overview of the hydrogeology of the eastern Snake River Plain, the Idaho National Engineering and Environmental Laboratory (INEEL), and a description of the INEEL Lithologic Core Storage Library, a source of data for many of the chapters in this volume. It also summarizes definitions and lithostratigraphic terminology for the volume. This volume summarizes geoscience research on the INEEL site in the 1990s. The chapters are written by scientists from many organizations, including INEEL contractors, universities, the U.S. Geological Survey, the state of Idaho, and the Idaho Water Resources Research Institute.

HISTORY

In 1949, the National Reactor Testing Station, a 2300 km^2 site on the eastern Snake River Plain in southeastern Idaho (Fig. 1), was established by the U.S. Atomic Energy Commission, which later became the U.S. Department of Energy (DOE). The site was used initially for peacetime atomic-energy applications, nuclear safety research, defense programs, and advanced energy concepts. The National Reactor Testing Station was renamed the Idaho National Engineering Laboratory (INEL) in 1974 to reflect the broad scope of engineering activities taking place at various facilities at the site. In 1997, the INEL was renamed the INEEL because of additional emphasis on environmental research. Current INEEL research activities emphasize spent nuclear-fuel management; hazardous and mixed waste management and minimization; cultural resources preservation; and environmental engineering, protection, and remediation (DOE-ID, 1996; Becker et al., 1998).

Various Federal Government contractors operate the INEEL under the supervision of three DOE offices: the Idaho Operations Office (DOE-ID), the Pittsburgh Naval Reactors Office, and the Chicago Operations Office. The government contractors and many other organizations conduct scientific research at the INEEL with authorization by DOE-ID. The State of Idaho INEEL Oversight Program is involved with public education, emergency response, and environmental monitoring. The Idaho Water Resources Research Institute and Inland Northwest Research Alliance (INRA) coordinate university research.

The U.S. Geological Survey has undertaken systematic research at the INEEL since 1949. This work initially characterized water resources before development of nuclear-reactor testing facilities (Walker, 1964; Barraclough et al., 1967, 1976; Nace et al., 1975). Since then, the U.S. Geological Survey has operated a ground-water quality and water-level measurement monitoring network to provide data for research on hydrologic trends and to delineate the movement of facility-related radiochemical and chemical wastes in the Snake River Plain aquifer.

Studies of hydrology, geology, and waste remediation at the INEEL are the focus of this Special Paper, and are needed because of historical waste-disposal practices; however, they also provide better understanding of the regional Snake River Plain-Yellowstone volcanic and hydrologic system. Wastewater containing chemical and radiochemical wastes was discharged

*E-mail: rcbarth@usgs.gov

Bartholomay, R.C., Davis, L.C., and Link, P.K., 2002, Introduction to the hydrogeology of the eastern Snake River Plain, *in* Link, P.K., and Mink, L.L., eds., Geology, Hydrogeology, and Environmental Remediation: Idaho National Engineering and Environmental Laboratory, Eastern Snake River Plain, Idaho: Boulder, Colorado, Geological Society of America Special Paper 353, p. 3–9.

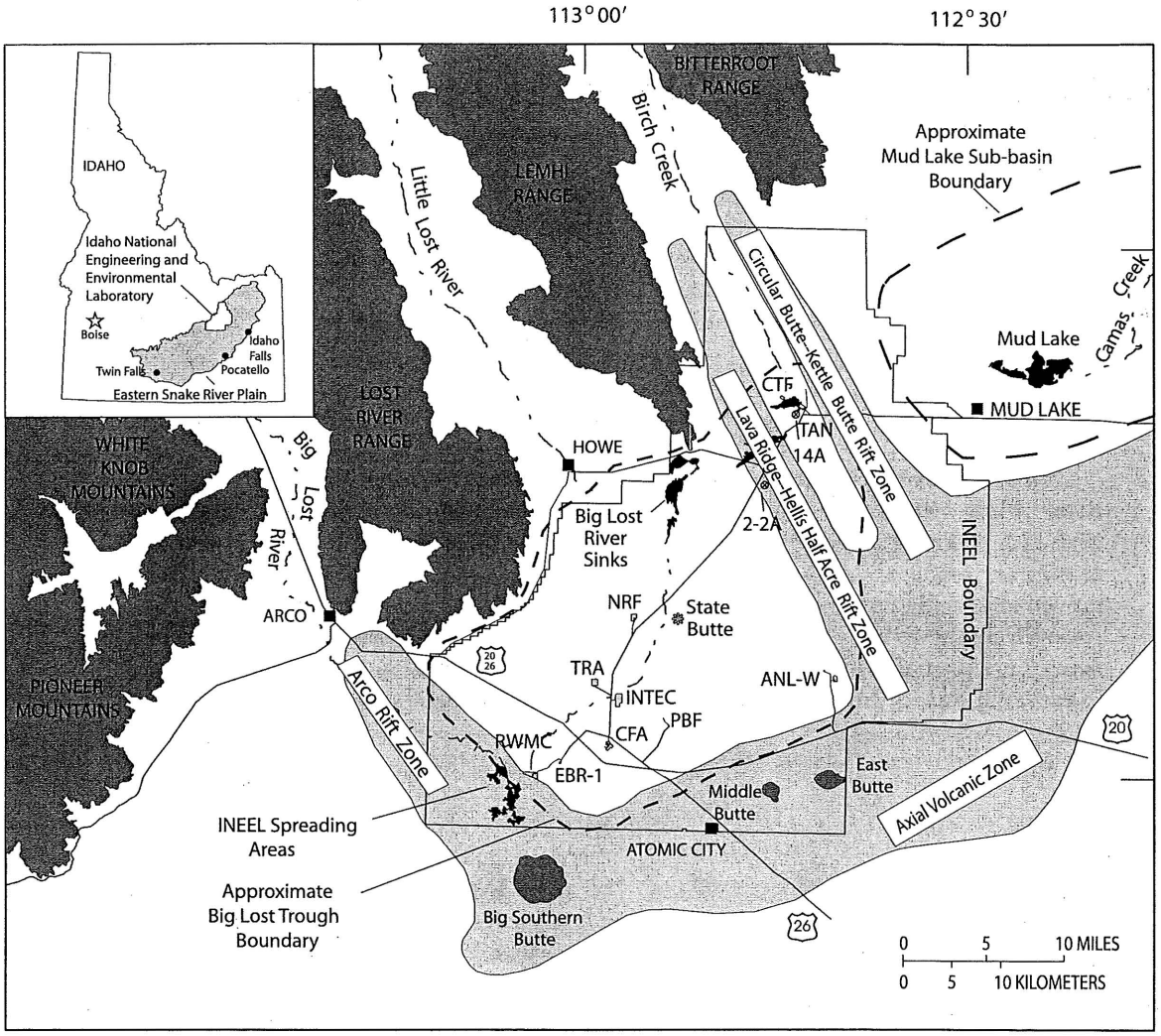

BOUNDARY OF THE IDAHO NATIONAL ENGINEERING AND ENVIRONMENTAL LABORATORY

APPROXIMATE RIFT ZONE BOUNDARIES

⊗ 2-2A LOCAL WELL IDENTIFIER

SELECTED FACILITIES AT THE IDAHO NATIONAL ENGINEERING AND ENVIRONMENTAL LABORATORY

ANL-W	ARGONNE NATIONAL LABORATORY--WEST	NRF	NAVAL REACTORS FACILITY
CFA	CENTRAL FACILITIES AREA	PBF	POWER BURST FACILITY
CTF	CONTAINED TEST FACILITY (Formerly called Loss of Fluid Test Facility--LOFT)	RWMC	RADIOACTIVE WASTE MANAGEMENT COMPLEX
EBR-1	EXPERIMENTAL BREEDER REACTOR NO. 1	TAN	TEST AREA NORTH
INTEC	IDAHO NUCLEAR TECHNOLOGY AND ENGINEERING CENTER	TRA	TEST REACTOR AREA

Figure 1. Map showing locations of major geologic features and Department of Energy facilities in the Idaho National Engineering and Environmental Laboratory (INEEL) area, eastern Snake River Plain.

Geological Society of America
Special Paper 353
2002

Pliocene and Quaternary stratigraphic architecture and drainage systems of the Big Lost Trough, northeastern Snake River Plain, Idaho

Jeffrey K. Geslin*
Paul Karl Link
James W. Riesterer
Department of Geosciences, Idaho State University, Pocatello, Idaho 83209, USA
Mel A. Kuntz
U.S. Geological Survey, Denver, Colorado 80225, USA
C. Mark Fanning
Research School of Earth Sciences, Australia National University, Canberra, ACT 2601, Australia

ABSTRACT

The geometry, volcanic-sedimentary stratigraphic architecture, and distribution of clastic sedimentary facies reflect a complex tectonic setting and fluctuations in climatic conditions during the past 2.5 m.y. in the Big Lost Trough on the eastern Snake River Plain. Interaction of the migrating Yellowstone hotspot and developing Basin and Range structures controlled the spatial distribution of volcanic rift zones that define the margins of the Big Lost Trough, an arid, underfilled basin. The volcanic-sedimentary stratigraphy of the basin is characterized by basaltic volcanic units that offlap eruptive centers and downlap into the basin, and clastic sedimentary units that onlap adjacent volcanic rift zones. Climatically influenced interactions of a fluvial-playa-eolian depositional system of the Big Lost River and a lacustrine system of Lake Terreton are reflected in the composition and architecture of the sedimentary basin fill.

Petrographic and U/Pb detrital-zircon geochronology analyses of subsurface sands compared with analyses of modern fluvial and eolian sands allow definitive determination of the provenance of the subsurface deposits. Petrographic and detrital-zircon data suggest that the Big Lost River has been the dominant source of sediment for at least the past 1 m.y. Big Lost River deposits found in the middle and northern parts of the basin suggest that the river system prograded northward during lowstands of Lake Terreton. Lowstands of Lake Terreton are also associated with development of an eolian system that reworked the fluvial deposits. The abundance of Big Lost River and eolian sands in the middle of the basin documents the effective damming of sediment by the volcanic rift zone that defines the northern basin margin. X-ray diffraction data suggest that subsurface playa or marginal lacustrine deposits along the northeastern basin margin contain abundant gypsum, indicating that ancient arid climate cycles were drier than the modern arid climate.

*Present address: ExxonMobil Upstream Research Company, P.O. Box 2189, Houston, TX 77252. E-mail: Jeff.K.Geslin@exxonmobil.com

Geslin, J.K., Link, P.K., Riesterer, J.W., Kuntz, M.A., and Fanning, C.M., 2002, Pliocene and Quaternary stratigraphic architecture and drainage systems of the Big Lost Trough, northeastern Snake River Plain, Idaho, *in* Link, P.K., and Mink, L.L., eds., Geology, Hydrogeology, and Environmental Remediation: Idaho National Engineering and Environmental Laboratory, Eastern Snake River Plain, Idaho: Boulder, Colorado, Geological Society of America Special Paper 353, p. 11–26.

INTRODUCTION

The Pliocene to Holocene Big Lost Trough is a small, closed sedimentary basin situated in the middle of the Idaho National Engineering and Environmental Laboratory (INEEL) on the eastern Snake River Plain, Idaho (Fig. 1). The northern INEEL, and the Test Area North (TAN) facility in particular, have been the focus of geological and hydrological investigations related to the remediation of contaminated groundwater in the Snake River Plain aquifer. Ultimately, it is crucial for hydrogeologic models and remediation technologies used in the northern INEEL to incorporate the stratal architecture of the vadose zone and aquifer in the northern end of the Big Lost Trough.

Volcanic rift zones and the Axial volcanic zone of the Snake River Plain (Fig. 1) define the boundaries of the Big Lost Trough on all but its northwestern side, and the stratal architecture under the INEEL reflects the interaction between basaltic volcanism and sedimentary systems operating in the intervening basin. The Lost River Range, Lemhi Range, and Beaverhead Mountains, part of the Basin and Range system, are located along the northwestern basin margin. Streams in valleys between these ranges, including the Big Lost River, Little Lost River, and Birch Creek, are the dominant source of clastic sediments in the Big Lost Trough (e.g., Geslin et al., 1999). The Circular Butte–Kettle Butte volcanic rift zone defines a low-relief ridge on the northeastern end of the Big Lost Trough, and serves as a barrier between the basin and the adjacent Mud Lake subbasin (Fig. 1; e.g., Anderson and Bowers, 1985; Geslin et al., 1997; Mark and Thackray, this volume).

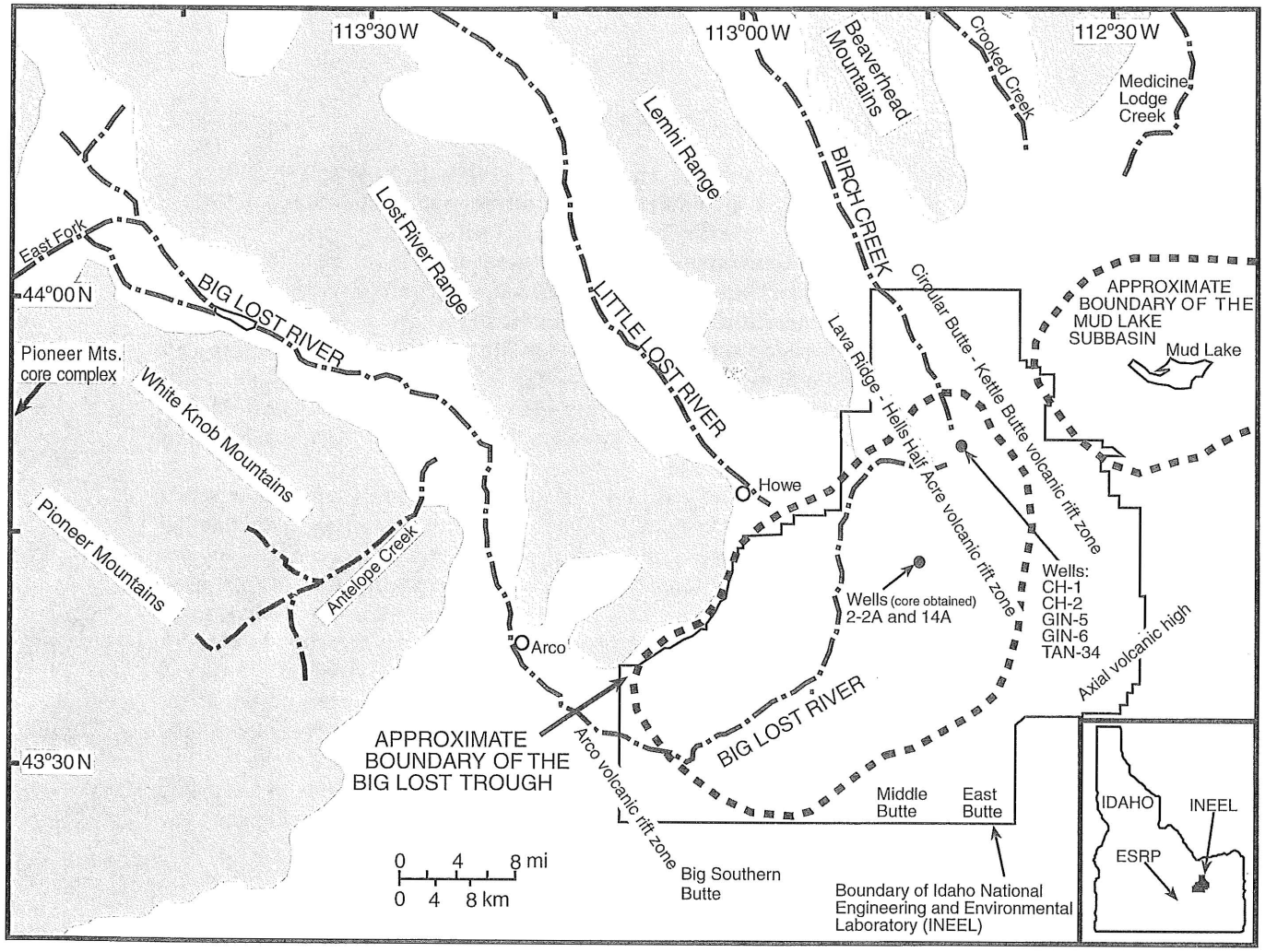

Figure 1. Map of study area showing location of approximate boundary of Big Lost Trough, adjacent basin and range features, streams that flow into basin, approximate locations of volcanic features on Snake River Plain, wells at Test Area North (CH-1, CH-2, GIN-5, GIN-6, TAN-34), and wells in middle of basin (2-2A, 14A).

The elevated topographic axis of the eastern Snake River Plain defines the southeastern side of the Big Lost Trough, and the Arco volcanic rift zone defines its southwestern border.

In this chapter we present the stratigraphic relationships of intercalated basalt flows and clastic sedimentary units in the northern Big Lost Trough, and discuss compositional analyses of sediments on the surface and in the shallow subsurface. We also document, using the results of detailed provenance analysis, the drainage history of the fluvial systems that deliver sand and gravel to the basin. These results predict that, in the upper part of Big Lost Trough strata, there is a progressively increasing abundance of high-permeability sediments (sands and gravels) from the northern end to the middle of the basin. X-ray diffraction analyses suggest that surficial fine-grained lacustrine and playa sediments, as well as subsurface fine-grained sediments from the middle of the basin, are composed predominantly of smectite, kaolinite, and chlorite; this probably reflects weathering of volcanic and fine-grained sedimentary rocks in fluvial source areas. Fine-grained subsurface sediments found at the northeastern basin margin, in the vicinity of the TAN facilities, contain abundant gypsum, reflecting evaporative depositional conditions.

GEOLOGIC SETTING

The Big Lost Trough is located within the eastern Snake River Plain, a semiarid lava- and loess-mantled plain that cuts across the northwest-trending Basin and Range structure of

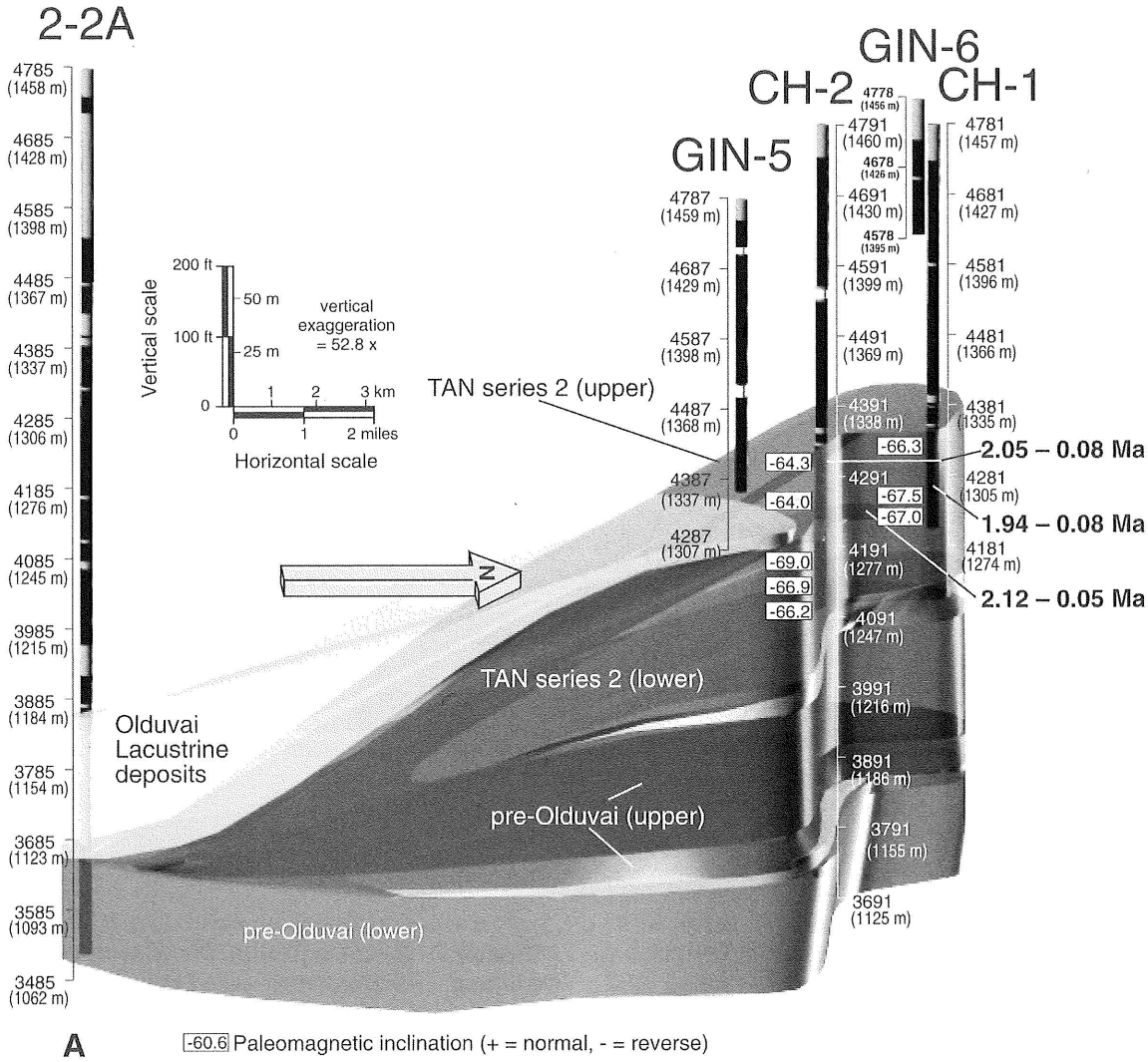

Figure 2. Three-dimensional correlation diagrams showing basalt flow groups and clastic sediments from northeastern basin margin (wells CH-1, CH-2, GIN-5, GIN-6) to middle of basin (well 2-2A). A: 2 Ma. B (page 14): 1 Ma. C (page 15): Modern. Well locations are shown in Figure 1. Basalt is darkly shaded and sedimentary units are lightly shaded. Abbreviations for lava flows Q-R and IJ reflect terminology of Hughes et al. (this volume).

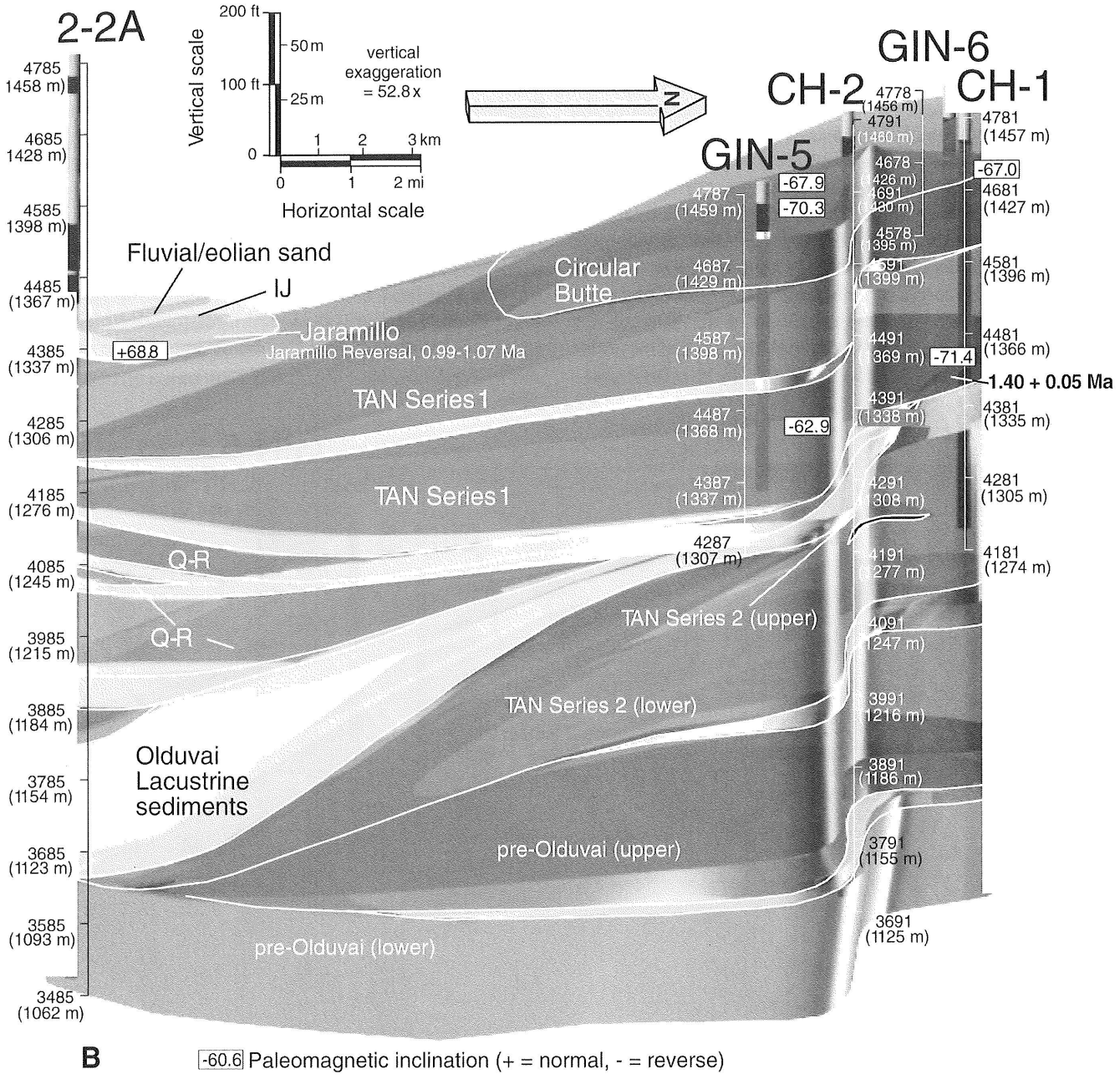

Figure 2. (*continued*)

eastern Idaho and is the track of the Yellowstone hotspot (e.g., Nace et al., 1975; Morgan, 1992; Pierce and Morgan, 1992). Topographic depressions that were created on the eastern Snake River Plain by differential subsidence or development of Basin and Range structures define several small sedimentary basins, including the Big Lost Trough (Fig. 1; Geslin et al., 1999) and, to the northeast, the Mud Lake subbasin (Gianniny et al., this volume). Geologic maps of the INEEL area (e.g., Scott, 1982; Kuntz et al., 1994) establish the general sedimentary-volcanic setting of the Big Lost Trough. Strata of the basin are part of the Pliocene to Holocene Snake River Group, and overlie a series of rhyolitic ignimbrites and minor sedimentary interbeds (Morgan et al., 1984; Champion et al., 1988; Anders et al., 1989; Hackett and Smith, 1992; Kuntz et al., 1992; Morgan, 1992; Pierce and Morgan, 1992).

Basaltic lava fields define many of the landforms on the eastern Snake River Plain and basalt flows dominate the upper part of the subsurface geology of the area. Surficial features

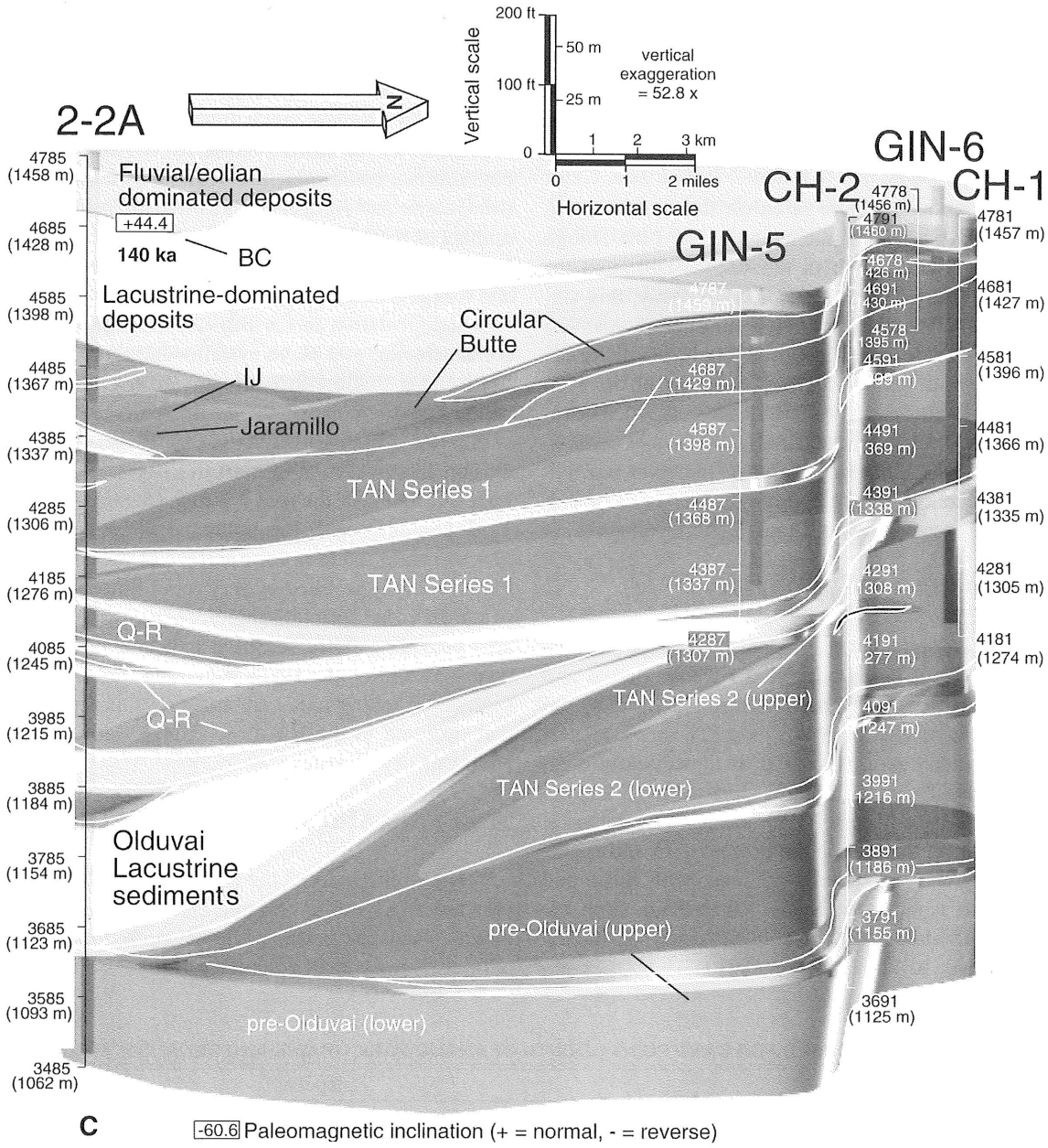

Figure 2. (*continued*)

also include small shield volcanoes and rhyolite domes (e.g., Kuntz et al., 1994). Basalt flows erupted along volcanic rift zones that parallel the northwest-southeast orientation of the adjacent Basin and Range structures (e.g., Kuntz et al., 1992). One of these volcanic rift zones, the Circular Butte–Kettle Butte volcanic rift zone, defines the northeastern end of the Big Lost Trough (Fig. 1). The stratigraphic architecture of the northern end of the basin (see following) reflects the interaction between basaltic volcanism along this volcanic rift zone and sedimentation in the basin.

Sediments are delivered to the Big Lost Trough primarily by three fluvial systems: the Big Lost River, the Little Lost River, and Birch Creek, which drain mountains to the northwest of the basin (Fig. 1; Geslin et al., 1999). Small streams that drain the southern end of the Beaverhead Mountains, north of the basin, and eolian systems operating on the eastern Snake River Plain contribute volumetrically less abundant clastic sediments. Eolian processes primarily winnow and redeposit sediments delivered by the fluvial systems. Examination of the modern configuration of the fluvial systems shows that both the

Little Lost River and Birch Creek have relatively small drainage areas and terminate in playas or sinks at the mouths of their respective valleys. However, the Big Lost River has a relatively large drainage area in the mountains of central Idaho and it traverses nearly the entire length of the Big Lost Trough, terminating in a series of playas near the northern end of the basin (Fig. 1; Kuntz et al., 1994).

The stratigraphic architecture of basalt flows and fluvial, eolian, playa, and lacustrine sediments in the Big Lost Trough controls groundwater flow, both in the vadose zone and the Snake River Plain aquifer (e.g., Mark and Thackray, this volume). In the Snake River Plain aquifer, ~60 m below the surface at the northern end of the Big Lost Trough, flow is to the south and southwest, driven by the regional head of the Mud Lake system (e.g., Whitehead; 1992; Spinazola, 1994). The regional flow in the aquifer suggests that as groundwater contaminants below the TAN facility migrate, their transport rate will be increasingly influenced by the hydrologic properties of sediments in the basin (see Mark and Thackray, this volume).

TECTONIC AND CLIMATIC SETTING

The Big Lost Trough is an arid, underfilled basin (cf. Carroll and Bohacs, 1999). It is underfilled because fluvial and lacustrine systems never breach basin margins defined by the surrounding topographically high volcanic rift zones. Generally, the basin geometry is a byproduct of these volcanic rift zones; however, fluvial systems that transport sediment into the basin are controlled by adjacent Basin and Range structures. The volcanic rift zones that define the northeastern and southwestern basin margins are generally collinear with Basin and Range structures adjacent to the Snake River Plain. Both the Basin and Range structures and volcanic rift zones are related to regional northeast to southwest extension (Kuntz et al., 1992). Local subsidence of the Big Lost Trough could have resulted from crustal thinning and contraction related to the rhyolite caldera history of the Snake River Plain, specifically the 6.0 Ma Blue Creek caldera that underlies the area (Kuntz et al., 1992; Morgan, 1992; Blair and Link, 2000). Large-scale subsidence of the eastern Snake River Plain is probably due to both thermal contraction and loading by a midcrustal mafic sill (McQuarrie and Rodgers, 1998). Therefore, the tectonic development of the Big Lost Trough represents complex interactions between the migration of the Yellowstone hotspot and Basin and Range extension.

Sedimentation in the Big Lost Trough was dominated by eolian, fluvial, and playa systems during drier climatic conditions and a shallow lacustrine system, Lake Terreton, during wetter climatic conditions (Geslin et al., 1997, 1999; Gianniny et al., 1997; Blair and Link, 2000). Pleistocene Lake Terreton existed intermittently in both the Big Lost Trough and Mud Lake subbasin for the past ~2 m.y. (Stearns et al., 1939; Scott, 1982; Gianniny et al., this volume; Bestland et al., this volume). The low-relief nature of the surface of the eastern Snake River Plain probably resulted in very rapid fluctuations in the lateral extent of Lake Terreton; therefore, lacustrine sediments in the area provide a fairly sensitive indicator of relatively wet climates. Geslin et al. (1999) suggested that fluvial-playa-eolian systems operating today are analogous to depositional systems that operated in the Big Lost Trough during Pleistocene and Holocene dry climates.

VOLCANIC AND SEDIMENTARY STRATIGRAPHY

The stratigraphy of the Big Lost Trough is somewhat complex because basaltic volcanic units offlap eruptive centers and downlap into the basin, while clastic sedimentary units onlap adjacent volcanic rift zones (e.g., Hughes et al., 1998). Three-

TABLE 1. CATEGORIES USED FOR SAND POINT COUNTS OF FRAMEWORK GRAINS AND RECALCULATED PLOTS

Grain category definitions		Categories*	Recalculated parameters
Qp	Aphanitic polycrystalline quartz	Qp	*QFLt:*
Qm	Monocrystalline quartz	Qm	Q = Qm
P	Plagioclase feldspar	P	F = P + K
K	Potassium feldspar	K	Lt = Lv + Lm + Ls + Qp
Lvv	Vitric volcanic lithic fragments	Lv	
Lvf	Felsitic volcanic lithic fragments	Lv	*LmLvLst:*
Lvml	Microlitic volcanic lithic fragments	Lv	Lm = Lm
Lvl	Lathwork volcanic lithic fragments	Lv	Lv = Lv
Lmi	Low-grade metaigneous lithic fragments	Lmv	Lst = Ls + Qp
PolyM	Polycrystalline phyllosilicates	Lms	
QMF(t)	Quartz-mica-feldspar aggregate with tectonite fabric	Lms	*QpLvmLsm:*
			Qp = Qp
QMF(a)	Quartz-mica-feldspar aggregate without tectonite fabric	Lms	Lvm = Lv + Lmv
			Lsm = Ls + Lms
Ls(arg)	Argillaceous sedimentary lithic fragments	Ls	
Ls(cb)	Carbonate sedimentary lithic fragments	Ls	*QmKP:*
Mica	Monocrystalline phyllosilicates	M	Qm = Qm
Dense	Dense mineral grains	D	K = K
C	Carbonate cement (not a grain category)	C	P = P

*See Ingersoll et al. (1984)

dimensional stratigraphic diagrams, constructed from well data, were created to illustrate the development of the stratal architecture in the northern end of the Big Lost Trough (Fig. 2). Figure 2 encompasses a region that includes TAN, the focus of geologic, hydrologic, and environmental studies, and areas hydrologically downgradient to the south. The three-dimensional stratigraphic diagrams correlate basalt flow groups (flow group classification based on Hughes et al. [this volume] as modified from Lanphere et al. [1994] and Anderson and Bowers [1995]) and clastic sedimentary successions from wells CH-1, CH-2, GIN-5, GIN-6, and TAN-34 at TAN to well 2-2A near the middle of the basin (Fig. 1). Geochronology data for basalt flow groups are from whole-rock $^{40}Ar/^{39}Ar$ analyses (Lanphere et al., 1994). A single date of 140 ka in the upper sedimentary succession in well 2-2A is from Geslin et al. (1999) and is based on amino acid racemization in ostracode shells. Paleomagnetic data are from Champion et al. (1988). The stratigraphy shown in these diagrams represents basaltic lava flows and clastic sediments deposited over the past ~2.5 m.y.

The stratal architecture of the northern end of the basin (Fig. 2) documents the construction of basaltic eruptive centers along the Circular Butte-Kettle Butte volcanic rift zone. The southward downlapping or offlapping of pre-Olduvai, TAN series 1 and 2, and Circular Butte basalt flow groups (Fig. 2), along with surface data (Kuntz et al., 1994), suggests that many of the flows moved generally northeast to southwest, from the volcanic rift zone toward the middle of the basin. Basalt flow group geometry, along with the northward onlap of sediments onto the volcanic rift zone, suggests that the volcanic rift zone was a positive topographic feature throughout basin history. Some of the smaller post-Olduvai flow groups present in well 2-2A (Fig. 2B) are not present in wells along the northern basin margin, and could have erupted from a volcanic center to the south, and then flowed northward into the basin. The strati-

TABLE 2. RECALCULATED MODAL POINT-COUNT DATA FOR SURFICIAL SEDIMENTS OF THE BIG LOST TROUGH AND ADJACENT DRAINAGES

	QmFLt			LmLvLst			QpLvmLsm			QmKP		
Sample No.	Qm	F	Lt	Lm	Lv	Lst	Qp	Lvm	Lsm	Qm	K	P
Big Lost River channel												
1PL96	20.4	14.9	64.7	12.3	69.4	18.3	7.9	69.4	22.7	57.8	0.0	42.2
7JG97	22.4	25.1	52.5	35.3	41.8	22.9	10.4	41.8	47.8	47.1	19.6	33.3
8JG97	12.9	15.8	71.4	32.3	45.3	22.4	13.7	45.3	41.0	44.9	16.7	38.4
9JG96	18.3	14.6	67.1	1.2	67.9	31.0	11.2	67.9	20.9	55.6	17.3	27.2
10JG96	12.5	15.7	71.8	18.0	67.1	15.0	8.7	67.1	24.3	44.3	21.4	34.4
15JG96	27.3	10.6	62.1	9.1	67.1	23.8	5.2	67.1	27.8	72.1	4.5	23.4
mean	19	16	65	18	60	22	10	60	31	54	13	33
σ	6	5	7	13	13	5	3	13	11	11	9	7
Little Lost River channel												
3JG97	36.0	10.5	53.4	29.4	44.0	26.6	13.8	44.0	42.2	77.4	7.9	14.7
4JG97	10.7	2.8	86.5	4.0	5.3	90.7	25.7	5.3	69.0	79.0	6.5	14.5
5JG96	27.6	2.2	70.2	11.5	26.2	62.3	2.6	26.2	71.2	92.6	1.2	6.2
5JG97	37.0	7.4	55.6	18.9	47.2	33.9	15.9	47.2	36.9	83.3	3.8	12.9
6JG97	40.9	4.9	54.2	18.7	45.9	35.4	25.7	45.9	28.4	89.4	0.5	10.1
mean	31	6	64	17	34	50	17	34	49	84	4	12
σ	12	4	14	9	18	27	10	18	19	7	3	4
Birch Creek channel												
1JG97	18.0	6.4	75.6	6.2	3.8	90.0	35.0	3.8	61.2	73.9	21.8	4.2
2JG97	14.6	5.8	79.6	54.7	3.9	41.4	20.7	3.9	75.4	71.4	19.4	9.2
3JG96	15.6	4.1	80.2	0.0	40.3	59.7	10.0	40.3	49.7	79.2	7.3	13.5
11JG96	14.9	9.2	75.8	6.9	13.0	80.1	12.5	13.0	74.5	61.7	20.0	18.3
mean	16	6	78	17	15	68	20	15	65	72	17	11
σ	1	2	2	26	17	22	11	17	12	7	7	6
Small drainages north of Big Lost Trough (Medicine Lodge Creek)												
1JR97	32.6	4.9	62.5	20.8	28.3	50.8	26.1	28.3	45.6	87.0	4.3	8.7
2JR97	65.9	6.3	27.8	29.5	19.1	51.4	31.4	19.0	49.5	91.2	6.6	2.2
4JR97	57.4	6.9	35.7	39.2	16.9	43.8	33.1	16.9	50.0	89.3	6.0	4.7
5JR97	32.4	9.3	58.3	38.5	22.5	39.0	22.5	22.5	55.0	77.6	6.3	16.1
mean	47	7	46	32	22	46	28	22	50	86	6	8
σ	17	2	17	8	5	6	5	5	4	6	1	6
Eolian (sand dunes)												
1JG96	22.8	29.6	47.6	9.2	52.1	38.7	2.8	52.1	45.2	43.5	17.6	38.9
2PL96	28.0	5.4	66.6	1.2	17.6	81.1	13.9	17.6	68.4	84.0	0.0	16.0
7JR96	31.5	16.0	52.6	5.4	43.8	50.8	8.7	43.8	47.5	66.5	5.0	28.4
12JG96	27.8	15.1	57.1	15.6	49.4	34.9	2.2	49.4	48.3	64.9	8.9	26.2
14JG96	30.0	9.8	60.2	8.2	30.9	61.0	1.1	30.9	68.0	75.3	7.9	16.9
mean	28	15	57	8	39	53	6	39	55	67	8	25
σ	3	9	7	6	14	19	6	14	12	15	7	9

graphically highest basalt flow group at the northern end of the Big Lost Trough (Circular Butte flows, Fig. 2C) is ca. 1 Ma, suggesting that the area has been volcanically quiet through much of the Pleistocene (Anderson and Lewis, 1989; Anderson, 1991; Anderson et al., 1996).

A thick sedimentary succession is present, most notably in the upper part of the stratigraphic section near the site of well 2-2A, in the north-central part of the basin (Fig. 2C; Anderson and Bowers, 1995; Geslin et al., 1997; 1999; Blair and Link, 2000). Although there are no data on interwell geometry, these sediments apparently onlap the northern basin margin (Fig. 2C), documenting the closed nature of the basin. Strata in the upper part of well 2-2A record the interaction of eolian, fluvial, playa, and lacustrine depositional systems (e.g., Geslin et al., 1997, 1999; Gianniny et al., 1997). These strata document a general shift from lacustrine-dominated sedimentation to fluvial- and/or eolian-dominated sedimentation, suggesting an overall drying of the climate (e.g., Bestland et al., this volume). In this volume Geslin et al. and Gianniny et al. argue that modern fluvial, playa, and eolian systems are excellent analogs for ancient depositional systems operating in the basin during relatively dry climatic conditions; lacustrine clays and fine sands deposited in Lake Terreton probably represent relatively wetter climatic conditions. Gianniny et al. (this volume) discuss the timing of multiple recent fluctuations of Lake Terreton. Bestland et al. (this volume) discuss older lacustrine sedimentation documented in the deeper core from well 2-2A (Fig. 2A) and emphasize weak paleosols developed on fluvial, playa, eolian, and lacustrine sediments in the upper part of the 2-2A core.

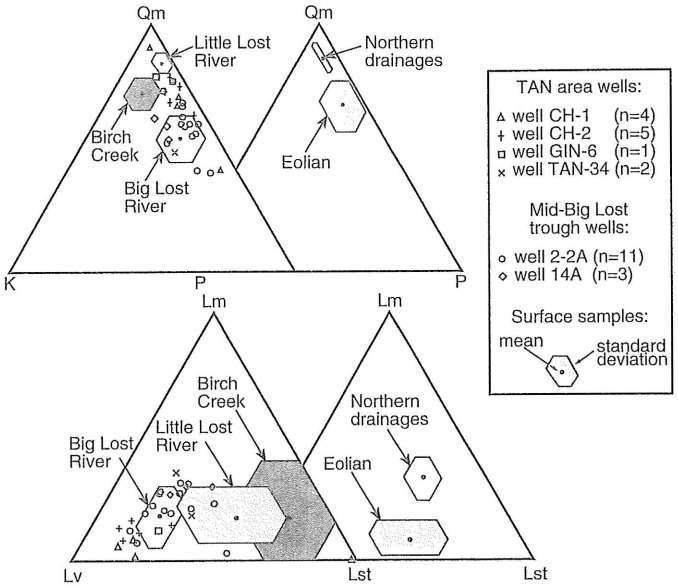

Figure 3. Standard ternary plots of detrital modes from petrographic analysis of sand samples. Qm—monocrystalline quartz, K—potassium feldspar, P—plagioclase feldspar, Lm—metamorphic lithic grains, Lv—volcanic lithic grains, Lst—total sedimentary lithic grains. Polygons represent mean and standard deviation for samples collected from modern drainages (Big Lost River, $n = 6$; Little Lost River, $n = 5$; Birch Creek, $n = 4$; northern drainages, $n = 4$; eolian deposits, $n = 5$). Symbols represent individual samples collected from wells (locations in Fig. 1) in central and northern parts of Big Lost Trough ($n = 29$).

COMPOSITIONAL ANALYSIS OF SEDIMENTARY UNITS

We examined both modern and shallow subsurface sands from the Big Lost Trough using petrographic analysis. Provenance interpretations of fluvial sands, based on modal recalculation of petrographic data, were supported by U/Pb geochronology of detrital zircons. Provenance results, particularly at the northern end of the basin, are used to interpret the evolution of the fluvial systems and document the role of volcanic eruptive centers in controlling the distribution of depositional systems.

The compositions of modern and shallow subsurface fine-grained sediments were evaluated using semiquantitative X-ray diffraction analysis, and are used to characterize depositional environments. Hughes et al. (this volume) present compositional analyses of the basalts and correlations of the basalt flow groups found in the Big Lost Trough.

Provenance of sands

Petrographic analyses. Sand samples were collected from modern fluvial and eolian deposits, and from core retrieved from wells in the middle and northern parts of the basin (Fig. 1). All modern fluvial systems that flow into the Big Lost Trough, including the Big Lost River, Little Lost River, and Birch Creek, were sampled, as were several small streams that flow out of the southern Beaverhead Mountains and terminate near the northeastern margin of the basin. Sand samples were examined petrographically; compositions were determined by the Gazzi-Dickinson point-count method (Ingersoll et al., 1984); raw point-count data were recalculated into detrital modes (Table 1). Samples from modern fluvial and eolian deposits, summarized in Table 2, were first compared to each other by plotting detrital mode data on ternary diagrams (Fig. 3). The source areas of the modern streams are generally well differentiated using fields defined by the statistical average and standard deviation for the samples (Fig. 3). Big Lost River sands are distinguished by abundant volcanic lithic material, probably reflecting both the abundance of Challis volcanic rocks in the source area and the abundant Snake River Plain basalts over which the stream flows in its lower reach. Modern eolian sands have an average composition that overlaps several of the fluvial fields (Fig. 3), indicating mixing and redeposition.

To evaluate the provenance of shallow subsurface sands, their recalculated modal compositions (Table 3) were compared to modern sands by plotting subsurface samples individually on the ternary diagrams (Fig. 3). The majority of the shallow subsurface sand samples have modal compositions that are similar

TABLE 3. RECALCULATED MODAL POINT-COUNT DATA FOR SUBSURFACE SEDIMENTS OF THE BIG LOST TROUGH

	Depth	QmFLt			LmLvLst			QpLvmLsm			QmKP		
Sample No.	(m)	Qm	F	Lt	Lm	Lv	Lst	Qp	Lvm	Lsm	Qm	K	P
Corehole 2-2A													
18JG96	19.8	26.7	17.4	55.9	21.0	58.0	21.0	17.8	58.0	24.2	60.5	9.7	29.8
19JG96	21.3	24.4	14.8	60.8	21.8	48.2	29.9	25.4	48.2	26.4	62.3	8.2	29.5
20JG96	36.6	26.7	17.9	55.3	31.9	44.1	23.9	16.0	44.1	39.9	59.9	4.1	36.0
21JG96	41.2	20.9	30.4	48.9	4.4	44.4	51.2	0.0	44.4	55.6	40.7	13.9	45.4
22JG96	42.4	30.9	20.9	48.2	22.8	60.8	16.4	4.2	60.8	34.9	59.6	7.4	33.0
23JG96	44.8	15.1	22.1	62.8	13.1	73.5	13.5	2.9	73.5	23.6	40.5	9.8	49.7
24JG96	50.6	23.4	11.5	65.1	23.9	39.1	37.0	25.0	39.1	35.9	67.1	5.9	27.0
25JG96	55.2	15.7	13.0	71.3	27.9	49.1	22.9	15.6	49.1	35.3	54.7	9.5	35.8
26JG96	58.6	27.2	12.7	60.2	28.1	56.1	15.8	10.1	56.1	33.8	68.2	5.3	26.5
27JG96	72.4	30.2	9.3	60.5	20.4	64.6	15.0	10.2	64.6	25.2	76.5	4.5	19.0
28JG96	75.3	25.5	17.4	57.1	29.3	55.0	15.7	12.4	55.0	32.5	59.4	8.6	32.1
29JG96	113.6	19.4	18.0	62.7	19.9	56.0	24.1	17.3	56.0	26.7	51.9	19.1	29.0
30JG96	118.8	21.6	17.2	61.2	32.2	46.4	21.4	11.2	46.4	42.4	55.6	7.0	37.4
31JG96	191.9	41.2	15.2	43.8	7.7	74.0	18.4	16.3	74.0	9.7	73.0	10.3	16.7
Corehole TAN CH1													
34JG96	122.5	44.7	4.7	50.6	0.0	1.6	98.4	25.4	1.6	73.0	90.5	5.4	4.1
36JG97	125.4	17.4	25.2	57.4	1.9	77.4	20.6	7.1	77.4	15.5	40.9	6.1	53.0
37JG96	136.0	33.4	16.2	50.3	6.0	81.2	12.8	7.4	81.2	11.4	67.3	6.8	25.9
38JG96	136.2	31.1	12.7	56.1	8.8	74.5	16.8	11.7	74.5	13.9	71.0	4.7	24.3
Corehole TAN CH2													
39JG96	73.0	35.4	12.9	51.7	12.5	70.1	17.4	15.8	70.1	14.1	73.3	7.2	18.0
41JG96	143.1	34.2	9.0	56.8	14.2	76.5	9.3	9.3	76.5	14.2	79.1	4.3	16.6
42JG96	224.2	35.8	16.2	47.5	9.3	77.6	13.1	9.8	77.6	12.6	68.3	9.4	22.3
43JG96	224.8	29.1	17.4	53.5	14.6	58.7	26.7	14.1	58.7	27.2	62.6	4.5	33.0
44JG96	225.5	32.2	10.6	57.1	17.2	70.6	12.3	10.8	70.6	18.6	75.2	3.3	21.6
Corehole GIN 6													
33JG96	35.7	32.8	8.7	58.5	13.2	64.0	22.8	12.7	64.0	23.2	79.0	9.3	11.7
Borehole 14A													
9JG97	4.2	26.0	18.0	56.0	29.9	35.6	34.4	7.3	35.6	57.1	59.0	15.1	25.9
10JG97	8.8	28.8	18.0	53.2	29.9	45.0	25.1	6.4	45.0	48.6	61.5	18.1	20.4
11JG97	15.0	17.4	15.3	67.2	27.2	51.9	20.9	13.9	51.9	34.2	53.2	16.9	29.9
Borehole TAN 34 (cuttings)													
15-20	4.6–6.1	36.7	11.2	52.1	19.0	48.6	32.4	22.4	48.6	29.0	76.7	4.1	19.2
25–30	7.6–9.1	19.5	21.2	59.3	35.7	46.2	18.1	11.6	46.2	42.2	47.9	18.4	33.7

to those of modern sands from the Big Lost River; a few samples are compositionally similar to modern eolian sands. These data suggest that the Big Lost River has been the dominant source of fluvial sands in the basin since at least the Pliocene.

The abundance of Big Lost River and eolian sands in the middle of the basin documents the effective damming of sediment by the volcanic rift zone that defines the northern basin margin (Fig. 2). These results also suggest that deposition by the Big Lost River in the middle of the basin is commonly associated with dry climatic conditions favorable for the development of an eolian system, similar to present-day conditions.

Detrital-zircon U/Pb geochronology. Sand samples for detrital-zircon analysis were collected from modern fluvial deposits, from shallow core retrieved from well 2-2A in the southern Big Lost Trough, and wells TAN-34, CH-1, and CH-2 at TAN. Detrital zircons were separated from the samples and ~50 zircon grains from each sample were analyzed on SHRIMP I at the Australian National University (Table 4). The ages of individual zircon grains were derived from the weighted mean of $^{206}Pb/^{238}U$-, $^{207}Pb/^{235}U$- and $^{207}Pb/^{206}Pb$-corrected ages, and relative-probability spectra were created by assigning Gaussian distributions to individual ages and errors and then summing them together in 1 m.y. bins.

It is easy to differentiate the detrital-zircon age spectra for the fluvial systems that provide sediment to the Big Lost Trough (Fig. 4). There are distinctive populations of detrital zircons in the sands from Birch Creek and the small northern drainages (Fig. 4, C–F): (1) several groups of <20 Ma zircons derived from Snake River Plain volcanic rocks; (2) 700-100 Ma zircons derived from the Cretaceous Idaho batholith (Worl et al., 1995); (3) ca. 500 Ma zircons derived from the Ordovician Beaverhead pluton exposed in the Beaverhead Mountains (Evans and Zartman, 1988); and (4) a large group of 1000–2000 Ma zircons and a small group of 2500–3000 Ma zircons likely recycled from Mesoproterozoic to Ordovician strata exposed in the Beaverhead Mountains and Lemhi Range (Oaks et al., 1977; Skipp and Link, 1992; Winston and Link, 1993). Detrital zircons from the Little Lost River (Fig. 4B) also contain a large Paleoproterozoic zircon population (1500–2000 Ma), but this sample can be differentiated from other samples by the presence of a large ca. 50 Ma zircon population, derived from the Eocene Challis Volcanic Group, and by the lack of 500 Ma and <20 Ma zircon populations. The detrital-zircon population in the Big Lost

TABLE 4. DETRITAL-ZIRCON AGE DATA FOR SURFACE AND SUBSURFACE SANDS OF THE BIG LOST TROUGH AND ADJACENT DRAINAGES

Sample 9JG96 Big Lost River			Sample 5JG96 Little Lost River			Sample 11JG96 Birch Creek			Sample 1JR96 Beaver Creek			Sample 2JR96 Crooked Creek			Sample 2JR97 Medicine Lodge Creek			Sample 50JG96 Well 2-2A 55.4 m		
Grain spot	Age $^{206}Pb/^{238}U$	±	Grain spot	Age $^{206}Pb/^{238}U$	±	Grain spot	Age $^{206}Pb/^{238}U$	±	Grain spot	Age $^{206}Pb/^{238}U$	±	Grain spot	Age $^{206}Pb/^{238}U$	±	Grain spot	Age $^{206}Pb/^{238}U$	±	Grain spot	Age $^{206}Pb/^{238}U$	±
1.1	2628	57	1.1	1841	43	1.1	503	22	1.1	1851	40	1.1	1646	34	1.1	1669	47	1.1	46.8	0.7
2.1	46.9	0.9	2.1	1614	70	2.1	493	32	2.1	50.2	1.2	3.1	2.1	0.1	2.1	2669	111	2.1	2644	29
3.1	45.4	1.5	3.1	1774.4	36.1	3.1	1055	27	3.1	51.0	1.2	4.1	10.7	1.0	3.1	1730	44	3.1	56.1	1.3
4.1	707	21	4.1	49.9	1.4	4.1	1859	44	4.1	52.1	1.2	5.1	7.7	0.7	4.1	1650	51	4.1	47.0	1.3
5.1	611	40	5.1	1728	38	5.1	33.0	0.9	5.1	52.9	1.3	6.1	1817	50	5.1	1103	59	5.1	46.8	1.0
6.1	46.6	1.9	6.1	49	2	6.1	1289	22	6.1	47.1	2.3	7.1	1399	32	6.1	1429	43	6.1	971	22
7.1	46.5	1.5	7.1	1275.7	47.4	7.1	482	29	7.1	51.2	1.2	8.1	1775	34	7.1	1488	58	7.1	1266	115
8.1	1441	59	8.1	2254	65	8.1	1.1	0.3	8.1	50.9	2.1	9.1	1048	44	8.1	1345	49	8.1	1760	33
9.1	46.4	1.4	9.1	1666	35	9.1	1810	29	9.1	75.3	3.1	10.1	48.9	2.1	9.1	1627	32	9.1	48.6	1.6
10.1	47.3	1.1	10.1	1728	35	10.1	496	13	10.1	91.9	2.0	11.1	1028	18	10.1	1835	46	10.1	1760	50
11.1	49.6	1.5	11.1	1787	41	11.1	44.3	1.2	11.1	50.3	1.4	12.1	1548	64	11.1	1352	32	11.1	48.6	1.0
12.1	48.6	2.0	12.1	1687.4	27.0	12.1	2574	148	12.1	50.9	1.3	13.1	6.5	0.4	12.1	1656	27	12.1	51.5	1.3
13.1	52.9	2.4	13.1	2728	72	13.1	491	29	13.1	64.8	3.9	14.1	32.4	1.5	13.1	6.4	0.6	13.1	1767	23
14.1	50.9	4.7	14.1	51	2	14.1	485	13	14.1	49.2	1.1	15.1	11.9	0.7	14.1	536	26	14.1	1118	32
15.1	45.7	2.1	15.1	668	13	15.1	1665	36	15.1	2.7	0.3	16.1	26.9	7.6	15.1	1703	38	15.1	88.0	2.8
16.1	49.9	2.0	16.1	50.6	1.8	16.1	46.8	1.6	16.1	1791	41	17.1	1598	44	16.1	1693	59	16.1	83.3	2.2
17.1	49.1	1.5	17.1	1667	44	17.1	33.1	2.2	17.1	227	10	18.1	8.4	0.5	17.1	91.5	4.2	17.1	1922	50
18.1	48.3	2.3	18.1	1830	38	18.1	1408	25	18.1	50.4	1.7	19.1	1406	49	18.1	93.9	3.6	18.1	49.5	1.6
19.1	47.4	1.1	19.1	1744	50	19.1	1808	38	19.1	16.6	0.5	20.1	1610	29	19.1	1530	43	19.1	49.2	1.2
20.1	52.4	2.2	20.1	1716.2	46.1	20.1	485	24	20.1	50.4	1.4	21.1	1738	37	20.1	18.4	9.5	20.1	11.3	1.3
21.1	689	39	21.1	1713.0	41.0	21.1	38.2	1.5	21.1	1083	22	22.1	1829	55	21.1	6.3	0.5	21.1	1690	28
22.1	47.9	1.3	22.1	1633	38	22.1	495	13	22.1	1406	52	23.1	1571	95	22.1	1588	105	22.1	50.1	1.7
23.1	51.2	1.9	23.1	1707	44	23.1	1698	39	23.1	47.4	2.4	24.1	2079	38	23.1	92	2	23.1	46.0	1.3
24.1	42.8	1.0	24.1	1812	36	24.1	1809	46	24.1	49.9	1.5	25.1	1594	35	24.1	1072	25	24.1	10.4	0.4
25.1	49.6	1.7	25.1	48	1	25.1	1570	45	25.1	1420	59	26.1	484	22	25.1	1750	72	25.1	2047	44
26.1	49.0	1.2	26.1	1713.8	69.8	26.1	488	13	26.1	49.5	1.2	27.1	484	18	26.1	1750	37	26.1	50.5	1.1
27.1	46.0	0.9	27.1	1402	74	27.1	462	13	27.1	7.6	1.4	28.1	1594	36	27.1	63.5	4.1	27.1	1768	39
28.1	674	16	28.1	48	3	28.1	1857	33	28.1	13.5	0.9	29.1	2682	60	28.1	1765	46	28.1	46.8	1.3
29.1	1449	24	29.1	2546	49	29.1	1454	35	29.1	509	10	30.1	10.3	0.3	29.1	419	12	29.1	93.6	2.1
30.1	49.6	2.3	30.1	1815	51	30.1	1066	25	30.1	1729	40	31.1	1678	36	30.1	1205	44	30.1	2262	32
31.1	570	15	31.1	1661	40	31.1	1418	29	31.1	2785	55	32.1	1777	40	31.1	1782	49	31.1	1058	13
32.1	54.1	1.0	32.1	2615	62	32.1	266	7	32.1	48.8	2.7	33.1	2633	60	32.1	9.8	1.8	32.1	50.2	1.2
33.1	45.4	1.0	33.1	48	1	33.1	1661	38	33.1	48.0	1.7	34.1	47.9	1.1	33.1	101	2	33.1	46.5	1.4
34.1	48.0	1.2	34.1	501	13	34.1	498	28	34.1	1419	38	35.1	49.7	1.9	34.1	1770	27	34.1	1658	23
35.1	48.1	1.5	35.1	2813	76	35.1	452	34	35.1	8.2	5.0	36.1	67.7	1.9	35.1	1774	82	35.1	47.5	1.1
36.1	1248	32	36.1	1840	56	36.1	1081	25	36.1	11.0	7.3	37.1	1686	32	36.1	1715	52	36.1	48.9	1.0
37.1	46.2	1.2	37.1	1355	51	37.1	1255	39	37.1	1275	43	38.1	1160	31	37.1	1789	40	37.1	2180	64
38.1	43.8	2.2	38.1	49.5	1.7	38.1	463	16	38.1	208	8	39.1	1639	37	38.1	1730	39	38.1	49.4	1.1
39.1	1245	32	39.1	1721	39	39.1	489	12	39.1	1288	46	40.1	474	18	39.1	2115	54	39.1	49.4	1.5
40.1	53.8	2.9	40.1	1732	31	40.1	17.2	1.6	40.1	52.3	4.5	41.1	6.7	0.8	40.1	1453	27	40.1	47.2	0.8
41.1	44.0	1.1	41.1	2025.0	45.7	41.1	46.2	1.9	41.1	97.3	3.6	42.1	3.5	0.8	41.1	1144	16	41.1	45.5	1.1
42.1	49.5	2.0	42.1	1817	56	42.1	8.9	1.0	42.1	101	7	43.1	7.7	1.2	42.1	1007	21	42.1	438	10
15.2	44.1	1.5	43.1	2694	45	43.1	1451	28	43.1	96.3	4.5	44.1	1743	38	43.1	1710	42	43.1	45.3	0.9
19.2	46.3	2.0	44.1	1839	37	44.1	637	23	44.1	153	3	45.1	83	29	44.1	1010	51	44.1	48.9	1.5
43.1	47.8	1.1	45.1	1959	77	45.1	8.4	0.8	45.1	47.6	1.4	46.1	929	30	45.1	1729	44	45.1	48.4	1.0
44.1	44.6	1.7	46.1	1	0	46.1	6.6	1.4	46.1	97.6	2.7	47.1	1054	21	46.1	98.3	1.3	46.1	11.0	0.5
28.2	706	21	47.1	1761.8	28.6	47.1	106	6	47.1	77.3	5.7	48.1	13.9	0.5	47.1	1016	26	47.1	613	27
20.2	49.9	1.8	48.1	2677.8	56.2	48.1	1431	54	48.1	48.5	1.2	49.1	1549	50	48.1	1694	34	48.1	1379	55
12.2	50.8	2.1	49.1	1753	29	49.1	1787	37	49.1	1372	26	50.1	1708	35	49.1	395	7	49.1	47.9	1.2
13.2	50.2	1.6	50.1	1521	46	50.1	962	27	50.1	517	18				50.1	1069	65	50.1	46.8	1.0

TABLE 4. DETRITAL-ZIRCON AGE DATA (continued)

Sample 51JG96 Well 2-2A 113.7 m			Sample 52JG96 Well 2-2A 191.9 m			Sample 3JG96 Well TAN 34 ~5.8 m			Sample 47JR96 Well CH 2 136.8 m			Sample 48JR96 Well CH 2 224.4 m			Sample 49JR96 Well CH 1 136.0 m		
Grain spot	Age $^{206}Pb/^{238}U$	±	Grain spot	Age $^{206}Pb/^{238}U$	±	Grain spot	Age $^{206}Pb/^{238}U$	±	Grain spot	Age $^{206}Pb/^{238}U$	±	Grain spot	Age $^{206}Pb/^{238}U$	±	Grain spot	Age $^{206}Pb/^{238}U$	±
1.1	51	1	1.1	49.7	1.1	1.1	741	24	1.1	525	20	1.1	1718	27	1.1	48.5	1.3
2.1	49	1	2.1	51.8	1.1	1.2	734	17	2.1	1849	30	2.1	52.9	2.5	2.1	1.9	0.1
3.1	1853	29	3.1	46.6	1.7	2.1	48.9	1.5	3.1	50.6	1.0	3.1	2674	91	3.1	9.3	0.5
4.1	49	1	4.1	1544	39	3.1	65.0	1.6	4.1	52.2	0.9	4.1	1217	39	4.1	1795	39
5.1	696	14	5.1	1228	74	4.1	1559	68	5.1	1765	34	5.1	1.7	0.2	5.1	1441	21
6.1	49	2	6.1	680	12	5.1	47.6	2.8	6.1	1622	114	6.1	1055	25	6.1	1821	39
7.1	47	1	7.1	49.0	1.1	6.1	47.9	1.4	7.1	8.9	0.6	7.1	34.1	1.9	7.1	1865	32
8.1	48	1	8.1	50.8	1.3	7.1	446	15	8.1	1049	23	8.1	2524	93	8.1	1888	58
9.1	1300	19	9.1	1861	91	8.1	837	23	9.1	1889	28	9.1	49.0	2.0	9.1	57.1	2.1
10.1	1408	25	10.1	545	19	9.1	47.5	1.5	10.1	1109	14	10.1	50.9	1.2	10.1	2030	30
11.1	2105	24	11.1	1751	28	10.1	85.6	3.9	11.1	1249	46	11.1	6.3	0.4	11.1	1119	31
12.1	49	1	12.1	48.9	1.5	11.1	49.1	2.8	12.1	50.4	0.8	12.1	1181	30	12.1	1644	59
13.1	696	14	13.1	47.9	2.6	12.1	1135	101	13.1	1285	14	13.1	1342	35	13.1	1630	26
14.1	1505	27	14.1	47.2	2.3	13.1	80.3	2.8	14.1	1227	18	14.1	1542	37	14.1	1679	32
15.1	48	1	15.1	48.2	2.7	14.1	1747	48	15.1	1279	15	15.1	32.1	2.0	15.1	1638	35
16.1	655	18	16.1	47.8	1.5	15.1	47.0	1.9	16.1	49.3	1.1	16.1	1590	32	16.1	48.2	1.5
17.1	49	1	17.1	573	21	16.1	45.4	2.4	17.1	525	24	17.1	452	7	17.1	1597	37
18.1	91	2	18.1	1836	51	17.1	44.8	1.6	18.1	1204	15	18.1	2700	84	18.1	1651	33
19.1	2445	54	19.1	50.2	2.2	18.1	48.1	1.5	19.1	506	8	19.1	1633	76	19.1	1665	39
20.1	691	9	20.1	49.3	1.2	19.1	46.9	1.7	20.1	47.7	1.3	20.1	7.1	0.3	20.1	2624	59
21.1	49	1	21.1	1185	19	20.1	27.4	0.9	21.1	49.8	1.3	21.1	49.5	1.2	21.1	51.1	1.8
22.1	47	1	22.1	2407	68	21.1	338	13	22.1	149	8	22.1	1693	24	22.1	1740	21
23.1	48	1	23.1	1614	47	22.1	48.0	1.3	23.1	1523	28	23.1	1.9	0.4	23.1	1.6	0.7
24.1	2062	28	24.1	49.1	3.7	23.1	620	14	24.1	509	11	24.1	5.9	0.4	24.1	1915	28
25.1	46	2	25.1	50.5	2.1	24.1	680	18	25.1	963	14	25.1	1949	24	25.1	648	7
26.1	107	5	26.1	48.5	2.9	25.1	757	32	26.1	50.0	0.8	26.1	1379	15	26.1	1418	16
27.1	1392	16	27.1	648	21	26.1	1717	36	27.1	1773	30	27.1	1666	31	27.1	48.7	0.7
28.1	207	4	28.1	729	14	27.1	82.1	3.5	28.1	1578	25	28.1	2664	61	28.1	1035	27
29.1	1479	23	29.1	46.3	4.5	28.1	45.6	1.8	29.1	1890	31	29.1	1727	18	29.1	2536	35
30.1	1492	28	30.1	45.6	3.0	29.1	47.8	1.4	30.1	1750	29	30.1	1666	30	30.1	1351	20
31.1	1707	23	31.1	1125	32	30.1	46.5	1.2	31.1	1538	41	31.1	1466	25	31.1	1925	30
32.1	50.5	0.8	32.1	48.9	1.9	31.1	48.1	1.4	32.1	1508	27	32.1	47.9	1.0	32.1	48.2	1.0
33.1	48.8	1.2	33.1	1753	48	32.1	653	15	33.1	496	11	33.1	77.2	1.4	33.1	49.9	1.2
34.1	710	42	34.1	44.1	2.6	33.1	1006	42	34.1	1159	31	34.1	1865	33	34.1	47.8	0.7
35.1	1505	23	35.1	51.2	2.7	34.1	50.9	1.8	35.1	1838	30	35.1	676	9	35.1	1.9	0.1
36.1	1804	27	36.1	91.2	7.2	35.1	45.5	1.5	36.1	2344	57	36.1	1666	32	36.1	50.4	0.9
37.1	48.5	1.6	37.1	41.8	1.9	36.1	42.5	1.6	37.1	896	32	37.1	48.6	0.8	37.1	48.6	2.3
38.1	696	11	38.1	679	22	37.1	1817	156	38.1	10.4	0.7	38.1	1981	23	38.1	1785	51
39.1	49.6	0.7	39.1	45.3	1.1	38.1	47.1	1.2	39.1	534	12	39.1	1531	15	39.1	1548	46
40.1	1030	18	40.1	595	14	39.1	47.1	1.5	40.1	1617	27	40.1	1405	16	40.1	1544	38
41.1	48.4	1.0	41.1	46.5	1.0	40.1	372	13	41.1	9.8	1.1	41.1	36.0	0.5	41.1	1756	52
42.1	1764	26	42.1	1300	20	41.1	45.4	1.4	42.1	858	35	42.1	1526	27	42.1	1699	24
43.1	46.1	1.0	43.1	43.3	1.5	42.1	48.1	2.9	43.1	475	12	43.1	2827	58	43.1	1210	30
44.1	48.8	1.5	44.1	1511	51	43.1	1855	44	44.1	2553	78	44.1	2322	26	44.1	1721	100
45.1	2890	54	45.1	89.9	1.7	44.1	57.9	1.5	45.1	3359	229	45.1	1780	25	45.1	983	13
46.1	46.9	0.8	46.1	48.4	2.3	45.1	46.9	2.3	46.1	1019	16	46.1	43.2	2.5	46.1	1840	22
47.1	1631	37	47.1	1296	37	46.1	138	10	47.1	48.6	0.9	47.1	1260	21	47.1	1398	32
48.1	2231	40	48.1	645	32	47.1	56.5	3.1	48.1	50.8	2.3	48.1	1327	22	48.1	2.3	0.4
49.1	49.5	0.9	49.1	49.3	2.4	48.1	46.5	1.1	49.1	1839	27	49.1	1473	26	49.1	49.6	0.8
50.1	49.1	1.2	50.1	1348	27	49.1	49.7	3.7	50.1	1223	30	50.1	757	10	50.1	1860	35
						50.1	112	7									

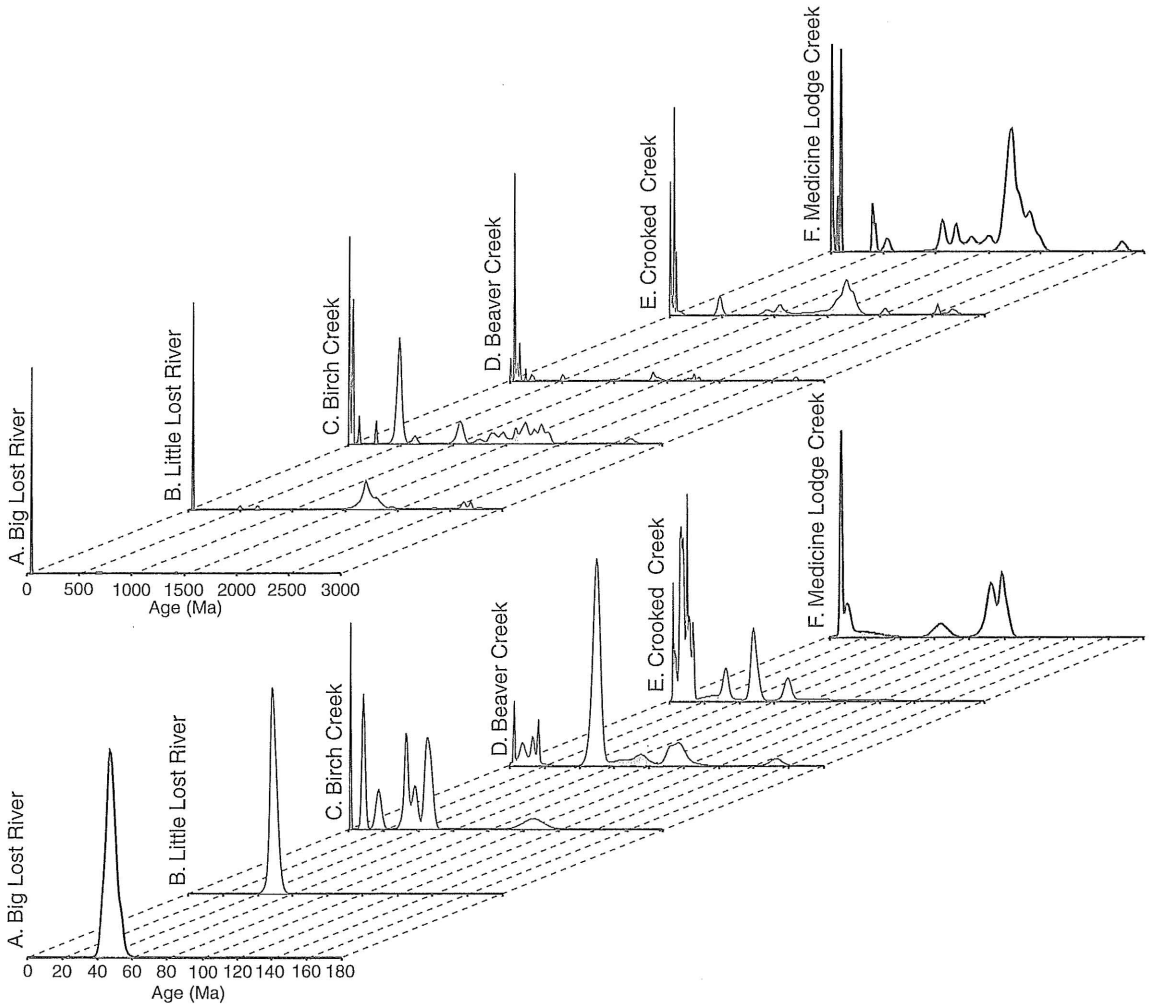

Figure 4. Relative probability plots for detrital-zircon ages determined for modern fluvial sands. Big Lost River, Little Lost River, and Birch Creek (A–C) are primary fluvial systems flowing into Big Lost Trough; smaller streams (D–F) are north of basin. Upper graphs contain results of all analyses (0–3000 Ma zircons); lower graphs are for young (<180 Ma) zircon populations.

River sample (Fig. 4A) is characterized by an abundance of ca. 50 Ma zircon grains and by a relative lack of older zircons.

Subsurface sands from well 2-2A in the central Big Lost Trough have detrital-zircon age spectra (Fig. 5) that are characterized by an abundance of ca. 50 Ma zircons and very few Paleozoic and older zircon grains. Small populations of 70–100 Ma zircons probably indicate derivation from the Cretaceous Idaho batholith. On the basis of visual comparison, detrital-zircon age spectra for these samples are most similar to the age spectra for the modern Big Lost River (Fig. 4A). These data suggest that the Big Lost River drainage was the dominant source, and are in agreement with modal compositional data (Fig. 3).

Subsurface samples from core collected in wells at TAN, near the northern margin of the basin, have detrital-zircon age spectra (Fig. 6) that suggest changing source areas through time. The detrital-zircon age spectrum of a near-surface sand sample (depth of 6.1–7.6 m in TAN-34; Fig. 6A) is most similar to the signature of the Big Lost River (Fig. 4A). However, deeper samples (Fig. 6, B–D) have detrital-zircon signatures similar to Birch Creek (Fig. 4C) or Crooked Creek (Fig. 4E).

Mineralogy of fine-grained sediments

The compositions of fine-grained sediments from surficial lacustrine and playa deposits were evaluated and compared to fine-grained deposits from the shallow subsurface (Figs. 7 and 8). X-ray diffraction analysis was used to determine the semiquantitative mineralogy of the <4 μm fraction of the samples, typically clay and evaporite minerals. Semiquantitative mineral abundance was based on the relative intensity of the diffraction peak for the clay or evaporite mineral. Material comprising the remainder of the samples, including quartz silt to very fine sand, organic matter, and detrital or authigenic carbonate, was not

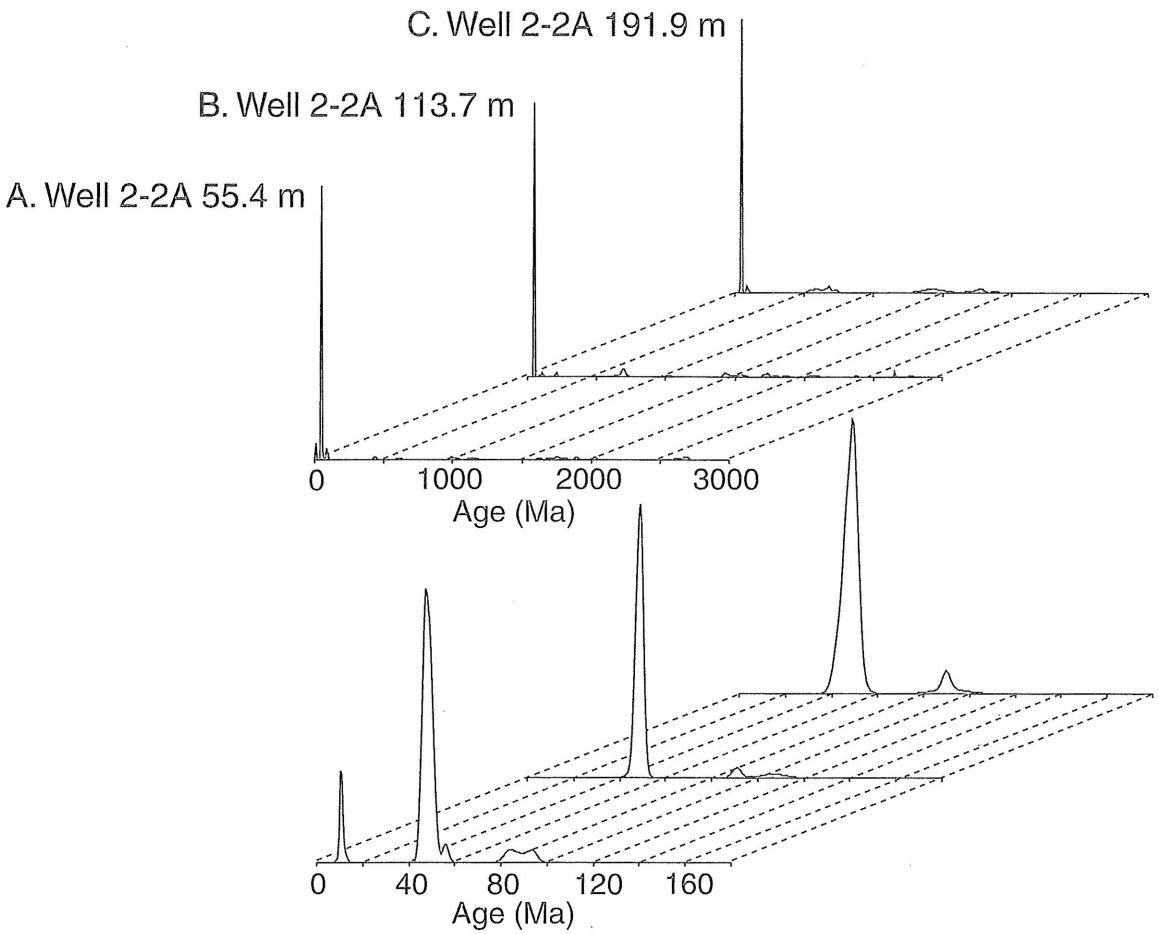

Figure 5. Relative probability plots for detrital-zircon ages determined for subsurface sands from well 2-2A, in middle of Big Lost Trough (Fig. 1). Upper graphs contain results of all analyses (0–3000 Ma zircons); lower graphs are for young (<180 Ma) zircon populations.

analyzed. Analysis of the samples included glycolization, to determine the presence of expanding clays (e.g., smectite), and 550°C heat treatment to differentiate chlorite and kaolinite.

X-ray diffraction data for shallow subsurface samples from well 2-2A (Fig. 8A) are generally similar to the surficial lacustrine and playa deposits (Fig. 7) in that they contain primarily smectite, kaolinite, and chlorite. This mineral assemblage probably reflects weathering of abundant volcanic and sedimentary rocks in fluvial source areas. However, several samples from the TAN wells (Fig. 8B) are distinctly different in that they contain gypsum. These data suggest that ancient evaporative playas or evaporative marginal lacustrine environments existed along the margin of the basin and that climatic conditions during deposition were probably drier than modern conditions.

DISCUSSION

The geometry and stratigraphic architecture of the Big Lost Trough was strongly influenced by the volcanic rift zones that define most of the basin margins. The locations of these volcanic rift zones, as well as local and regional subsidence patterns, reflect the interaction between basaltic volcanism and rhyolite caldera formation related to the Yellowstone hotspot and development of Basin and Range structures. Offlapping basalt flow groups and onlapping clastic sedimentary units along the northern margin of the basin (e.g., Fig. 2) represent growth of the volcanic rift zones and simultaneous clastic sedimentation in the basin. A general volcanic quiescence over the past ~1 m.y. has allowed fluvial, playa, eolian, and lacustrine systems to infill the basin to its modern configuration (Fig. 2C).

Sediments deposited in the middle of the basin over the past ~1 m.y. contain fluvial, eolian, and minor playa deposits interbedded with lacustrine sediment; this could represent alternating relatively wetter and relatively drier climatic conditions. This argument is based on documented fluctuations of Lake Terreton over the past 2 m.y. (e.g., Scott, 1982; Gianniny et al., this volume) and the presence of fluvial sands from the Big Lost River in the middle of the basin (Figs. 3–6).

Provenance studies in the Big Lost Trough that involve a comparison of modern fluvial and eolian sands with sands from

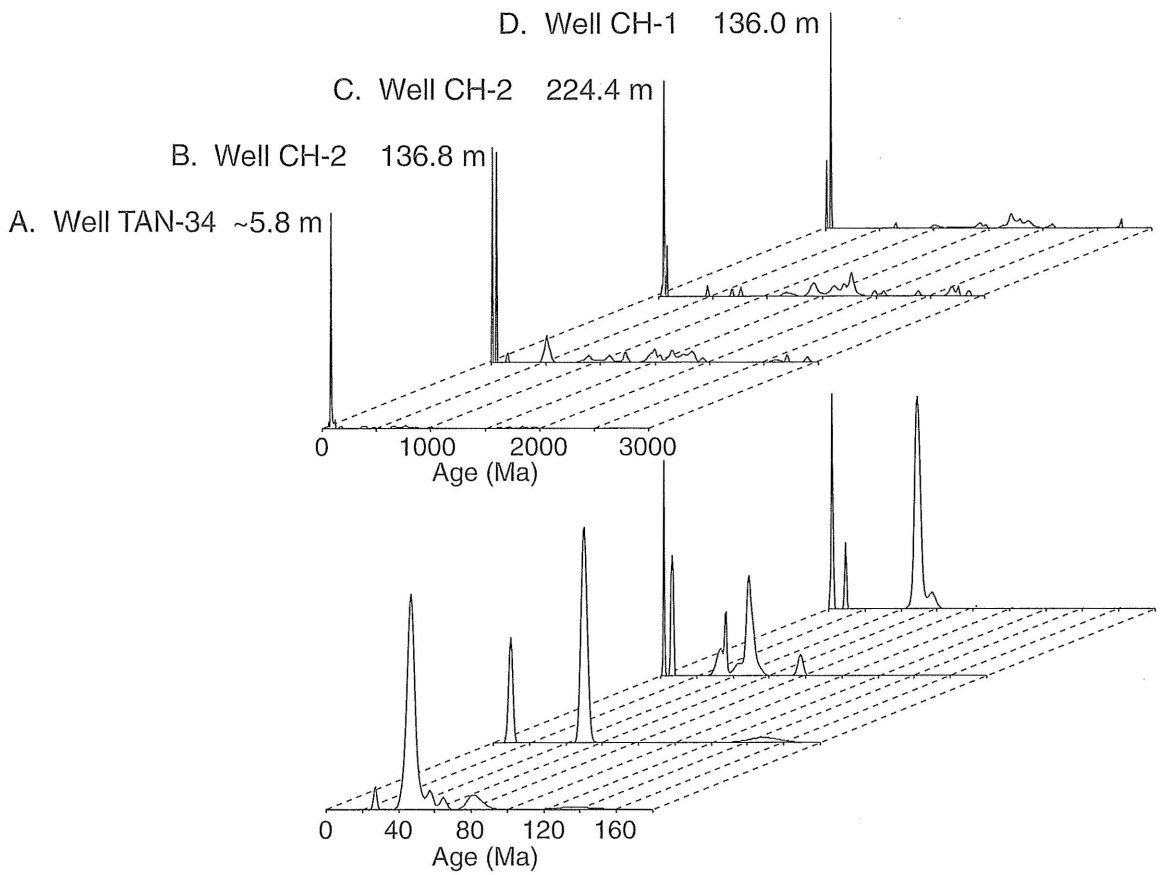

Figure 6. Relative probability plots for detrital-zircon ages determined for subsurface sands from wells at Test Area North, along northeastern margin of Big Lost Trough (Fig. 1). Upper graphs contain results of all analyses (0–3000 Ma zircons); lower graphs are for young (<180 Ma) zircon populations.

the subsurface using both petrography and U/Pb geochronology of detrital zircons provide very robust correlations (Figs. 4–6; Geslin et al., 1999). However, relating the detrital-zircon age spectra from modern Big Lost River sand and correlative subsurface sands to those of bedrock exposures in the source area is somewhat difficult. It is surprising that the Proterozoic to Archean detrital-zircon signature in these samples is faint despite the fact that the upper reaches of the Big Lost River drain the Pioneer Mountains core complex (Fig. 1), where abundant Paleoproterozoic metamorphic rocks crop out (Worl et al., 1995). Possible explanations for this observation include: (1) the great abundance of Eocene Challis volcanics cropping out in the middle reaches of the river have diluted the detrital zircon population; or (2) smaller streams that drain the Pioneer Mountains core complex were captured by the Big Lost River relatively recently, and Proterozoic to Archean zircons have yet to be transported to the lower reaches of the river. These data suggest that provenance determination, even in a well-documented setting like the Big Lost Trough, is a complex task, and that the zircon signature of the Big Lost River requires further study (e.g., Link et al., 1999, 2000).

Subsurface sands in the middle of the Big Lost Trough have provenance signatures indicating deposition by the Big Lost River, suggesting that the proportion of Big Lost River fluvial sand in the subsurface increases from northeast to southwest, toward the point where the river enters the basin (Fig. 1). The southwestward increase in abundance of subsurface sand-rich sediments, the increase in the thickness of strata from the northern basin margin to basin center (Fig. 2C), and the regional northeast to southwest groundwater gradient all suggest that water flowing in the upper part of the Snake River Plain aquifer will encounter progressively more abundant and more conductive sediments as it migrates down gradient from the TAN facilities toward the middle of the basin. This information should be incorporated into regional hydrologic models of the unsaturated zone and upper part of the Snake River Plain aquifer.

CONCLUSIONS

The Big Lost Trough is an arid underfilled basin, the geometry and volcanic-sedimentary stratigraphic architecture of which reflect the development of surrounding volcanic rift zones. The pattern of volcanic rift zones that define the basin margins, subsidence of the area, and the fluvial systems that provide clastic sediments to the basin reflect the interaction of the migrating Yellowstone hotspot and developing Basin and

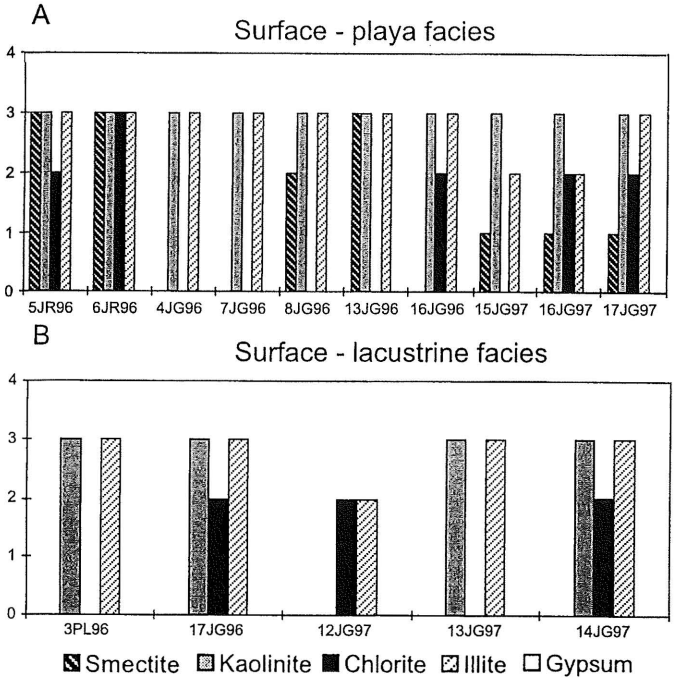

Figure 7. Semiquantitative mineralogy of fine-grained fraction of surficial playa and lacustrine sediments determined using X-ray diffraction analyses. Ranking from 0 to 4 indicates relative abundance of mineral: 4 = mineral dominant in sample, 3 = mineral present in sample, 2 = trace amounts of mineral in sample, 1 = mineral possibly present in sample.

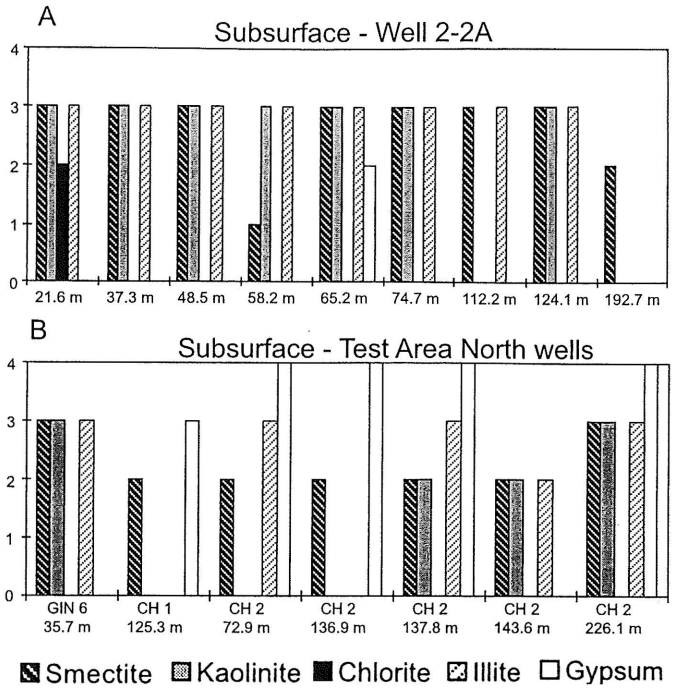

Figure 8. Semiquantitative mineralogy of fine-grained fraction of subsurface deposits determined using X-ray diffraction analyses for samples from well 2-2A, in middle of basin, and from wells at Test Area North, along northeastern margin of basin. Ranking from 0 to 4 indicates relative abundance of mineral: 4 = mineral dominant in sample, 3 = mineral present in sample, 2 = trace amounts of mineral in sample, 1 = mineral possibly present in sample.

Range structures. Correlations of basalt flow groups and sedimentary successions from the basin margin at TAN to the middle of the basin at well 2-2A show the complex stratigraphic relationships created by basalt flows that downlap into the basin and sediments that onlap onto the adjacent volcanic high. Architecture within the clastic sedimentary fill of the basin reflects deposition during climatically influenced progradation and retrogradation of a fluvial-playa-eolian depositional system and transgressions and regressions of Lake Terreton.

Because the Big Lost Trough is still an active basin with easily identifiable sediment source areas, it provides an excellent natural laboratory for conducting provenance studies. By conducting both petrographic and U/Pb detrital-zircon geochronology analyses on subsurface sands, as well as modern fluvial and eolian deposits, the provenance of the subsurface sands has been very tightly defined. These analyses suggest that the Big Lost River has been the dominant source of sediment to the basin for at least the past 1 m.y., and that the river system frequently prograded across the basin during lowstands of Lake Terreton. Fluvial progradation during lowstands of Lake Terreton was associated with eolian reworking of fluvial deposits.

Semiquantitative compositional analyses, using X-ray diffraction, indicate that subsurface playa or marginal lacustrine deposits along the basin margin (at TAN) contain abundant gypsum, suggesting that ancient dry climate cycles were drier than the modern dry climate.

ACKNOWLEDGMENTS

This study was funded by grant DE-FG07-96ID13420 from the Department of Energy to the Idaho Water Resources Research Institute and Idaho Universities Consortium. Mary Kauffman and Savona Anderson assisted with sample collection and analysis. Fruitful discussions of sedimentary systems on the Snake River Plain were held with Gary Gianniny and Glenn Thackray. Access to core was provided by Linda Davis (U.S. Geological Survey). The manuscript was improved by comments from reviewers Larry Middleton, Dick Smith, and Brad Ritts.

REFERENCES CITED

Anders, M.H., Geissman, J.W., Piety, L., and Sullivan, T., 1989, Parabolic distribution of circum-eastern Snake River Plain seismicity and latest Quaternary faulting: mMigratory pattern and association with the Yellowstone hotspot: Journal of Geophysical Research, v. 94, p. 1589–1621.

Anderson, S.R., 1991, Stratigraphy of the unsaturated zone and uppermost part of the Snake River Plain aquifer at the Idaho Chemical Processing Plant and Test Reactors Area, Idaho National Engineering Laboratory, Idaho: U.S. Geological Survey Water-Resources Investigations Report 91-4010, 71 p.

Anderson, S.R., and Bowers, B., 1995, Stratigraphy of the unsaturated zone and uppermost part of the Snake River Plain aquifer at Test Area North, Idaho National Engineering Laboratory, Idaho: U.S. Geological Survey Water-Resources Investigations Report 95-4130, 47 p.

Anderson, S.R., and Lewis, B.D., 1989, Stratigraphy of the unsaturated zone at Radioactive Waste Management Complex, Idaho National Engineering Laboratory, Idaho: U.S. Geological Survey Water-Resources Investigations Report 89-4065, 54 p.

Anderson, S.R., Liszewski, M.J., and Ackerman, D.J., 1996, Thickness of surficial sediment at and near the Idaho National Engineering Laboratory, Idaho: U.S. Geological Survey Open-File Report 96-330, 16 p.

Blair, J.J., and Link, P.K., 2000, Pliocene and Quaternary sedimentation and stratigraphy of the Big Lost Trough from coreholes at the Idaho National Engineering and Environmental Laboratory, Idaho: Evidence for a regional Pliocene lake during the Olduvai normal polarity subchron, *in* Robinson, L., ed., Proceedings of the 35th Symposium on Engineering Geology and Geotechnical Engineering: Pocatello, Idaho, Idaho State University, College of Engineering, p. 163–179.

Carroll, A.R., and Bohacs, K.M., 1999, Stratigraphic classification of ancient lakes: Balancing tectonic and climatic controls: Geology, v. 27, p. 99–102.

Champion, D.E., Lanphere, M.A., and Kuntz, M.A., 1988, Evidence for a new geomagnetic reversal from lava flows in Idaho: Discussion of short polarity reversals in the Brunhes and late Matuyama polarity chrons: Journal of Geophysical Research, v. 93, p. 11667–11680.

Evans, K.V., and Zartman, R.E., 1988, Early Paleozoic alkalic plutonism in east-central Idaho: Geological Society of America Bulletin, v. 100, p. 1981–1987.

Geslin, J.K., Gianniny, G.L., Link, P.K., and Riesterer, J.W., 1997, Subsurface sedimentary facies and Pleistocene stratigraphy of the northern Idaho National Engineering Laboratory: Controls on hydrogeology, *in* Sharma, S., and Hardcastle, J. H., eds., Proceedings of the 32nd Annual Symposium on Engineering Geology and Geotechnical Engineering: Moscow, Idaho, University of Idaho, p. 15–28.

Geslin, J.K., Link, P.K., and Fanning, C.M., 1999, High-precision provenance determination using detrital-zircon ages and petrography of Quaternary sands on the eastern Snake River Plain, Idaho: Geology, v. 27, p. 295–298.

Gianniny, G.L., Geslin, J.K., Riesterer, J.W., Link, P.K., and Thackray, G.D., 1997, Quaternary surficial sediments near Test Area North (TAN), northeastern Snake River Plain: An actualistic guide to aquifer characterization, *in* Sharma, S., and Hardcastle, J.H., eds., Proceedings of the 32nd Annual Symposium on Engineering Geology and Geotechnical Engineering: Moscow, Idaho, University of Idaho, p. 29–44.

Hackett, W.R., and Smith, R.P., 1992, Quaternary volcanism, tectonics, and sedimentation in the Idaho National Engineering Laboratory area: *in* Wilson J.R., ed., Field guide to geologic excursions in Utah and adjacent areas of Nevada, Idaho, and Wyoming: Utah Geological Survey Miscellaneous Publication 92-3, p. 1–18.

Ingersoll, R.V., Bullard, R.R., Ford, R.L., Grimm, J.P., Pickel, J.P., and Sares, S.W., 1984, The effect of grain size on detrital modes: A test of the Gazzi-Dickinson point-counting method: Journal of Sedimentary Petrology, v. 54, p. 103–116.

Kuntz, M.A., Covington, H.R., and Schorr, L.J., 1992, An overview of basaltic volcanism of the eastern Snake River Plain, Idaho, *in* Link, P.K., Kuntz, M.A., and Platt, L.B., eds., Regional geology of eastern Idaho and western Wyoming: Geological Society of America Memoir 179, p. 227–267.

Kuntz, M.A., Skipp, B., Lanphere, M.A., Scott, W.E., Pierce, K.L., Dalrymple, G.B., Champion, D.E., Embree, G.F., Page, W.R., Morgan, L.A., Smith, R.P., Hackett, W.R., and Rodgers, D.W., 1994, Geological map of the Idaho National Engineering Laboratory and adjoining areas, eastern Idaho: U.S. Geological Survey Miscellaneous Investigations Series Map I-2330, scale 1:100 000.

Lanphere, M.A., Kuntz, M.A., and Champion, D.E., 1994, Petrography, age, and paleomagnetism of basaltic lava flows in coreholes at the Test Area North (TAN), Idaho National Engineering Laboratory: U.S. Geological Survey Open-File Report 94–686, 49 p.

Link, P.K., Geslin, J.K., Thackray, G.T., Gianniny, G.L., 1999, Basin architecture of the Pleistocene Bit Lost Trough, eastern Snake River Plain, Idaho: Geological Society of America Abstracts with Programs, v. 31, no. 4, p. A22.

Link, P.K., Geslin, J.K., and Fanning, C.M., 2000, Detrital zircon 'barcodes' from modern and Neogene sands of the Snake River Plain, Idaho: Defining a provenance area requires several grains and single grains mean little: Geological Society of America Abstracts with Programs, v. 32, no. 6, p. A25.

Morgan, L. A., 1992, Stratigraphic relations and paleomagnetic and geochemicial correlations of ignimbrites of the Heise Volcanic Field, Eastern Snake River Plain, eastern Idaho and western Wyoming, *in* Link, P.K., Kuntz, M.A., and Platt, L.B., eds., Regional geology of eastern Idaho and western Wyoming, Geological Society of America Memoir 179, p. 215–226.

Morgan, L.A., Doherty, D.J., and Leeman, W.P., 1984, Ignimbrites of the eastern Snake River Plain: Evidence for major caldera forming eruptions: Journal of Geophysical Research, v. 89, p. 8665–8678.

McQuarrie, N., and Rodgers, D.W., 1998, Subsidence of a volcanic basin by flexure and lower crustal flow: The eastern Snake River Plain, Idaho: Tectonics, v. 17, p. 203–220.

Nace, R.L., Voegeli, P.T., Jones, J.R., and Deutsch, M., 1975, Generalized geologic framework of the National Reactor Testing Station, Idaho: U.S. Geological Survey Professional Paper 725-B, 49 p.

Oaks, R.Q., Jr., James, W.C., Francis, G.G., and Schulingkamp, W.J., 1977, Summary of Middle Ordovician stratigraphy and tectonics, northern Utah, southern and central Idaho, *in* Heisey, E.L., Lawson, D.E., Norwood, E.R., Wach, P.H., and Hale, L.A., eds., Rocky Mountain thrust belt geology and resources: Casper, Wyoming, Wyoming Geological Association Guidebook, p. 101–118.

Pierce, K.L., and Morgan, L.A., 1992, The track of the Yellowstone hot spot, *in* Link, P.K., Kuntz, M.A., and Platt, L.B., eds., Regional geology of eastern Idaho and western Wyoming: Geological Society of America Memoir 179, p. 1–53.

Scott, W.E., 1982, Surficial geologic map of the eastern Snake River Plain and adjacent areas, 111°–115° W, Idaho and Wyoming: U.S. Geological Survey Miscellaneous Investigations Series Map I-1372, scale 1:250000, 2 sheets.

Skipp, B., and Link, P.K., 1992, Middle and Late Proterozoic rocks and Late Proterozoic tectonics in the southern Beaverhead Mountains, Idaho and Montana, a preliminary report, *in* Link, P.K., Kuntz, M.A., and Platt, L.B., eds., Regional geology of eastern Idaho and western Wyoming: Geological Society of America Memoir 179, p. 141–153.

Spinazola, J.M., 1994, Geohydrology and simulation of flow and water levels in the aquifer system in the Mud Lake area of the eastern Snake River Plain, eastern Idaho: U.S. Geological Survey Water-Resources Investigations Report 93–4227, 78 p.

Stearns, H.T., Crandall, L., and Steward, W.G., 1939, Geology and groundwater resources of the Mud Lake region, Idaho, including the Island Park area: U.S. Geological Survey Water-Supply Paper 818, 125 p.

Whitehead, R.L., 1992, Geohydrologic framework of the Snake River Plain regional aquifer system, Idaho and eastern Oregon: U.S. Geological Survey Professional Paper 1409-B, 32 p., 6 plates.

Winston, D., and Link, P.K., 1993, Middle Proterozoic rocks of Montana, Idaho, and Washington: The Belt Supergroup, *in* Reed., J., Simms, P., Houston, R., Rankin, D., Link, P., Van Schmus, R., and Bickford, P., eds., Precambrian of the conterminous United States: Boulder, Colorado, Geological Society of America, Geology of North America, v. C-3, p. 487–521.

Worl, R.G., Link, P.K., Winkler, G.R., and Johnson, K.M., editors., 1995, Geology and mineral resources of the Hailey 1° × 2° quadrangle and the western part of the Idaho Falls 1° × 2° quadrangle, Idaho: Washington, D.C., U.S. Geological Survey Bulletin 2064, v. 1, chapters A-R, separate pagination.

MANUSCRIPT ACCEPTED BY THE SOCIETY NOVEMBER 2, 2000

Printed in the U.S.A.

Geological Society of America
Special Paper 353
2002

Accumulation and subsidence of late Pleistocene basaltic lava flows of the eastern Snake River Plain, Idaho

Duane E. Champion*
Marvin A. Lanphere
U.S. Geological Survey, 345 Middlefield Road, Menlo Park, California 94025, USA
Steven R. Anderson
U.S. Geological Survey, Department of Geology, Idaho State University, Pocatello, Idaho 83209-8072, USA
Mel A. Kuntz
U.S. Geological Survey, Box 25046, Denver Federal Center, Denver, Colorado 80225, USA

ABSTRACT

Studies of cores from drill holes with detailed petrographic descriptions, paleomagnetic characterization and correlation, and conventional K-Ar and $^{40}Ar/^{39}Ar$ dating allow examination of the process of accumulation of basaltic lava flows in a part of the eastern Snake River Plain, Idaho. Core holes at various locations in the Idaho National Engineering and Environmental Laboratory (INEEL) demonstrate variable accumulation rates that can be fitted by linear regression lines with high correlation coefficients. Hiatuses of several hundred thousand years are represented in many of the core holes, but accumulation of flows resumed in most of the areas sampled by these core holes at rates nearly identical to previous rates. The studies show that an area of the eastern Snake River Plain north of its topographic axis, including the area of the INEEL, has undergone a hiatus in eruptive activity for the past ~200 k.y. The data also allow enhanced interpretations of the volcanic hazard to the INEEL with regard to lava flow inundation, prediction of lava flow thickness, and assessment of eruption recurrence-time intervals.

GEOLOGIC SETTING

The eastern Snake River Plain rises 1000 m in elevation from Twin Falls, Idaho, to the Yellowstone Plateau. The relatively flat surface has a northeast-southwest–trending central axis that connects those two areas. The plain is bounded on the northwest and southeast by Tertiary block-faulted mountains of the Basin and Range Province, underlain mainly by folded and thrust-faulted Precambrian, Paleozoic, and Mesozoic sedimentary rocks and Mesozoic and younger plutonic rocks. The plain terminates to the northeast in the Pliocene and Quaternary Yellowstone Plateau volcanic field. The Snake River flows along the southern boundary of the eastern Snake River Plain (Fig. 1) along a course defined in part by the extrusion of the lava flows; there is no evidence that the river ever crossed the lava surface (Walker, 1964).

At the surface, the eastern Snake River Plain comprises basaltic lava flows, shield volcanoes, minor associated pyroclastic deposits, and more widespread sedimentary accumulations of variable thicknesses. The surface is locally covered by a thin discontinuous mantle of loess. Most of the surface flows have normal magnetic polarity associated with the Brunhes Normal Polarity Chron, and are thus younger than 780 ka. Pleistocene and Holocene lava fields cover large parts of the eastern Snake River Plain, suggesting that renewed lava shield formation must be considered a possibility anywhere along the length of the eastern Snake River Plain. Several andesitic to rhyolitic flows and domes crop out along the axial area of the eastern

*E-mail: dchamp@mojave.wr.usgs.gov

Champion, D.E., Lanphere, M.A., Anderson, S.R., and Kuntz, M.A., 2002, Accumulation and subsidence of late Pleistocene basaltic lava flows of the eastern Snake River Plain, Idaho, *in* Link, P.K., and Mink, L.L., eds., Geology, Hydrogeology, and Environmental Remediation: Idaho National Engineering and Environmental Laboratory, Eastern Snake River Plain, Idaho: Boulder, Colorado, Geological Society of America Special Paper 353, p. 175–192.

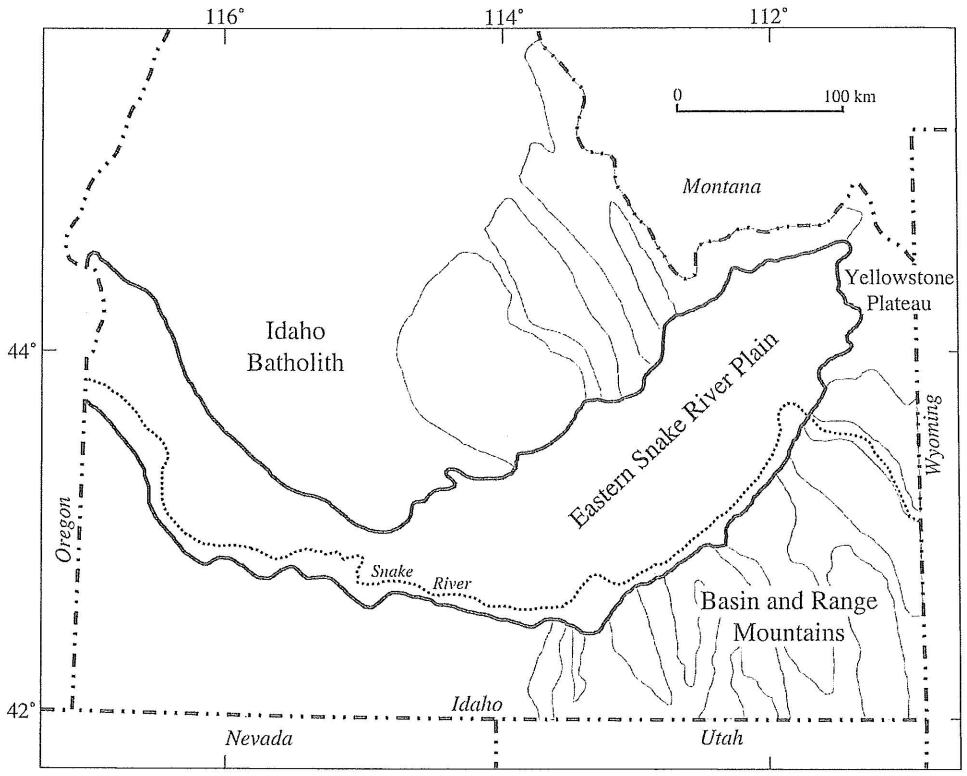

Figure 1. Generalized map of southern Idaho showing geologic and geographic features referred to in text, including eastern Snake River Plain.

Snake River Plain and have ages ranging from 1.4 to 0.3 Ma (Kuntz et al., 1994). Lava flows of evolved composition have been considered to be a very minor constituent of the eastern Snake River Plain, but recent work suggests that a larger amount of higher silica lava flows may be found at depth (Hughes et al., 1997). Outcrops of rhyolite pumice-fall deposits and welded tuff only occur at the margins of the plain; similar rocks occur at great depth (>730 m) in the deepest wells of the Idaho National Engineering and Environmental Laboratory (INEEL), but play no part in the surface or near-surface stratigraphy of the plain.

The distinctive low relief and low-slope morphology of basalt lava flows of the eastern Snake River Plain prompted Greeley (1982) to give the name "basaltic plains volcanism" to the eruptions of the eastern Snake River Plain to distinguish them from the more voluminous flood-basalt eruptions of plateau volcanism and from Hawaiian volcanism, which produces greater surface relief. Basaltic plains volcanism is dominated by low shield volcanoes of modest overall volume (5 ± 3 km^3) formed from fluid, gas-rich lavas. Eruptions may begin from a system of fissures and typically consolidate in long-lived eruptions to one or several vents along the original fissure system. The eruptions produce hundreds of lava flow units that extend tens of kilometers from the vent during a time no longer than a few decades. This type of eruption doesn't flood a surface 100 m thick with single flow units or pile up an equant mass of lava. Rather, flow directions follow subtle creases in the topography, moving great distances by endogenous flow when the effusion rate is appropriately maintained. The net effect is to produce nearly planar surfaces puddled by successive effusions, and widespread overlapping of lava fields.

The subsurface record of the eastern Snake River Plain is generally similar to the lava and sediment accumulations at the surface environment (Walker, 1964; Anderson et al., 1996; Anderson and Liszewski, 1997). In many core holes in the southern half of the INEEL, fine-grained sediments separate flows of significantly different ages. Anderson and Liszewski (1997) suggested an average sediment content of 15% for wells drilled in or near the INEEL. Sands and gravels recovered in southern INEEL core holes suggest that these are fluvial deposits associated with buried courses of the Big Lost River. The course of that stream has been displaced frequently as the plain has subsided to positions peripheral to new lava fields. Thick accumulations of sediments are typical of wells drilled or cored in the sinks area of the Big Lost or Little Lost Rivers or in the Mud Lake area. Sediment contents range from 26% to 46% for the deepest of the wells from those areas (Lanphere et al., 1994). By contrast, the proportion of sediment in core holes and drill holes along the southern boundary of the INEEL near the topographic axis of the eastern Snake River Plain is generally low, typically <5%. For example, Core Hole #1, located on the axis of the plain between East and Middle Buttes, has <1% sediments over a depth range of 600 m.

Kuntz et al. (1992) suggested that as many as nine volcanic rift zones cross the eastern Snake River Plain following Basin and Range trends. Four of these, the Arco–Big Southern Butte, Howe–East Butte, Lava Ridge–Hell's Half Acre, and Circular Butte–Kettle Butte volcanic rift zones cross the INEEL. The

Lava Ridge–Hell's Half Acre volcanic rift zone can be documented through the Test Area North (TAN) area of the INEEL (Fig. 2); core holes show that the subsurface section is composed of sediment-poor, flow-on-flow sequences to depths >300 m. Topographic freeboard arising from frequent eruptions prevents accumulation of sediments, thus sediment-poor sequences indicate near-vent locations for nearly all flows. In comparison, core holes to the northeast and south of the TAN area contain more than 100 m of sediment over the same depth range, indicating that their locations are on the flanks of volcanic edifices located in the vent zone.

PURPOSE OF THE PRESENT STUDY

We studied the stratigraphy of basaltic lava flows and sediments in 20 core holes at the INEEL by conventional logging, petrographic, paleomagnetic, $^{40}Ar/^{39}Ar$, and conventional K/Ar dating methods. These studies have yielded detailed information about the rates at which the lava flows and sediments have accumulated. The data indicate that the flows and sediments accumulate predictably with linear accumulation rates. The data for some core holes show that episodes of nearly constant accumulation rates were separated by hiatuses of several hundred thousand years. However, the hiatuses were followed by the resumed accumulation of lava flows and sediments, typically, but not universally, at a linear rate nearly identical to the prior rate. Accumulation rates also varied considerably in magnitude at various locations in the study area.

In this chapter we document the techniques used in this study, describe the accumulation rates found, and discuss the influences of these rates and their geographic distribution on the character of basaltic volcanism and on the potential volcanic hazards of the eastern Snake River Plain.

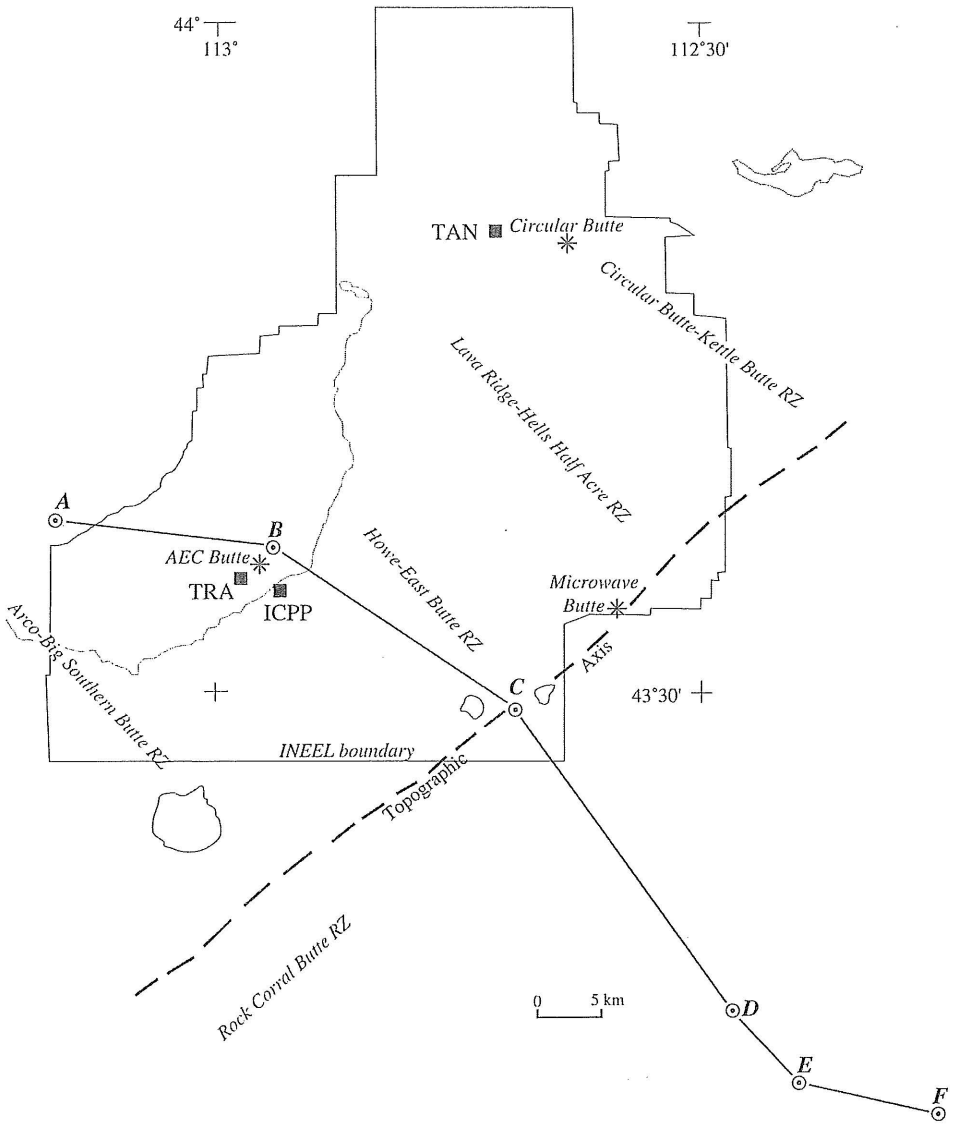

Figure 2. Map of part of eastern Snake River Plain at and near Idaho National Engineering and Environmental Laboratory (INEEL) showing geologic and geographic features referred to in text. Line A-F shows location of cross section in Figure 17. TAN, Test Area North; ICPP, Idaho Chemical Processing Plant; TRA, Test Reactor Area, RZ, rift zone.

ANALYTICAL TECHNIQUES

Each core hole was logged to establish tops and bottoms of individual lava flows, positions of sedimentary interbeds and unrecovered intervals, and generally to sample the cores for thin-section petrographic examination. Detailed petrographic descriptions were made of lava flows and flow units. Multiple paleomagnetic samples (typically seven for each flow or flow unit) were taken to establish mean remanent inclination values, and then compared one to another, assuming that lava flows of the same age share identical inclinations while lava flows of different ages typically have different mean inclinations or even different polarities. The inclination values were based on the assumption that each sampled core slug was vertical; this assumption can be tested using borehole deviation logs. The analytical techniques associated with the sampling, measurement, and demagnetization of basalt lava flow paleomagnetic specimens followed well-established protocols (Irving, 1964).

The K-Ar dating followed the established procedures of Dalrymple and Lanphere (1969). The application of those procedures to young basalts of very low potassium concentrations and the high success rate of our experiments merit some explanation. Careful thin-section evaluations were used to determine whether samples were suitable for dating (Mankinen and Dalrymple, 1972). The K_2O measurements were made in duplicate on each of two splits of powder by flame photometry (Ingamells, 1970). Argon mass analyses were done on a computerized multiple-collector mass spectrometer (described by Stacey et al., 1981). Weighted-mean ages for duplicate samples (some triplicate) were calculated by the method of Taylor (1982). These methods produced ages that stack well, generally in ascending age order with decreasing depth. In addition, ages from different core holes on flows correlated by petrography or remanent magnetization are the same, within analytical uncertainty.

Some basalt samples were also analyzed by the $^{40}Ar/^{39}Ar$ technique, which employs the radioactive decay of ^{40}K to ^{40}Ar as a chronometer in a different way (Dalrymple and Lanphere, 1971, 1974; Lanphere and Dalrymple, 1971). In the $^{40}Ar/^{39}Ar$ method, the sample is irradiated with fast neutrons, along with a monitor mineral of known age, to induce the reaction $^{39}K(n, p)^{39}Ar$. The age of the sample is calculated from the measured $^{40}Ar/^{39}Ar$ ratio after determining the fraction of ^{39}K converted to ^{39}Ar by analyzing the monitor mineral. The important difference between the two methods is that while quantitative measurements of the contents of radiogenic ^{40}Ar and ^{40}K are required by the conventional method, for the $^{40}Ar/^{39}Ar$ method only the ratios of Ar isotopes are measured. There is currently a widespread mistaken belief that $^{40}Ar/^{39}Ar$ dating has rendered conventional K-Ar dating obsolete. A direct comparison of the two dating techniques (Lanphere, 2000) finds consistency between ages determined by the two techniques. Whereas the mean K-Ar and $^{40}Ar/^{39}Ar$ ages are statistically identical, the precision of individual $^{40}Ar/^{39}Ar$ ages is generally better than the precision of K-Ar ages.

Accumulation rates were calculated from graphs of age of lava flows plotted against depth. A linear regression was fitted to the depth versus age data points, yielding the accumulation rate and regression coefficient, R.

CORE DESCRIPTIONS

Because most of the following cores have been described previously (Lanphere et al., 1993, 1994; Champion et al., 1988, 1981; Champion and Lanphere, 1997; Kuntz et al., 1980; Doherty, 1979), this section includes only information specific to the discussion of accumulation rates; i.e., the number of eruptive events, their K-Ar and $^{40}Ar/^{39}Ar$ ages, and thicknesses. In some cases, age information has improved since the original reports, either through the acquisition of new ages or by averaging multiple ages from what we have later learned to be the same flow in adjacent core holes. A diagram (Fig. 3) shows the locations of core holes examined for this study, and Tables 1–4 contain the detailed data pertinent to our study of lava flow and sediment accumulation through time. In addition, data on lava flow thicknesses and recurrence intervals are given in Tables 1–4 for use in a later discussion concerning volcanic hazards.

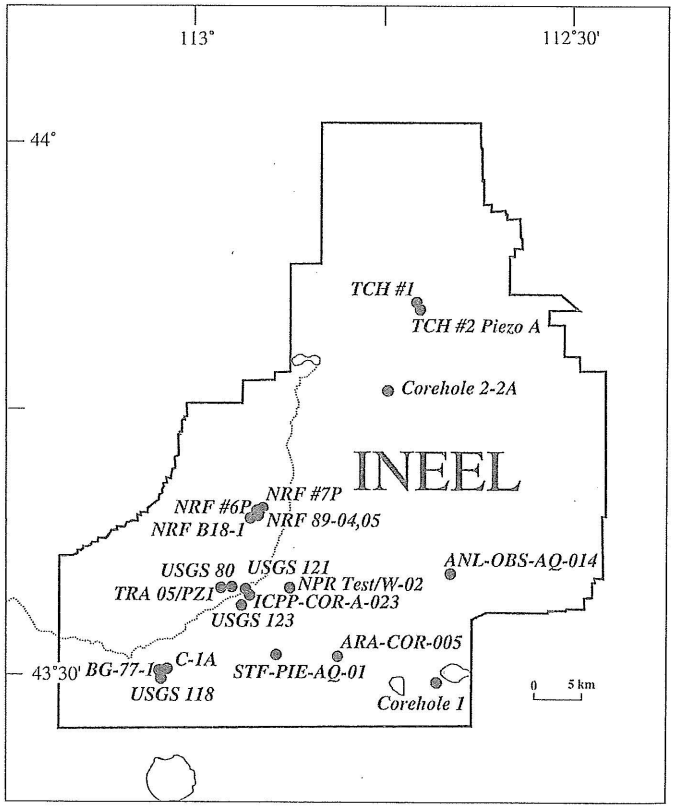

Figure 3. Map of Idaho National Engineering and Environmental Laboratory (INEEL) showing locations of core holes examined for this study (see text for designations).

TABLE 1. AGE, RECURRENCE INTERVAL, DEPTH AND THICKNESS DATA FOR LAVA FLOWS SAMPLED BY DRILL CORES NEAR FACILITIES IN THE SOUTH-CENTRAL PART OF THE INEEL*

Flow number	Age (ka)	Recurrence interval (1 k.y.)	Flow top depth (m/*ft*)	Thickness (m/*ft*)
USGS 80		*419+*		
1	419 ± 33	(−5)	13/*44′*	9/*29′*
2	[414 ± 8]	161	23/*76′*	18/*60′*
3	(575)	62	44/*144′*	5/*18′*
4	[637 ± 35]	—	54/*177′*	8/*27′* +
USGS 123		*229+*		
1	[229 ± 28]	73	10/*34′*	23/*74′*
2	(302)	4	34/*113′*	1/*4′*
3	(306)	44	36/*118′*	11/*36′*
4	[350 ± 40]	26	50/*163′*	13/*43′*
5	(376)	30	64/*209′*	12/*39′*
6	(406)	55	76/*248′*	9/*31′*
7	[461 ± 35]	30	87/*284′*	29/*98′*
8	[491 ± 80]	52	116/*382′*	12/*38′*
9	(543)	56	129/*424′*	22/*73′*
10	(599)	18	151/*497′*	4/*12′*
11	[617 ± 22]	20	155/*509′*	17/*55′*
12	[637 ± 35]	112	172/*564′*	37/*123′*
13	(749)	26	211/*691′*	10/*33′*
14	(775)	—	221/*724′*	5/*17′*
NPR Test/W-02		*229+*		
1	[229 ± 28]	82	2/*7′*	29/*96′*
2	(311)	39	34/*112′*	6/*21′*
3	350 ± 40	71	41/*136′*	33/*107′*
4	(421)	40	81/*267′*	9/*30′*
5	[461 ± 35]	30	92/*303′*	29/*96′*
6	491 ± 80	59	129/*424′*	10/*32′*
7	[550 ± 10]	67	139/*456′*	11/*35′*
8	[617 ± 22]	20	150/*492′*	20/*65′*
9	[637 ± 35]	—	182/*596′*	30/*98′*†
10	B/M-780 ± 5		216–234/*710–768′*	
ICPP-COR-A-023		*229+*		
1	[229 ± 28]	62	12/*41′*	16/*51′*
2	(291)	29	28/*92′*	3/*9′*
3	(320)	30	38/*126′*	5/*18′*
4	[350 ± 40]	22	52/*170′*	4/*12′*
5	(372)	89	57/*188′*	5/*18′*
6	[461 ± 35]	57	63/*206′*	46/*152′*
7	(518)	(−27)	110/*360′*	3/*10′*
8	[491 ± 80]	125	113/*371′*	6/*19′*
9	[616 ± 61]	(−6)	119/*390′*	24/*78′*
10	(610)	55	143/*468′*	19/*61′*
11	(665)	(−28)	162/*533′*	2/*7′*
12	[637 ± 35]	144	165/*540′*	40/*131′*
13	(781)	(−22)	205/*671′*	6/*21′*
14	[759 ± 12]	—	211/*692′*	14/*47′*
USGS 121		*77+*		
1	77 ± 39	—	10/*34′*	6/*19′*
2	—	—	16/*53′*	12/*39′*
3	—	—	28/*92′*	7/*22′*
4	—	—	35/*114′*	5/*16′*
5	376 ± 81	30	41/*134′*	16/*54′*

(*continued on next page*)

USGS 80

The stratigraphy, petrography, age, and paleomagnetic inclination stratigraphy of flows in core hole USGS 80 were originally reported by Lanphere et al. (1993), who found four lava flows of normal polarity to a depth of 62 m (Fig. 4; Table 1). Pairs of K-Ar ages on three of the flows define an ~220 k.y. span, from 637 to 419 ka. Anderson et al. (1997) fit the age versus depth data with a regression line of high correlation ($R = 0.998$), yielding an accumulation rate of ~18 m/100 k.y. Additional age measurements have altered the accumulation-rate calculation. Flow #2 is paleomagnetically and petrograph-

TABLE 1. AGE, RECURRENCE INTERVAL, DEPTH AND THICKNESS DATA FOR LAVA FLOWS SAMPLED BY DRILL CORES NEAR FACILITIES IN THE SOUTH-CENTRAL PART OF THE INEEL* (*continued*)

Flow number	Age (ka)	Recurrence interval (1 k.y.)	Flow top depth (m/*ft*)	Thickness (m/*ft*)
USGS 121 (continued)		*77+*		
6	(406)	55	57/*188'*	17/*56'*
7	[461 ± 35]	82	76/*248'*	23/*76'*
8	543 ± 48	(−52)	99/*324'*	21/*68'*
9	[491 ± 80]	125	126/*412'*	2/*6'*
10	616 ± 61	(−12)	129/*422'*	14/*46'*
11	(604)	41	143/*468'*	16/*54'*
12	(645)	(−8)	160/*525'*	5/*15'*
13	[637 ± 35]	51	165/*540'*	14/*46'*
14	(688)	12	179/*586'*	5/*16'*
15	(700)	29	184/*603'*	12/*41'*
16	(729)	30	196/*644'*	18/*60'*
17	759 ± 12	—	215/*704'*	9/*30'*
TRA 05/PZ1		*365+*		
1	(365)	49	21/*69'*	5/*18'*
2	[414 ± 8]	120	27/*89'*	19/*61'*
3	(534)	59	47/*155'*	5/*15'*
4	(593)	44	56/*185'*	6/*21'*
5	[637 ± 35]	149	67/*220'*	16/*54'*
6	786 ± 23	—	84/*276'*	6/*21+*
ANL-OBS-AQ-014				
1			0/*1'*	15/*50'*
2			16/*51'*	3/*12'*
3	358 ± 46		19/*63'*	35/*115'*
4			55/*181'*	24/*80'*
5			80/*261'*	33/*110'*
6			113/*372'*	9/*29'*
7			122/*400'*	12/*40'*
8	565 ± 94		134/*440'*	37/*122'*
ARA-COR-005				
1	[229 ± 28]		3/*10'*	26/*85'*
2			30/*98'*	26/*86'*
3			56/*185'*	2/*6'*
4			59/*193'*	57/*187'*
5			116/*380'*	19/*61'*
6			135/*443'*	5/*15'*
7			140/*458'*	43/*142'*
8			183/*602'*	20/*64'*
9			202/*666'*	14/*46'*
10	[550 ± 10]		217/*712'*	16/*53'*
STF-PIE-AQ-01				
1			6/*20'*	16/*52'*
2	[229 ± 28]		26/*84'*	16/*54'*
3			43/*141'*	13/*43'*
4			56/*184'*	6/*21'*
5			63/*208'*	26/*86'*
6			90/*295'*	69/*228'*
7	[550 ± 10]		166/*543'*	30/*100'*

Note: Ages in square brackets from another core, or from averaging ages in multiple cores; ages in parentheses derived from accumulation rate line fits; negative recurrence intervals in parentheses due to errors in age determinations or in line fits to same data.
*INEEL—Idaho National Engineering and Environmental Laboratory.
†Thickness of flow 9, core hole NPR-Test derived from basal depth estimate in adjacent core W-02.

ically correlated with flow #2 in adjacent well TRA-05, and the pooled age estimate from the original K-Ar and new $^{40}Ar/^{39}Ar$ ages is 414 ± 8 ka, substantially younger than the original estimate of 461 ± 24 ka. Flow #4, which is correlated with flows from AEC Butte, also has a different age than originally presented; averaging two pairs of K-Ar ages from wells USGS 80 and USGS 123 and one pair of ages from a nearby surface outcrop yields a slightly younger age of 637 ± 35 ka instead of 643 ± 64 ka. These revised ages decrease the accumulation rate for this core hole to 16 m /100 k.y. and lower the regression slightly (Fig. 4), but do not significantly alter conclusions regarding accumulation rates.

USGS 123

The stratigraphy, petrography, age, and paleomagnetic inclination stratigraphy of core hole USGS 123 were reported by Lanphere et al. (1993), who found 14 lava flows of normal polarity to a depth of 226 m (Fig. 5; Table 1). Pairs of K-Ar ages on five of the flows defined an ~550 k.y. span, from 775 to 229 ka. Petrographic and paleomagnetic correlations of numerous lava flows in USGS 123 to flows in core hole NPR Test (Fig. 1) allow ages in NPR Test to be pooled with ages from USGS 123, yielding six points of accumulation-rate measure. The accumulation rate is 39 m/100 k.y.; the linear regression coefficient is 0.994.

NPR Test/W-02

The stratigraphy, age, and paleomagnetic inclination stratigraphy of core hole NPR Test (where NPR refers to New Production Reactor) were reported by Champion et al. (1988), who found eight lava flows of normal polarity, and one of reversed polarity (Big Lost Reversed Polarity Subchron of the Brunhes Normal Polarity Chron) to a depth of 186 m (Fig. 6; Table 1). A detailed description of the petrography of the core hole was provided by Morgan (1990), who divided the uppermost flow into three flow units, raising the overall flow count to 11. Four pairs of K-Ar ages, one set of four K-Ar ages, and one single K-Ar age for six flows, provide age control and define an ~500 k.y. span, from 637 to 229 ka. In addition, core hole W-02, located only 100 m from NPR Test, includes the Matuyama Reversed Polarity Chron–Brunhes Normal Polarity Chron boundary (hereafter referred to as the Brunhes-Matuyama boundary) between the top of reversed polarity flows at 234 m and the base of normal polarity flows at 216 m. Petrographic and paleomagnetic correlation of numerous lava flows in these core holes with flows in core hole USGS 123 allows age data in that well to be pooled with ages in NPR Test and W-02 to yield seven points of accumulation-rate measure. The accumulation rate is 43 m/100 k.y.; the high regression coefficient is 0.984.

ICPP-COR-A-023

The stratigraphy, hand-specimen petrography, and paleomagnetic inclination stratigraphy of flows in core hole ICPP-023 (where ICPP stands for Idaho Chemical Processing Plant) is reported on by Jobe and Champion (2002), who describe 14 lava flows of normal polarity to a depth of 225 m (Fig. 7; Table 1). Although no K-Ar ages have been measured on this core, correlations of flows in ICPP-023 with flows in adjacent core holes (USGS 121 and USGS 123) together with paleomagnetic and petrographic data allow ages to be assigned to seven flows. The ages define an ~530 k.y. span, from 759 to 229 ka. The accumulation rate is 36 m/100 k.y., and the linear regression coefficient is 0.964. The lower coefficient of regression suggests errors in the dates, or possibly in correlations of flows from other wells.

TABLE 2. AGE, RECURRENCE INTERVAL, DEPTH AND THICKNESS DATA FOR LAVA FLOWS SAMPLED BY DRILL CORES NEAR THE NAVAL REACTOR FACILITY (NRF) AT THE IDAHO NATIONAL ENGINEERING AND ENVIRONMENTAL LABORATORY

Flow number	Age (ka)	Recurrence interval (1 k.y.)	Flow top depth (m/*ft*)	Thickness (m/*ft*)
NRF 89-04		*303+*		
1	[303 ± 30]	92	6/*21′*	26/*85′*
2	[395 ± 25]	126	36/*119′*	22/*71′*
3	521 ± 31	25	60/*196′*	7/*22′*
4	[546 ± 47]	—	67/*221′*	8/*27′* +
NRF 89-05		*303+*		
1	303 ± 30	92	6/*21′*	26/*86′*
2	[395 ± 25]	97	36/*118′*	23/*76′*
3	492 ± 56	29	60/*196′*	3/*12′*
4	521 ± 31	—	63/*208′*	10/*34′* +
NRF B18-1		*303+*		
1	[303 ± 30]	92	11/*35′*	16/*53′*
2	[395 ± 25]	97	*27/88′*	31/*102′*
3	[492 ± 56]	29	58/*190′*	10/*34′*
4	[521 ± 31]	—	68/*224′*	8/*27′* +
NRF #6P		*303+*		
1	[303 ± 30]	92	3/*11′*	24/*78′*
2	395 ± 25	126	*27/89′*	23/*76′*
3	[521 ± 31]	25	50/*165′*	14/*45′*
4	546 ± 47	181	64/*210′*	44/*143′*
5	727 ± 31	157	108/*354′*	29/*64′*
6	[884 ± 53]	—	127/*418′*	25/*83′* +
NRF #7P		*303+*		
1	[303 ± 30]	92	7/*25′*	20/*67′*
2	[395 ± 25]	126	32/*105′*	14/*46′*
3	[521 ± 31]	25	46/*152′*	6/*20′*
4	[546 ± 47]	181	52/*172′*	56/*184′*
5	[727 ± 31]	*(53)*	109/*358′*	13/*44′*
6	<780	*(104)*	123/*404′*	6/*21′*
7	884 ± 53	—	130/*428′*	22/*73′* +

Note: Ages in square brackets from another core, or from averaging ages in multiple cores; depths in parentheses from limiting age data in core hole NRF #7P.

USGS 121

The lithology and paleomagnetic inclination stratigraphy of core hole USGS 121 are reported by Jobe and Champion (2002), who describe 17 lava flows of normal polarity to a depth of 227 m (Fig. 8; Table 1). A single K-Ar age and four $^{40}Ar/^{39}Ar$ ages, as well as three K-Ar ages correlated from adjacent wells, establish a set of eight age and depth measures. The data define lava flow accumulation for the entire span of the Brunhes Normal Polarity Chron, ~780 k.y. The age versus depth graph displays a distinct "dog leg" in the upper 35 m of the well (not shown in Fig. 8), reflecting an interval of slower accumulation. An accumulation rate of 43 m/100 k.y., and a regression coefficient of 0.953, is derived for the majority of the core hole. This somewhat lower regression coefficient may reflect errors in the ages, or possibly in the correlations of flows from other wells.

TABLE 3. AGE, RECURRENCE INTERVAL, DEPTH AND THICKNESS DATA FOR LAVA FLOWS SAMPLED BY DRILL CORES NEAR THE RADIOACTIVE WASTE MANAGEMENT COMPLEX (RWMC) AT THE IDAHO NATIONAL ENGINEERING AND ENVIRONMENTAL LABORATORY

Flow number	Age (ka)	Recurrence interval (1 k.y.)	Flow top depth (m/ft)	Thickness (m/ft)
BG 77-1		*95+*		
1	95 ± 50	37	1/*4′*	12/*41′*
2	(132)	79	16/*51′*	16/*51′*
3	211 ± 16	19	32/*105′*	38/*126′*
4	230 ± 85	*(285)*	77/*252′*	10/*33′*
5	515 ± 85	35	88/*288′*	23/*76′*
6	550 ± 10	—	112/*367′*	57/*188′*
7	—	—	170/*557′*	13/*43′* +
C-1A		*95+*		
1	95 ± 50	25	2/*8′*	9/*28′*
2	(120)	91	11/*36′*	23/*75′*
3	211 ± 16	19	34/*111′*	36/*118′*
4	230 ± 85	(—)	73/*239′*	15/*50′*
5	—	(—)	89/*293′*	12/*39′*
6	515 ± 85	35	101/*333′*	20/*64′*
7	550 ± 10	133	121/*397′*	48/*158′*
8	(683)	37	173/*569′*	15/*50′*
9	(720)	19	189/*620′*	7/*25′*
10	(739)	41	197/*645′*	16/*53′*
11	B/M-780 ± 5	—	213/*700′*	—
USGS 118				
1	<180	—	4/*14′*	28/*92′*
2	211 ± 16	(—)	34/*112′*	34/*112′*
3	—	(—)	76/*250′*	4/*13′*
4	—	(—)	81/*265′*	10/*33′*
5	515 ± 85	35	91/*300′*	25/*81′*
6	550 ± 10	—	116/*381′*	57/*186′*

Note: Ages in parentheses derived from accumulation rate line fits; recurrence intervals in parentheses represent hiatuses in accumulation.

TRA 05/PZ1

In core hole TRA 05/PZ1, six lava flows of normal polarity occur to a depth of 91 m (Fig. 9; Table 1). The K-Ar ages on three lava flows, redating by $^{40}Ar/^{39}Ar$ on two of the flows, and correlation of lava flows to those in well USGS 80 define an ~400 k.y. span, from 786 to 365 ka. The three points of age control define an accumulation rate of 16 m/100 k.y., and a high regression coefficient of 0.994.

STF-PIE-AQ-01

There is no report on the stratigraphy, petrography, age, and paleomagnetism of a 218 m core hole drilled at the Safety Test Facility (STF). Paleomagnetic studies have designated nine lava flows; thicknesses and depths to tops of flows are listed (Table 1). A preliminary accumulation rate for the upper seven lava flows can be derived from age information correlated to this core hole for flows #2 and #7. Flow #2 can be paleomagnetically correlated with the top flow in core holes NPR Test/W-02 and USGS 123. The weighted mean K-Ar age of these two flows is 229 ± 28 ka. Flow #7 is part of the sequence of flow units of the Big Lost Reversed Polarity Subchron, which has an age of 550 ± 10 ka (Champion et al., 1996). The age and depth data suggest an average accumulation rate of 50 m/100 k.y. for this core hole.

ARA-COR-005

There is no report on the stratigraphy, petrography, age, and paleomagnetism of a 261 m core hole drilled at the Auxiliary Reactor Area (ARA). Paleomagnetic studies have designated 11 lava flows; thicknesses and depths to tops of flows are listed in Table 1. A preliminary accumulation rate for the upper 10 flows can be derived from age information correlated to this core hole for flows #1 and #10. Flow #1 can be correlated with the top flows in core holes NPR Test, W-02, and USGS 123 that have a weighted mean K-Ar age of 229 ± 28 ka. Flow #10 is one of the sequence of flow units of the Big Lost Reversed Polarity Subchron, which has an age of 550 ± 10 ka (Champion et al., 1996). The age versus depth data suggest an average accumulation rate of 67 m/100 k.y. for this location.

ANL-OBS-AQ-014

The age and paleomagnetic inclination stratigraphy of core hole ANL-OBS-AQ-014 were reported by Champion and Lanphere (1997), who described 27 lava flows of both normal and reversed polarity to a depth of 582 m. Four $^{40}Ar/^{39}Ar$ ages and one K-Ar age (Kuntz et al., 1994) suggest a history of alternating fast and slow accumulation at this location close to the central axis of the eastern Snake River Plain. Until more age information and petrographic details are available for this core hole, a detailed accumulation analysis is premature. A preliminary accumulation rate for the majority of the Brunhes Normal Polarity Chron lava flows can be derived from the ages of 358 ± 46 ka for flow #3 and 565 ± 94 ka for flow #8 (Table 1). The age and depth data suggest an average mid-Brunhes Normal Polarity Chron accumulation rate of 56 m/100 k.y.

NRF core holes

The stratigraphy, petrography, age and paleomagnetic inclination stratigraphy of two core holes at the Naval Reactor Facility (NRF) (Fig. 3) were reported by Lanphere et al. (1993). They found five lava flows of normal polarity in the NRF 89-04 and NRF 89-05 core holes to depths of 76 m and 74 m, respectively. Other core holes in and near the facility, NRF B18-1, NRF #6P, and NRF #7P, have now been studied by paleomagnetic inclination methods and $^{40}Ar/^{39}Ar$ ages have been obtained on five flows (Table 2). Ages have been measured on virtually all lava flows within the shared section in core holes NRF #6P and NRF #7P. The horizontal separation of the different core holes is only 1000 m, so they can be interpreted with a single accumulation rate for a single location. Core holes NRF #6P (Fig. 10A) and NRF #7P (Fig. 10B) were both cored

TABLE 4. AGE, RECURRENCE INTERVAL, DEPTH AND THICKNESS DATA FOR LAVA FLOWS SAMPLED BY DRILL CORES NEAR TEST AREA NORTH (TAN) AT THE IDAHO NATIONAL ENGINEERING AND ENVIRONMENTAL LABORATORY

Flow number	Age (Ma)	Recurrence interval (1 k.y.)	Flow top depth (m/*ft*)	Thickness (m/*ft*)
TCH #1		*1.09+*		
1	1.09 ± 0.09	0.06	13/*44'*	8/*26'*
2	(1.15)	0.10	21/*70'*	10/*34'*
3	1.25 ± 0.07	0.07	32/*104'*	37/*121'*
4	1.32 ± 0.02	0.26	69/*226'*	53/*175'*
5	1.58 ± 0.06	(0.42)	126/*412'*	9/*31'*
6	2.00 ± 0.06	0.12	137/*448'*	29/*96'*
7	2.12 ± 0.05	—	166/*544'*	17/*56'* +
TCH #2 Piezo A		*1.09+*		
1	1.09 ± 0.09	0.06	14/*47'*	9/*28'*
2	(1.15)	0.10	23/*75'*	18/*59'*
3	1.25 ± 0.07	0.07	41/*134'*	32/*105'*
4	1.32 ± 0.02	0.09	75/*247'*	61/*201'*
5	1.41 ± 0.05	(0.59)	138/*452'*	5/*17'*
6	2.00 ± 0.06	0.12	144/*473'*	34/*111'*
7	2.12 ± 0.05	0.40	179/*586'*	45/*147'*
8	2.52 ± 0.03	—	226/*742'*	107/*351'*
9			336/*1102'*	4/*12'* +
Corehole 2-2A				
1	*{Brunhes Chronozone}*		~3/*10'*	~17/*55'*
2	*{top of Matuyama*		76/*249'*	~16/*54'*
3	*Chronozone}*		~97/*319'*	~12/*41'*
4			120/*393'*	2/*7'*
5	*{Jaramillo*		124/*407'*	7/*22'*
6	*Subchronozone}*		131/*431'*	12/*38'*
7			144/*471'*	8/*28'*
8			152/*499'*	7/*22'*
9			159/*521'*	11/*37'*
10			170/*559'*	21/*69'*
11			194/*636'*	18/*58'*
12			212/*697'*	9/*28'*
13			226/*742'*	11/*35'*
14			237/*778'*	22/*71'*
15			273/*895'*	6/*21'*
16			280/*918'*	6/*19'*
17			287/*942'*	5/*16'*
	{Olduvai Subchronozone}			
18			350/*1147'*	22/*73'*
19			372/*1220'*	8/*28'*
20	2.45 ± 0.03		380/*1248'*	18/*60'*
21			399/*1308'*	4/*13'*
22			403/*1322'*	5/*15'*
23	*{approx. top of Gauss*		~477/*1564'*	~10/*33'*
24	*Chronozone}*		487/*1598'*	8/*26'*
25	*{Kaena Subchronozone}*		~541/*1775'*	~1/*3'*
26	3.26 ± 0.06		581/*1906'*	13/*43'*

Note: Ages in parentheses derived from accumulation rate line fits; recurrence intervals in parentheses represent hiatuses in accumulation; approximate depths and thicknesses in 2-2A from unrecovered cored intervals.

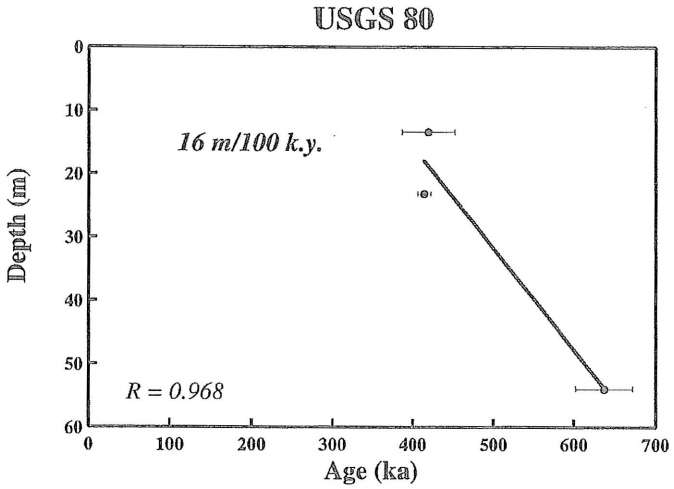

Figure 4. Graph of ages of lava flows plotted against depths to flow tops in core hole USGS 80 from Idaho National Engineering and Environmental Laboratory. One-sigma errors are plotted for age determinations, but small uncertainties in depth to tops of lava flows not shown. Accumulation rate in m/100 k.y. is calculated by straight line fit through data points; regression coefficient is also shown.

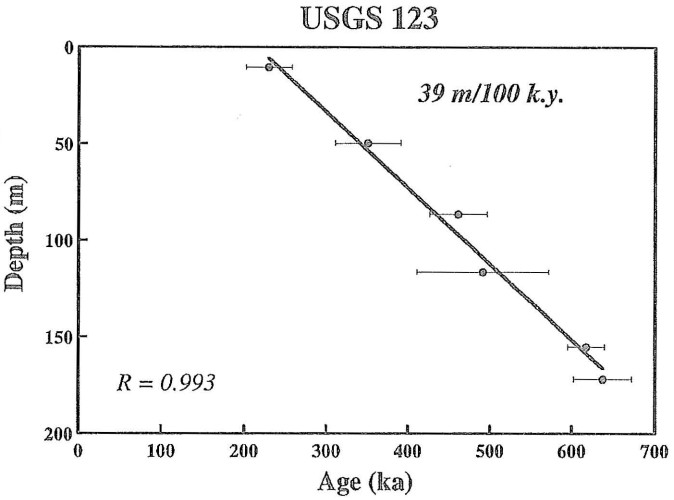

Figure 5. Graph of ages of lava flows plotted against depths to flow tops in core hole USGS 123 from Idaho National Engineering and Environmental Laboratory. Data are as in Figure 4.

to 153 m, deeper than the other NRF core holes, and have six and seven identified lava flows, respectively. The two core holes bottom in a reversed polarity lava flow, and thus have the most complete record of accumulation rate. All five core holes share similar accumulation rates, between 22 m and 27 m/100 k.y.; the shallowest and most southerly core holes record the higher rates.

Radioactive Waste Management Complex core holes

The stratigraphy, petrography, age, and paleomagnetic inclination stratigraphy of core hole BG-77-1 were reported by Kuntz et al. (1980) and Champion et al. (1981), who found seven lava flows, six having normal polarity and one having reversed polarity, to a depth of 183 m (Fig. 11; Table 3). The single reversed polarity flow, situated within the normal polarity lava flows, was initially miscorrelated with the Emperor Reversed Polarity Subchron of the Brunhes Normal Polarity Chron, but later identified as a new polarity event, the Big Lost

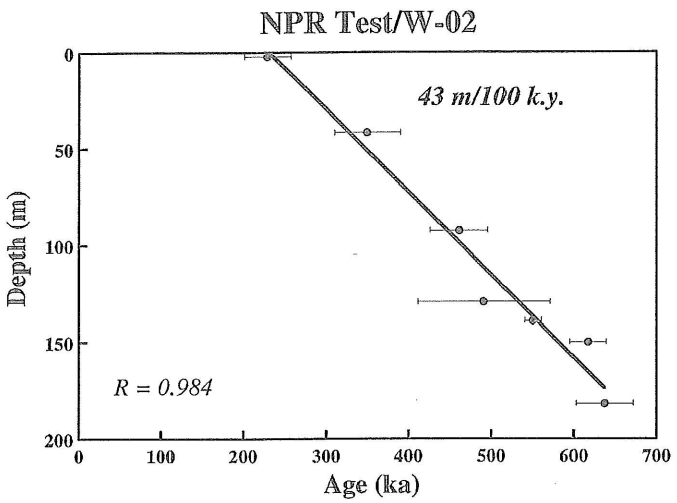

Figure 6. Graph of ages of lava flows plotted against depths to flow tops in core holes NPR Test and W-02 from Idaho National Engineering and Environmental Laboratory. Data are as in Figure 4.

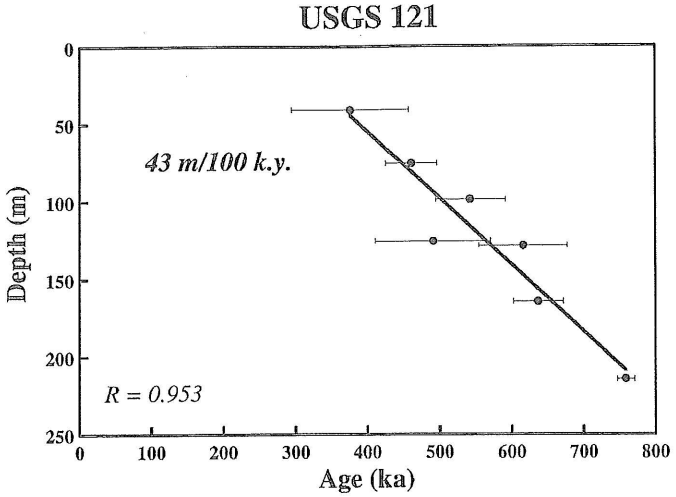

Figure 8. Graph of ages of lava flows plotted against depths to flow tops in core hole USGS 121 from Idaho National Engineering and Environmental Laboratory INEEL. Data are as in Figure 4. Data point at 77 ka is not plotted nor used in linear regression.

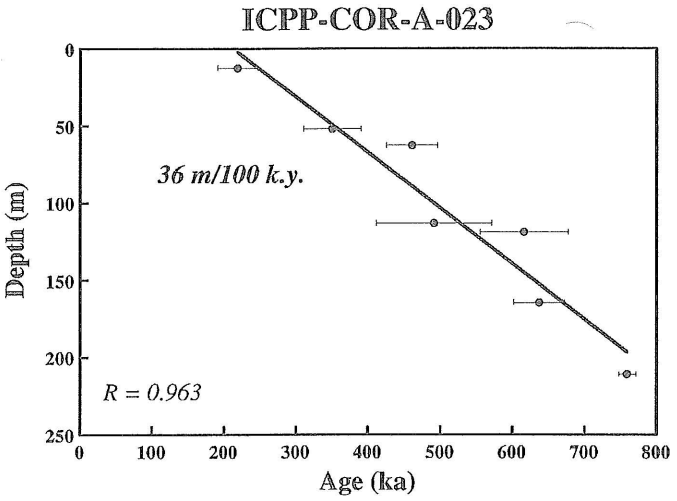

Figure 7. Graph of ages of lava flows plotted against depths to flow tops in core hole ICPP-COR-A-023 from Idaho National Engineering and Environmental Laboratory. Data are as in Figure 4.

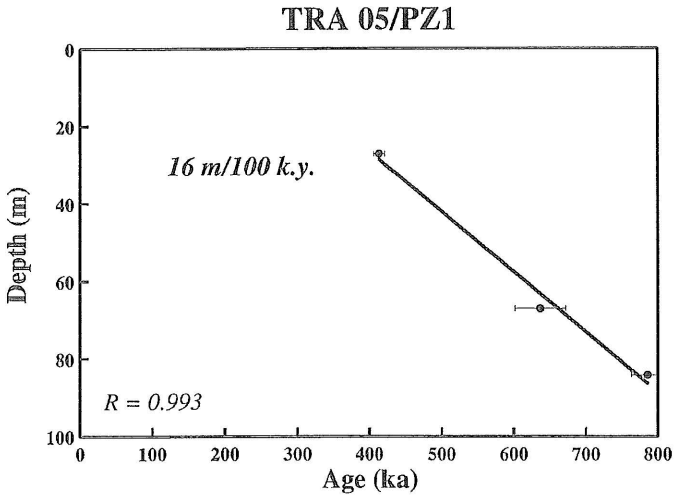

Figure 9. Graph of ages of lava flows plotted against depths to flow tops in core hole TRA 05/PZ1 from Idaho National Engineering and Environmental Laboratory. Data are as in Figure 4.

Reversed Polarity Subchron (Champion et al., 1988). The event was assigned an age of 565 ± 14 ka on the basis of K-Ar dating, but subsequent $^{40}Ar/^{39}Ar$ dating improved the age assignment to 550 ± 10 ka (Champion et al., 1996). Core hole BG-77-1 is near the Radioactive Waste Management Complex (RWMC) of the INEEL (Fig. 3). Like the Naval Reactor Facility area, dozens of wells have been drilled and cored to various depths in the vicinity of that facility. We have analyzed results from three of the deeper core holes, BG-77-1, C-1A, and USGS 118, that form a short north-south transect across the RWMC. These three core holes sample the same stratigraphic interval with minor variations. The Matuyama-Brunhes boundary in core hole C-1A occurs at a depth of about 213 m at the boundary between reversed and normal polarity flows (Fig. 12; Table 3). As many as six age versus depth pairs can be assigned to flows in these core holes, and accumulation rates can be calculated. Accumulation rates range between 20 m and 28 m/100 k.y. and have relatively low regression coefficients. The low (<0.95) coefficients of regression suggest these are apparent accumulation rates, to use a term coined by Anderson et al. (1997) to reflect hiatuses related to vent construction, periods of decreased volcanism, and differential subsidence and uplift. In particular, a hiatus was recognized at the ~90 m level in many RWMC wells by Anderson and Lewis (1989), and they assigned a duration of 285 k.y. to the hiatus based on flow ages in Champion et al. (1981). Consequently, we fit the ages to

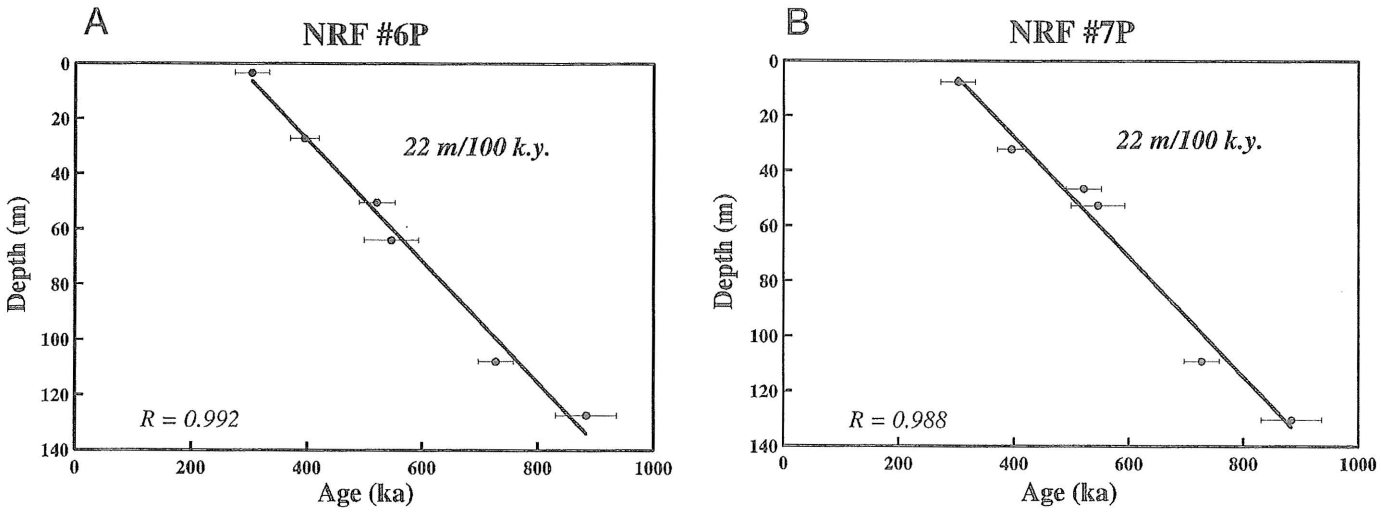

Figure 10. A: Graph of ages of lava flows plotted against depths to flow tops in core hole NRF #6P from Naval Reactor Facility (NRF) of Idaho National Engineering and Environmental Laboratory. B: Graph of ages of lava flows plotted against depths to flow tops in core hole NRF #7P. Data are as in Figure 4.

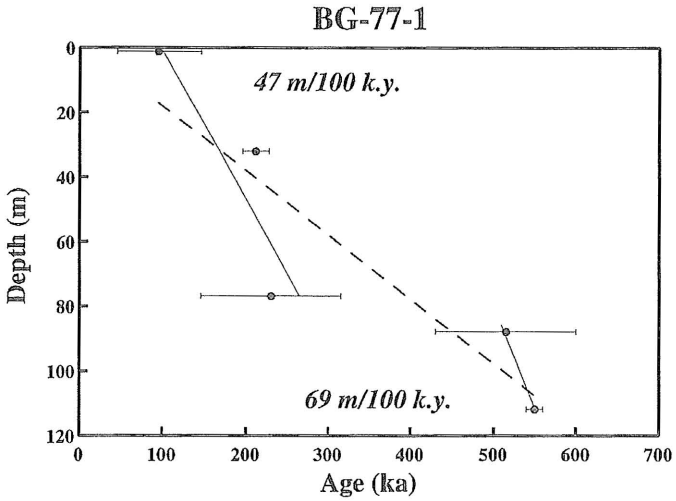

Figure 11. Graph of ages of lava flows plotted against depths to flow tops in core hole BG-77-1 at the Radioactive Waste Management Complex. Accumulation rate calculated without consideration of a hiatus between flows 4 and 5 shown as dashed line, accumulation rates calculated with a hiatus between those flows shown as two solid lines. Data shown as in Figure 4.

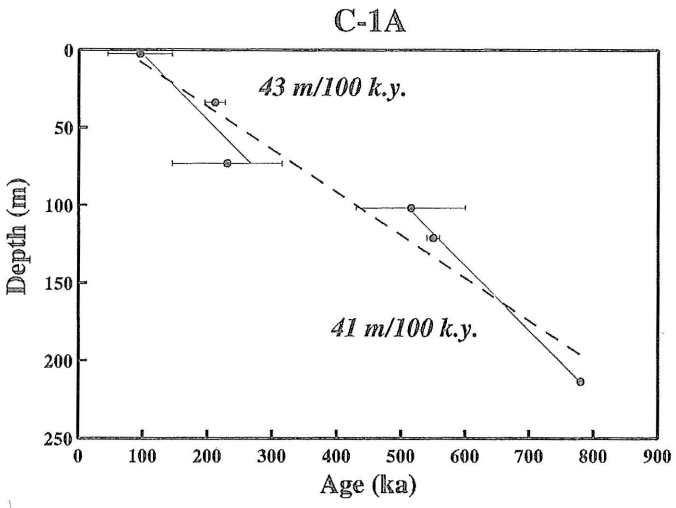

Figure 12. Graphs of ages of lava flows plotted against depths to flow tops in core hole C-1A at Radioactive Waste Management Complex. Accumulation rate calculated without consideration of hiatus between flows 4 and 6 is shown as dashed line; accumulation rates calculated with hiatus between those flows is shown as two solid lines. Data are as in Figure 4.

separate regression lines above and below the hiatus. Data from core hole C-1A define accumulation rates of 41 m/100 k.y. and 43 m/100 k.y. below and above the hiatus interval, respectively (Fig. 12).

TCH #1

The stratigraphy, petrography, age, and paleomagnetic inclination stratigraphy of core hole TCH #1 were reported by Lanphere et al. (1994), who described 14 lava flows of reversed polarity to a depth of 183 m (Fig. 13; Table 4). Similar mean-inclination values and the absence of intercalated sediments indicate that the number of flows in the core hole is fewer than earlier reported, based on the presumption that a feature observed in the cores represents multiple flow units within each of several eruptive events. An accumulation rate of 14 m/100 k.y. is derived from the six dated flows in the core hole, but the regression coefficient of 0.95 suggests that this should be considered an apparent accumulation rate. Thus, rates of 24 m/100 k.y. calculated for the periods before and after a hiatus of 420

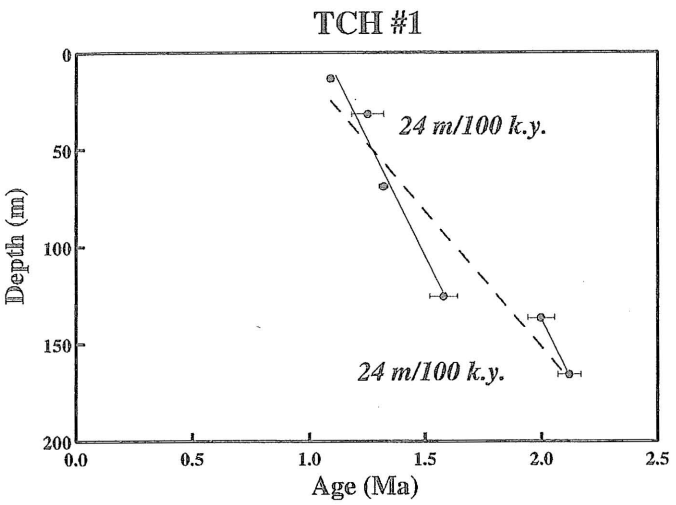

Figure 13. Graphs of age of lava flows plotted against depths to flow tops in core hole TCH #1 at Test Area North. Accumulation rate calculated without consideration of hiatus between flows 5 and 6 is shown as dashed line; accumulation rates calculated with hiatus between those flows are shown as two solid lines. Data are as in Figure 4.

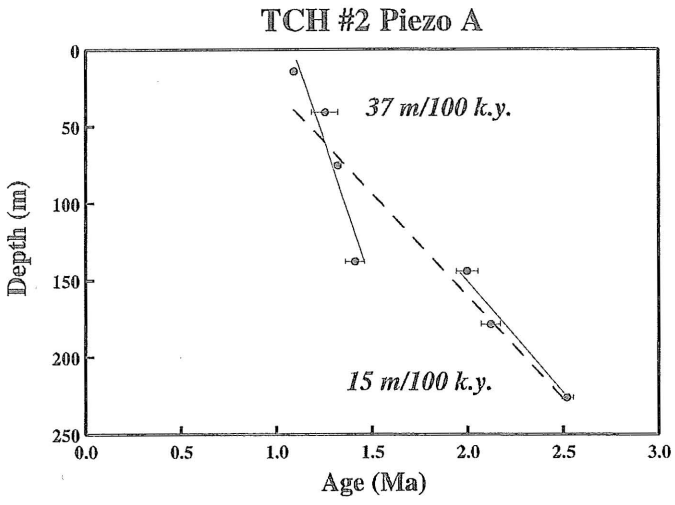

Figure 14. Graphs of ages plotted against depths to flow tops in core hole TCH #2 Piezo A at Test Area North. Accumulation rate calculated without consideration of hiatus between flows 5 and 6 is shown as dashed line; accumulation rates calculated with hiatus between those flows are shown as two solid lines. Data are as in Figure 4.

k.y. at a depth of ~137 m might be more realistic (Fig. 13). No flows of Brunhes age, younger than 780 ka, are known in the immediate TAN area. Normal polarity flows located just north of "TCH #1" and on top of the 1.09 Ma reversed polarity flows of Circular Butte are likely to have been erupted during the Jaramillo Normal Polarity Subchron of the Matuyama Reversed Polarity Chron, 1.07–1.0 Ma. It is unclear that the accumulation rates of the northern (TAN) INEEL area can be directly compared to the younger sections to the south.

TCH #2 Piezo A

The stratigraphy, petrography, age, and paleomagnetic inclination stratigraphy of core hole TCH #2 Piezo A were reported by Lanphere et al. (1994), who described 20 lava flows of reversed polarity to a depth of 340 m (Fig. 14; Table 4). Again, owing to similar mean-inclination values and the absence of intercalated sediments, fewer flows in the core have been interpreted on the presumption that some multiple flow units formed within each of several eruption events. A regression coefficient of 0.93 suggests that an accumulation rate of 13 m/100 k.y. derived from seven dated flows in the core hole (Fig. 14) is an apparent rate. Thus, a rate of 37 m/100 k.y., after a hiatus of 590 k.y. at a depth of ~137 m, preceded by a rate of 15 m/100 k.y. deeper in the core, are probably more realistic values (Fig. 14).

Core hole 2-2A

There is no detailed report on the stratigraphy, petrography, age, and paleomagnetism of the 915 m core hole 2-2A in the north-central part of the INEEL (Fig. 3). A general description of the stratigraphy of the core hole was produced by Doherty (1979). Core hole 2-2A is unique among the longer core holes at the INEEL in that more than one-third of the section consists of fine-grained lake and playa sediments that can span 100 m. The large amount of sediment in this core hole complicates the lava accumulation rate for the core hole. Preliminary paleomagnetic studies have designated 26 lava flows within the upper 604 m of the core. Paleomagnetic studies below this depth have been more cursory. Preliminary determination of flow thicknesses and depths to tops of flows are listed (Table 4). An accumulation rate for the top two-thirds of core hole 2-2A has been derived from a combination of four K-Ar ages on four lava flows within the core, the ages of flows correlated to the core hole, and the depths of magnetic polarity boundaries between lava flows (Fig. 15). These 11 points of age control yield an accumulation rate of 20 m/100 k.y., and a correlation coefficient of 0.998. This calculation of accumulation rate is different from that of the other data sets of this report in that the reported depths may have considerable error, whereas the ages may constitute proportionately a lower source of error. This results from the age being assigned to the top of a lava flow, so that for a thick flow the assigned depth may have a considerable uncertainty; instead of knowing that accumulation proceeded to a certain depth, we know that a polarity change of the magnetic field occurred at a particular time ($\pm$0.01 m.y.), but that no lava accumulation occurred between flows or while sediments accumulated. The accumulation rate for this core must be considered an apparent rate, averaging accumulation bursts and hiatuses into a longer term rate. It is remarkable, however, that the accumulation of lavas at this location progressed rather smoothly for nearly 5 m.y.

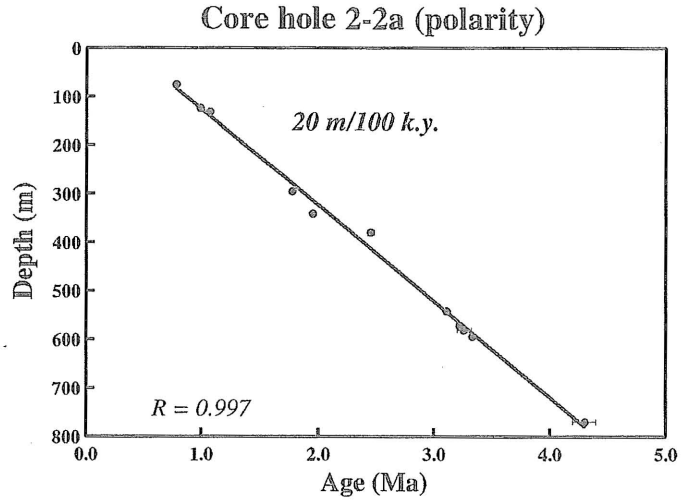

Figure 15. Graph of ages of lava flows plotted against depths to flow tops in core hole 2-2A in north-central part of Idaho National Engineering and Environmental Laboratory. See text for discussion of error sources.

RESULTS

Accumulation rate

The accumulation rates found in drill cores vary by a factor of 4, from 16 m/100 k.y. to 67 m/100 k.y. Regression coefficients of age versus depth plots are typically greater than 0.98 (Table 5). The graphical representations of accumulation rates are compelling and suggest a regular and controlled process of lava flow accumulation for the eastern Snake River Plain. This is well shown by those core holes for which complete or nearly complete K-Ar and $^{40}Ar/^{39}Ar$ age data are available.

Although the rates of accumulation varied from core hole to core hole, a contour map of their values suggests a simple overall pattern (Fig. 16). Only rates of accumulation of lava flows erupted during the Brunhes Normal Polarity Chron are included in the map; the rates from older sections in wells farther north in the INEEL may vary broadly through time. The data suggest a northwest-southeast gradient; contour trends are broadly parallel to the axis of the eastern Snake River Plain, and accumulation rates are greater at sites closer to the axis of the plain. The accumulation rates (Fig. 16) would require that lava accumulates in the vicinity of the axis of the eastern Snake River Plain, unless some other process is involved. This process must be subsidence, because the eastern Snake River Plain generally is rather flat. The higher accumulation rates toward the axis of the plain are compatible with subsidence that compensates for the higher accumulation rates. Proximity to lava flow source vents along the axis of the eastern Snake River Plain could explain the faster accumulation and/or subsidence of these areas, with waning lava flow accumulation to the northwest (Fig. 17).

Within the overall gradient of accumulation rates, there is an abrupt increase to higher values, centered in the TRA and ICPP area. The anomaly near TRA and ICPP suggests a zone of relative structural movement, such as a monocline or a fault. A cross section drawn through core locations TRA 05/PZ1, USGS 80, USGS 121, and NPR Test/W-02 (Fig. 18) shows the structural effect on the otherwise nearly horizontal flat-bedded age horizons of the lava section of the INEEL. Although this cross section has a vertical exaggeration of 10 for clarity, the parallelism of surfaces between core locations TRA 05/PZ1 and USGS 80 and between USGS 121 and NPR Test/W-02 is striking, compared to the tilted west to east zone between USGS 80 and USGS 121, where successively older surfaces are dropped proportionately to greater depths. The only lava flow present in all four of the core holes TRA 05/PZ1, USGS 80, USGS 121, and NPR Test/W-02 is the 640 ka flow from a vent exposed at AEC Butte (Fig. 2). This upper surface of this flow pitches downward on the southeast side >100 m between USGS 80 and USGS 121. The differences in depth of this upper surface of the flow could be explained by a great thickness of AEC Butte flow units in the near-vent locations of core holes TRA 05/PZ1 and USGS 80, the next deeper flow having a more nearly horizontal surface. Anderson (1991) suggested that AEC Butte flows are possibly 75 m thick beneath core hole USGS 80, which is 1.3 km from the vent at AEC Butte. The AEC Butte flow units are only 16 m thick in TRA 05/PZ1 and 14 m thick in USGS 121, core holes that are 1.9 km and 2.0 km, respectively, from the vent. If the AEC Butte flow units represent a thick accumulation of basalt forming a shield near these core holes, it is necessary to explain how thin flows in examples between 400 and 500 ka overlapped the edge of the shield to an aggregate depth of 100 m so soon after eruption of AEC Butte lavas.

Thickness

Mean thicknesses of basalt lava flows at INEEL vary from 10 to 39 m per eruptive event (Table 5), each eruptive event being defined by a combination of paleomagnetic and petrographic criteria. A given event may be a single lava flow or several flow units that together constitute a single lava accumulation. Changes in thicknesses define a north-northwest–trending decreasing gradient (Fig. 19); thus lava flows are thicker close to the vent locations than farther away. The thickness gradient decreases toward the areas of ICPP and TRA (Fig. 2), where mean thickness values are <12 m. The gradient of decreasing flow thicknesses (Fig. 19) is similar to the pattern of accumulation rates (Fig. 16); the core holes having thinner flows generally yield lower accumulation rates (USGS 80, TRA 05/PZ1), whereas most core holes having thicker flows yield high accumulation rates (USGS 121, ICPP-COR-A-023, USGS 123). In the vicinity of AEC Butte, the average flow thickness is <12 m; Anderson et al. (1997) speculated that this is an area of possible uplift. Whether by uplift or by a slower rate of

TABLE 5. MEAN RECURRENCE INTERVALS, MEAN THICKNESSES, ACCUMULATION RATES, AND LINEAR REGRESSION COEFFICIENTS FOR CORED WELLS OF THE IDAHO NATIONAL ENGINEERING AND ENVIRONMENTAL LABORATORY

Well name	Recurrence interval (1 k.y.)	Mean thickness (m)	Accumulation rate (m/100 k.y.)	Regression coefficient
USGS 80	73 ± 84	11 ± 7	16	0.968
USGS 123	42 ± 28	15 ± 10	39	0.994
NPR Test/W-02	51 ± 22	20 ± 11	43	0.984
ICPP-COR-A-023	41 ± 56	14 ± 14	36	0.964
USGS 121	32 ± 46	12 ± 6	43	0.953
TRA 05/PZ1	84 ± 47	10 ± 7	16	0.994
STF-PIE-AQ-01	(54)	25 ± 21	50	(1.0)
ARA-COR-005	(36)	23 ± 17	67	(1.0)
ANL-OBS-AQ-014	(41)	21 ± 13	56	(1.0)
NRF 89-04	81 ± 51	18 ± 10	24	0.992
NRF 89-05	73 ± 38	18 ± 12	26	0.994
NRF B18-1	73 ± 38	19 ± 11	27	0.990
NRF #6P	116 ± 61	25 ± 11	22	0.993
NRF #7P	97 ± 55	19 ± 19	22	0.989
BG-77-1	43 ± 26	26 ± 18	47/69	0.878/(1.0)
C-1A	50 ± 41	20 ± 13	43/41	0.898/0.999
USGS 118	—	26 ± 19	—	—
TCH #1	122 ± 81	25 ± 18	24/24	0.981/(1.0)
TCH #2 Piezo A	140 ± 129	39 ± 33	37/15	0.938/0.979
Core hole 2-2A	—	(11 ± 6)*	20	0.998

Note: Recurrence interval in parentheses are from incompletely studied core holes and preliminary; mean thickness for core hole 2-2A is preliminary due to insufficient data and an absolute minimum value; accumulation rates and regression coefficients separated by slash are for core holes with significant hiatuses in their sequence and represent before and after figures; regression coefficients in parentheses are on two-point lines and are unity by definition.

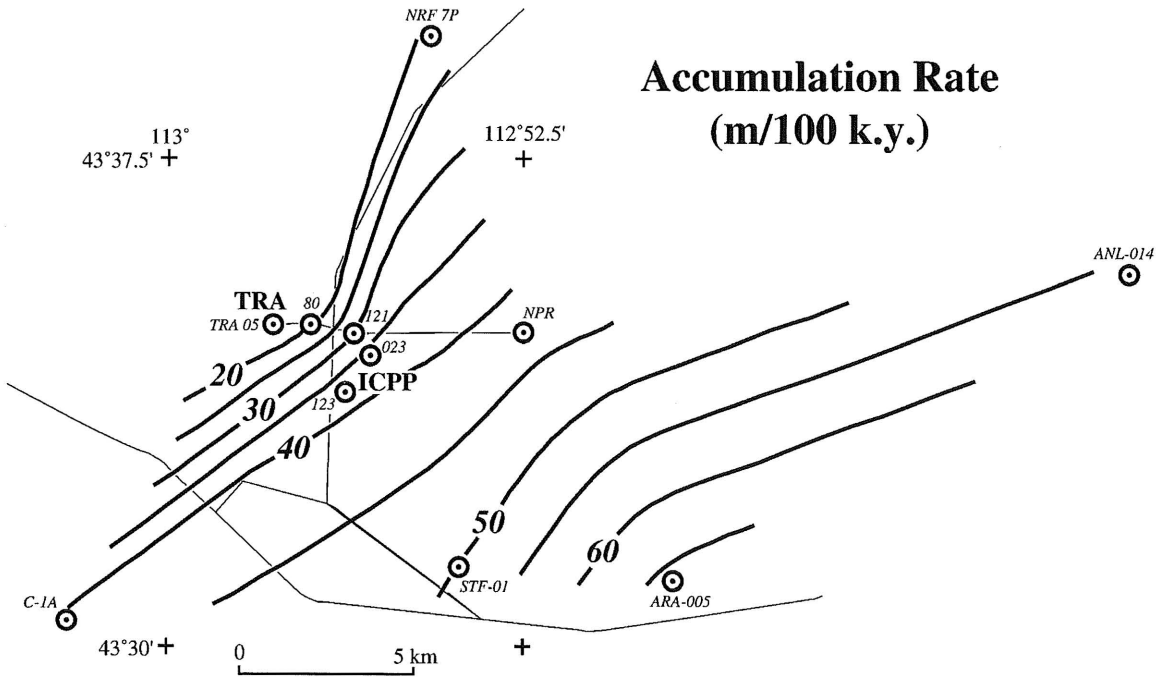

Figure 16. Contour map of basalt lava accumulation rates early to midway in Brunhes Normal Polarity Chron from core hole data in southern part of Idaho National Engineering and Environmental Laboratory. Values are in m/100 k.y., and contour interval is 5 m. Abbreviations: TRA, Test Reactor Area; ICCP, Idaho Chemical Processing Plant.

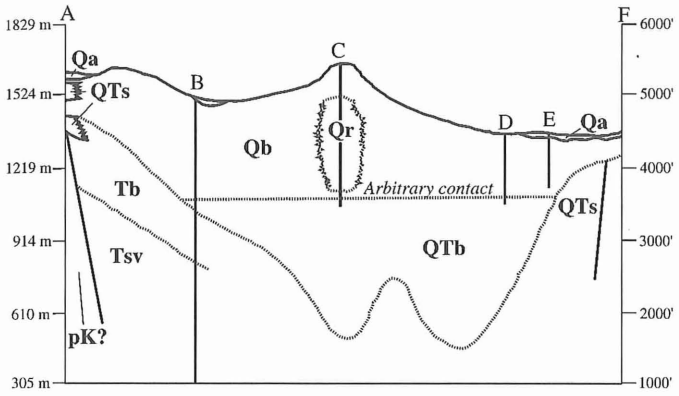

Figure 17. Northwest-southeast cross section showing subsidence of lava flows parallel to topographic axis of eastern Snake River Plain. Geologic units: Qa, Quaternary alluvium; Qr, Quaternary rhyolite; Qb, Quaternary basalt; QTs, Quaternary-Tertiary sediments; QTb, Quaternary-Tertiary basalts; Tb, Tertiary basalts; Tsv, Tertiary silicic volcanic rocks; pK, preCretaceous basement rocks. See Figure 2 for location of sections; after Whitehead (1992).

subsidence, the AEC Butte area seems to have served as a shoal for successive lava flow inundations.

Recurrence interval

The recurrence rate for eruptions can be estimated if we assume a linear age versus depth relationship in combination with a given number of flows within each core hole (Table 5). The recurrence intervals vary by a factor of four, from an eruption every 32 k.y. at USGS 121, to an eruption every 140 k.y. at TCH #2 Piezo A. Uncertainties in the ages of flows in USGS 118, and of age and flow-unit groupings in core hole 2-2A, prevent the calculation of mean recurrence intervals in those core holes. Estimates of mean recurrence intervals in core holes ANL-OBS-AQ-014, ARA-COR-005, and STF-PIE-AQ-01 were made by dividing the time interval between dated lava flows by the number of independent lava flows.

The ages used to calculate recurrence intervals come from two assessment processes. If the lava flow was directly dated or correlated to a flow in an adjacent core hole that was directly dated, then that age was used to calculate the recurrence interval between successive flows. For a lava flow for which no ages have been measured, an age estimate (parentheses in Tables 1–4) was generated from the linear age versus depth relationship in that core hole. In well-studied core holes such as NPR Test/W-02, TCH #2 Piezo A, and USGS 123, the recurrence intervals vary. For incompletely studied core holes, such as USGS 121 and ICPP-COR-A-023, in which much of the age information is provided by correlation with other core holes, negative apparent recurrence intervals are paired with long positive recurrence intervals that immediately precede or follow the negative calculated intervals. Only the mean recurrence value is used in geologic interpretations; we believe that the errors of age assessment only increase the standard deviation of the mean recurrence interval and not the mean value itself.

The contour pattern of the mean recurrence intervals is broadly smooth and roughly parallels the axis of the eastern Snake River Plain (Fig. 20). One would expect the mean recurrence interval to be shorter close to vents in fast accumulation zones and longer at locations farther from vents in zones of lower accumulation rate. This pattern is approximated (Fig. 20) with the important additional feature that a sharp gradient in recurrence interval mimics the strong gradient in accumulation rate (Fig. 16). The higher accumulation rates of USGS 121, ICPP-COR-A-023, and USGS 123 arise in part due to short recurrence intervals compared to core holes USGS 80 and TRA 05/PZ1. The recurrence intervals to the east and southeast of the sharp gradient suggest an area of relatively uniform recurrence intervals between 40 and 50 k.y. Mean recurrence intervals vary significantly, typically by 50%–100% of the mean values, and clearly indicate that recurrence of lava flow inundation at a given locality is nonuniform. These recurrence intervals pertain to a time from early to midway in the Brunhes Normal Polarity Chron. It is important to note that most of the eastern Snake River Plain at or near the INEEL underwent a hiatus in lava flow accumulation for the past 200 ka. However, it is important to note that the limited data from core holes that capture hiatuses suggest that these same recurrence intervals would again exist when eruptions resume.

APPLICATION OF ACCUMULATION-RATE DATA TO VOLCANIC HAZARDS AT INEEL

The data on accumulation rates, mean thicknesses, and mean-recurrence intervals generated from the INEEL core holes present an opportunity to further assess the volcanic hazard to the INEEL. Volcanic hazards were discussed by Hackett and Smith (1994) and Hackett et al. (2000), mostly on the basis of geologic data derived from the geologic map of the INEL (Kuntz et al., 1994). Hackett and Smith (1994) estimated recurrence intervals using vent density, lava flow area, and lava flow age. They estimated recurrence intervals for core holes NPR Test and BG-77-1 of 45 k.y., in close agreement with the respective values of 51 ± 22 k.y. and 43 ± 26 k.y. calculated in this study. They assigned single values for recurrence interval to individual volcanic rift zones as defined by Kuntz et al. (1992) and expressed the belief that recurrence intervals increase northward in the northwest-trending volcanic rift zones with increasing distance from the axis of the eastern Snake River Plain and decreasing vent density.

From our study, recurrence intervals do not seem to be related to the northwest-trending volcanic rift zones, possibly due to the distribution of core holes we studied. However, recurrence intervals are relatively short near the axis of the eastern Snake River Plain and relatively long in the north part of the

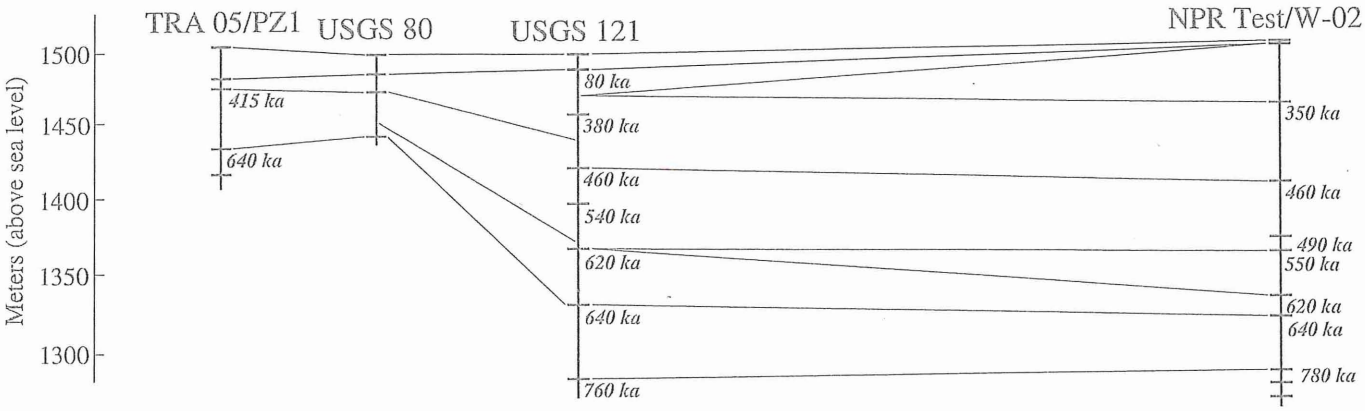

Figure 18. East-west vertical cross section between core holes TRA 05 and NPR Test/W-02 showing absolute depth position (in meters above sea level) of lava flows from AEC Butte (640 ka) and other dated flows correlated between these core holes. Gray halftone denotes surface sediment layer; numbers show age of horizons rounded to nearest 10 ka.

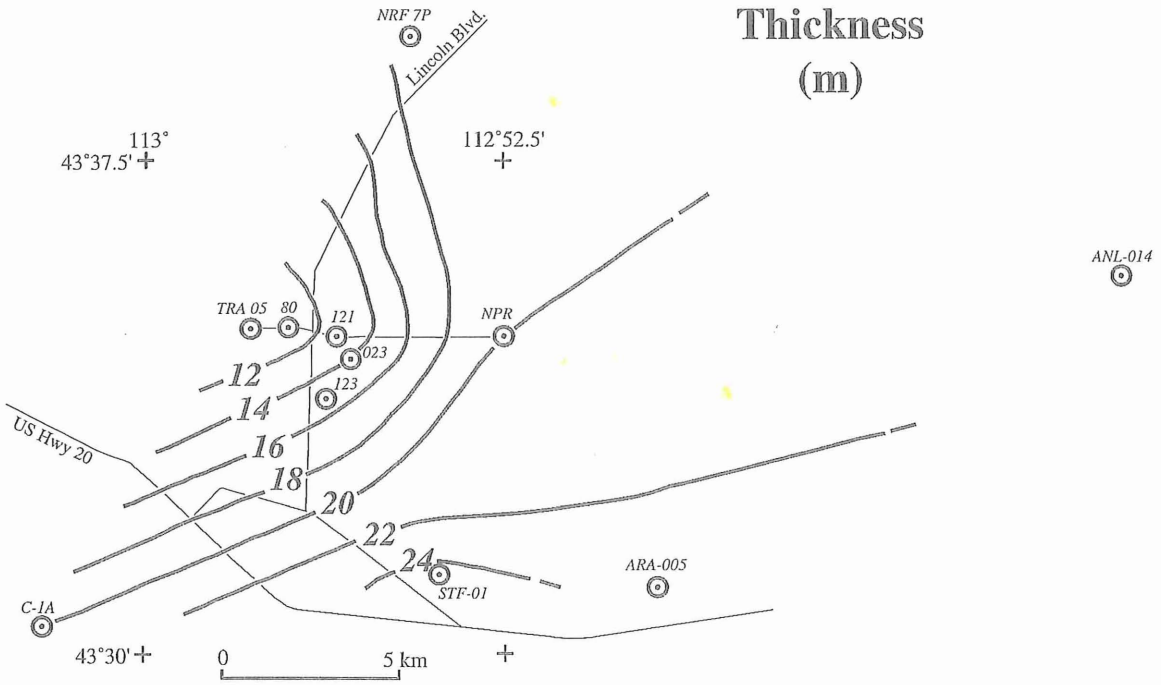

Figure 19. Contour map of average basalt lava flow thicknesses of lavas erupted early to midway in Brunhes Normal Polarity Chron, from core hole data in southern part of Idaho National Engineering and Environmental Laboratory. Values are in meters; contour interval is 2 m.

study area. Specific values computed from this study correspond to the 125 k.y. value estimated by Hackett and Smith (1994) only in the northern part of the Howe–East Butte, Lava Ridge–Hell's Half Acre, and Circular Butte–Kettle Butte volcanic rift zones, and generally for lava flows older than 780 ka. Appraisal of lava flow inundation hazards to sites on the INEEL must be viewed in light of the context that volcanic recurrence intervals are nonuniform, and that a hiatus of eruptions dominates the INEEL at present.

CONCLUSIONS

Our studies show that the accumulation of basaltic lava flows at 20 studied core holes in the eastern Snake River Plain is uniform at a given locality over very long periods of time. We also find that adjacent core holes yield remarkably different accumulation rates for strata of the same age (Fig. 16). The accumulation rates are highest near the axis of the eastern Snake River Plain and near volcanic rift zones, and lowest near the

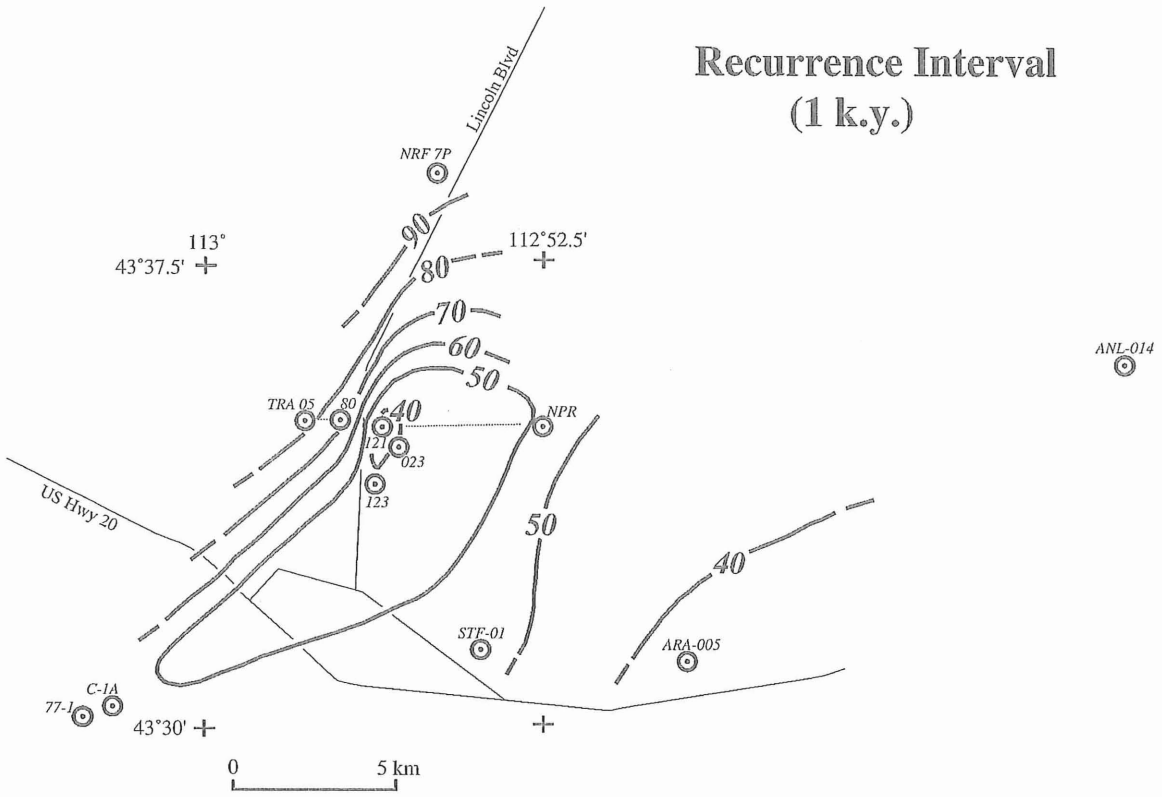

Figure 20. Contour map of average recurrence interval of basalt lava inundation during time period of early to midway through Brunhes Normal Polarity Chron from core hole data in southern part of Idaho National Engineering and Environmental Laboratory. Values are in k.y.; contour interval is 10 k.y.

margins of the eastern Snake River Plain and away from volcanic rift zones. In some core holes, the relatively steady accumulation history has been interrupted by hiatuses lasting several hundreds of thousands of years. When accumulation of flows began again at sites that underwent such a hiatus, the accumulation typically resumed at rates nearly identical to those before the hiatus.

These data provide strong evidence that basaltic volcanism in the eastern Snake River Plain is temporally and spatially predicable when viewed over hundreds of thousands or a few million years. Volcanism has occurred repeatedly along long-lived volcanic rift zones; areas away from the topographic axis of the eastern Snake River Plain and between volcanic rift zones have undergone fewer inundations by basaltic lava flows. The data can be used for long-term predictions about where and when future eruptions will occur and thus form a basis for volcanic-hazard evaluations for the INEEL area of the eastern Snake River Plain.

REFERENCES CITED

Anderson, S.R., 1991, Stratigraphy of the unsaturated zone and uppermost part of the Snake River Plain aquifer at the Idaho Chemical Processing Plant and Test Reactors Areas, Idaho National Engineering Laboratory: U.S. Geological Survey Water-Resources Investigations Report 91-4010 (DOE/ID-22095), 71 p.

Anderson, S.R., and Lewis B.D., 1989, Stratigraphy of the unsaturated zone at the Radioactive Waste Management Complex, Idaho National Engineering Laboratory, Idaho: Geological Survey Water-Resources Investigations Report 89-4065 (DOE/ID-22080), 54 p.

Anderson, S.R., Ackerman, D.J., Liszewski, M.J., and Freiburger, R.M., 1996, Stratigraphic data for wells at and near the Idaho National Engineering Laboratory, Idaho: U.S. Geological Survey Open-File Report 96-248 (DOE/ID-22095), 27 p. and 1 diskette.

Anderson, S.R., and Liszewski, M.J., 1997, Stratigraphy of the unsaturated zone and the Snake River Plain aquifer at and near the Idaho National Engineering Laboratory, Idaho: U.S. Geological Survey Water-Resources Investigations Report 97-4183 (DOE/ID-22095), 65 p.

Anderson, S.R., Liszewski, M.J., and Cecil, L.D., 1997, Geologic ages and accumulation rates of basalt-flow groups and sedimentary interbeds in selected wells at the Idaho National Engineering Laboratory, Idaho: U.S. Geological Survey Water-Resources Investigations Report 97-4010 (DOE/ID-22095), 39 p.

Champion, D.E., and Lanphere, M.A., 1997, Age and paleomagnetism of basaltic lava flows in corehole ANL-OBS-AQ-014 at Argonne National Laboratory-West, Idaho National Engineering and Environmental Laboratory: U.S. Geological Survey Open-File Report 97-700, 34 p.

Champion, D.E., Dalrymple, G.B., and Kuntz, M.A., 1981, Radiometric and paleomagnetic evidence for the Emperor Reversed Polarity Event at 0.46 ± 0.05 M.Y. in basalt lava flows from the eastern Snake River Plain, Idaho: Geophysical Research Letters, v. 8, p. 1055–1058.

Champion, D.E., Lanphere, M.A., and Kuntz, M.A., 1988, Evidence for a new geomagnetic reversal from lava flows in Idaho: Discussion of short po-

larity reversals in the Brunhes and late Matuyama polarity chrons: Journal of Geophysical Research, v. 93, p. 11667–11680.

Champion, D.E., Lanphere, M.A., and Anderson, S.R., 1996, Further verification and $^{40}Ar/^{39}Ar$ dating of the Big Lost reversed polarity subchron from drill core subsurface samples of the Idaho National Engineering Laboratory, Idaho: Eos (Transactions of the American Geophysical Union), v. 77, no. 46, p. F165.

Dalrymple, G.B., and Lanphere, M.A., 1969, Potassium-argon dating: New York, W.H. Freeman, 258 p.

Dalrymple, G.B., and Lanphere, M.A., 1971, $^{40}Ar/^{39}Ar$ technique of K-Ar dating: A comparison with the conventional technique: Earth and Planetary Science Letters, v. 12, p. 300–308.

Dalrymple, G.B., and Lanphere, M.A., 1974, $^{40}Ar/^{39}Ar$ age spectra of some undisturbed terrestrial samples: Geochemica et Cosmochemica Acta, v. 38, p. 715–738.

Doherty, D.J., 1979, Drilling data from exploration well 2-2A, NW1/4, sec. 15, T. 5 N., R. 31 E., Idaho National Engineering Laboratory, Butte County, Idaho: U.S. Geological Survey Open-File Report 79-851, 1 oversize plate.

Greeley, R., 1982, The Snake River Plain, Idaho: Representative of a new category of volcanism: Journal of Geophysical Research, v. 87, p. 2705–2712.

Hackett, W.R., and Smith, R.P., 1994, Volcanic hazards of the Idaho National Engineering Laboratory and adjacent areas: INEL-94/0276, 31 p.

Hackett, W.R., Smith, R.P., and Khericha, Soli, 2002, Volcanic hazards of the Idaho National Engineering and Environmental Laboratory, Southeast Idaho, *in* Bonnichsen, B., White, C.M., and McCurry, M., eds., Tectonic and magmatic evolution of the Snake River Plain Volcanic Province: Idaho Geological Survey Bulletin 30 (in press).

Hughes, S.S., Smith, R.P., Hackett, W.R., McCurry, M., Anderson, S.R., and Ferdock, G.C., 1997, Bimodal magmatism, basaltic volcanic styles, tectonics, and geomorphic processes of the eastern Snake River Plain, Idaho: Salt Lake City, Utah, National Geological Society of America Meeting, Fieldtrip Guidebook, p. 423–458.

Ingamells, C.O., 1970, Lithium metaborate flux in silicate analysis: Annals Chemica Acta, v. 52, p. 323–334.

Irving, E., 1964, Paleomagnetism and its application to geological and geophysical problems: New York, John Wiley & Sons, 399 p.

Jobe, S.A., and Champion, D.E., 2002, Petrography and paleomagnetism of core ICPP-COR-A-023 and correlation of a basalt lava flow sequence, Idaho National Engineering and Environmental Laboratory, Idaho: U.S. Geological Survey Open-File Report, 27 p. (in press).

Kuntz, M.A., Dalrymple, G.B., Champion, D.E., and Doherty, D.J., 1980, Petrography, age and paleomagnetism of volcanic rocks at the Radioactive Waste Management Complex, Idaho National Engineering Laboratory, Idaho, with an evaluation of volcanic hazards: U.S. Geological Survey Open-File Report 80-388, 63 p.

Kuntz, M.A., Covington, H.R., and Schorr, L.J., 1992, An overview of basaltic volcanism of the eastern Snake River Plain, Idaho, *in* Link, P.K., Kuntz, M.A., and Platt, L.B., eds., Regional geology of eastern Idaho and western Wyoming: Geological Society of America Memoir 179, p. 227–267.

Kuntz, M.A., Skipp, B., Lanphere, M.A., Scott, W.E., Pierce, K.L., Dalrymple, G.B., Champion, D.E., Embree, G.F., Page, W.R., Morgan, L.A., Smith, R.P., Hackett, W.R., and Rodgers, D.W., 1994, Geologic map of the Idaho National Engineering Laboratory and adjoining areas, eastern Idaho: U.S. Geological Survey Miscellaneous Investigations Map I-2330, scale 1:100 000.

Lanphere, M.A., 2000, Comparison of conventional K-Ar and $^{40}Ar/^{39}Ar$ dating of young mafic volcanic rocks: Quaternary Research, v. 53, p. 294–301.

Lanphere, M.A., and Dalrymple, G.B., 1971, A test of the $^{40}Ar/^{39}Ar$ age spectrum technique on some terrestrial materials: Earth and Planetary Science Letters, v. 12, p. 359–372.

Lanphere, M.A., Champion, D.E., and Kuntz, M.A., 1993, Petrography, age and paleomagnetism of basalt lava flows in coreholes Well 80, NRF 89-04, NRF 89-05, and ICPP-123, Idaho National Engineering Laboratory: U.S. Geological Survey Open-File Report 93-327, 40 p.

Lanphere, M.A., Kuntz, M.A., and Champion, D.E., 1994, Petrography, age and paleomagnetism of basaltic lava flows in coreholes at Test Area North (TAN), Idaho National Engineering Laboratory: U.S. Geological Survey Open-File Report 94-686, 49 p.

Mankinen, E.A., and Dalrymple, G.B., 1972, Electron microprobe evaluation of terrestrial basalts for whole-rock K-Ar dating: Earth and Planetary Science Letters, v. 17, p. 89–94.

Morgan, L.A., 1990, Lithologic description of the "Site E Corehole," Idaho National Engineering Laboratory, Butte County, Idaho: U.S. Geological Survey Open-File Report 90-487, 7 p.

Stacey, J.S., Sherrill, N.D., Dalrymple, G.B., Lanphere, M.A., and Carpenter, N.V., 1981, A five-collector system for the simultaneous measurement of argon isotope ratios in a static mass spectrometer: International Journal of Mass Spectrometry and Ion Physics, v. 39, p. 167–180.

Taylor, J.R., 1982, An introduction to error analysis: Mill Valley, California, University Science Books, 270 p.

Walker, E.H., 1964, Subsurface geology of the National Reactor Testing Station, Idaho: U.S. Geological Survey Bulletin 1133-E, 22 p.

Whitehead, R.L., 1992, Geohydrologic framework of the Snake River Plain Regional aquifer system, Idaho and eastern Oregon: U.S. Geological Survey Professional Paper 1408-B, 32 p.

MANUSCRIPT ACCEPTED BY THE SOCIETY NOVEMBER 2, 2000

Printed in the U.S.A.